https://ntrs.nasa.gov/search.jsp?R=20180008680 2019-08-31T17:44:56+00:00Z

10 meter Sub-Orbital Large Balloon Reflector (LBR)

Step I Phase B Report
31 May 2014

PI: Christopher K. Walker
University of Arizona

I COVER PAGE AND PROJECT SUMMARY

The realization of a large, space-based 10 meter class telescope for far-infrared/THz studies has long been a goal of NASA. Such a telescope could study the origins of stars, planets, molecular clouds, and galaxies; providing a much needed means of following-up on tantalizing results from recent successful missions such as Spitzer, Herschel, and SOFIA. Indeed, Herschel began its life in the US space program as the Large Deployable Reflector (LDR) – to be assembled in low Earth orbit by shuttle astronauts. Escalating costs and smaller federal budget allocations resulted in a downsizing of the mission. However, by combining successful suborbital balloon and ground-based telescope technologies, the dream of a 10 meter class telescope free of ~99% of the Earth's atmospheric absorption in the far-infrared can be realized. The same telescope can also be used to perform sensitive, high spectral and spatial resolution limb sounding studies of the Earth's atmosphere in greenhouse gases such as CO, ClO, O_3, and water, as well as serve as a high flying hub for any number of telecommunications and surveillance activities. Flight times of 100+ days will be possible, with instruments having mass and power requirements in excess of ~500 kg and ~1 kW.

Here we present the results of our NIAC Step 1, Phase B design study where each key aspect of the LBR concept is discussed and recommendations made for further study in Phase II. These aspects include realization of a large spherical reflecting surface, spherical corrector, pointing system, instrument module, and service module/gondola. Once each hardware component is introduced, a typical LBR Mission profile is described that enables the realization of a stratospheric 10 meter THz observatory and limb sounder. Verification of the design approach was achieved by using a combination of analytical modelling, lab testing of materials and techniques, and building a 3 meter rooftop LBR prototype.

LBR directly addresses NASA's Strategic Goals 2, 3, 5, and 6.

II FACT SHEET

The Large Balloon Reflector (LBR) is a game-changing concept to use the aluminized half-hemisphere of a balloon to form a 10 meter stratospheric observatory. The spherical balloon reflector is deployed *within* a larger carrier balloon that serves both as a launch vehicle and radome. Such a telescope could study the origins of stars, planets, molecular clouds, and galaxies; providing a much needed means of following-up on tantalizing results from recent successful missions such as Spitzer, Herschel, and SOFIA. LBR will perform high spectral/spatial resolution observations in astrophysically important atomic and molecular spectral lines only accessible from near space or from orbit. The proposed effort directly addresses NASA's Strategic Goals 2, 3, 5, and 6.

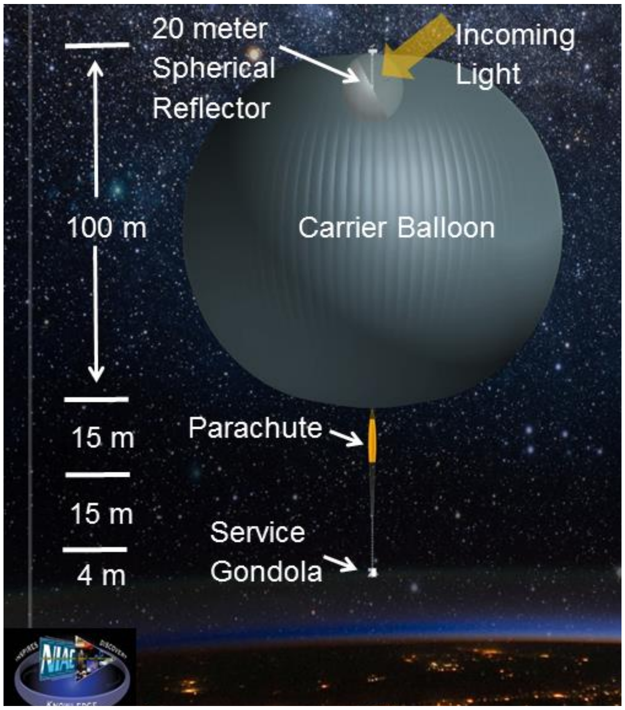

LBR: Prospecting for *Cosmic Origins*

Goal 1: Stellar Evolution & Planet Formation:
Use the ground state Water line at 557 GHz to probe the formation of planetary systems.

Goal 2: External Galaxies:
Use the ground state Water line at 557 GHz to probe the chemistry and physical conditions in Normal, Starburst, & High z galaxies.

Goal 3: Cosmic Evolution:
Use the LiH line at 444 GHz to determine the lithium abundance along multiple lines of sight through the Galaxy.

Data Products:
Spectroscopic data base of water and LiH lines toward a variety of galactic and extragalactic objects.

1. Key Mission Characteristics

Heritage: Echo I & II, IAE
Mode: Ultra-Long Duration Balloon (ULDB)
Duration: 100 days (ULDB baseline)
Float altitude: 39 km
Power: 510 W
Mass: 1501 kg

2. Key Instrument Characteristics

Heritage: Herschel, ODIN, SWAS, STO
Instrument type: Heterodyne receivers
System Sensitivity: <1500K DSB
Spectrometer: ~1 km/s resolution,
347-552 km/s velocity coverage per pixel
Cryogenic system: closed-cycle cryostat

3. ***Key Gondola Characteristics***

Heritage: Flare Genesis, SBI, STO
Attitude Control: 3-axis stabilized
Pointing requirements: 3 arcsec (knowledge)
Science data storage capability: >500 GB
Science data transfer rate: 1 GB/day

III TABLE OF CONTENTS

I Cover Page and Project Summary ... 2

II Fact Sheet ... 3

III Table Of Contents ... 4

IV Executive Summary ... 6

V Detailed Description of Concept ... 8
- V.A Spherical Reflectors ... 8
  - V.A.1 History ... 8
  - V.A.2 Using LBR as a Parabola ... 11
    - V.A.2a Analytic LBR Performance Description ... 11
    - V.A.2b Numerical LBR Performance Description ... 14
  - V.A.3 Spherical Correctors ... 17
- V.B Large Balloon Reflector (LBR) Design ... 30
  - V.B.1 Materials ... 30
  - V.B.2 Fabrication methods ... 36
  - V.B.3 Internal structural supports ... 40
  - V.B.4 Instrument Unit integration ... 40
  - V.B.5 Steering mechanisms ... 40
  - V.B.6 Surface figure measurement system ... 42
  - V.B.7 Pressure/thermal management system ... 44
  - *V.B.8 LBR control computers ... 45*
- V.C Instrument Unit (IU) Design ... 46
- V.D Pointing Control System (PCS) ... 47
  - V.D.1 LBR Guidance Package ... 47
  - V.D.2 PCS Computer ... 49
- V.E Service Gondola ... 51
  - V.E.1 Structure ... 51
  - V.E.2 Avionics Computers ... 51
  - V.E.3 Command & Data Handling ... 52
  - V.E.4 Power ... 54
  - V.E.5 Thermal Control ... 56
  - V.E.6 Balloon Control and Telecommunications ... 56
  - V.E.7 Distribution to LBR ... 57
- V.F Mission Profile ... 60
  - V.F.1 Ground System ... 60
  - V.F.2 Flight Line Integration & Test ... 61

V.F.3 Launch Sequence 62
V.F.4 Ascent 62
V.F.5 LBR Deployment 62
V.F.6 Science Mission Operations 63
V.F.7 Data Management 63
V.F.8 Termination Sequence 63
V.F.9 Descent 63
V.F.10 Landing and Recovery 63

VI Example Applications to NASA Mission 66
VI.A Sub-Orbital 10 Meter THz Telescope 66
VI.A.1 Science Investigation 66
VI.B THz Earth Observing System 73

VII Approach Used to Evaluate the ConcepT 76
VII.A Rooftop 3 meter LBR Prototype 76
VII.A.1 Design 76
VII.A.2 Lessons Learned 79
VII.B Laboratory Measurements of Balloon Materials 80

VIII LBR COST Projection 82

IX Remaining Challenges 83

X References 84

XI Acronyms and Abbreviations 85

IV EXECUTIVE SUMMARY

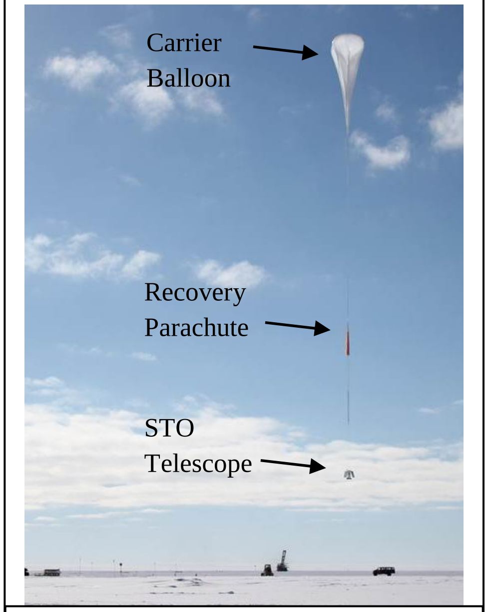

Figure IV.1: Conventional LDB Payload launched by the PI's team in January 2012.

Water vapor in the Earth's atmosphere absorbs much of the far-infrared emission and absorption lines from atoms and molecules in space needed to understand the origins of stars, planets, and galaxies. It is for this reason that telescopes designed to observe far-infrared spectral lines are placed on high, dry, mountain peaks or on the frozen high plateau of Antarctica. However, even these 10 to 12 meter class telescopes (ALMA – Atacama desert, Chile; Caltech Submillimeter Telescope – Mauna Kea, Hawaii; Heinrich Hertz Telescope – Mt. Graham, Arizona; South Pole Telescope - Antarctica) are essentially blind due to atmospheric absorption over much of the far-infrared. The Stratospheric Observatory for Far-Infrared Astronomy (SOFIA) provides some relief, but with only a modest 2.5 meter aperture, has limited sensitivity for the high angular resolution observations needed to probe distant galaxies and forming stellar and planetary systems in the Milky Way. Herschel's larger 3.5 meter aperture is somewhat better, but still falls short of what is needed. The James Webb telescope at 6.5 meters will do an excellent job probing these regions with its dedicated, fixed suite of instruments, but lacks the high spectral resolution provided by heterodyne instruments to disentangle the complex velocity fields associated with much of the interstellar medium. What is required is a 10 meter telescope in near space able to conduct high spectral resolution ($R > 10^5$) observations.

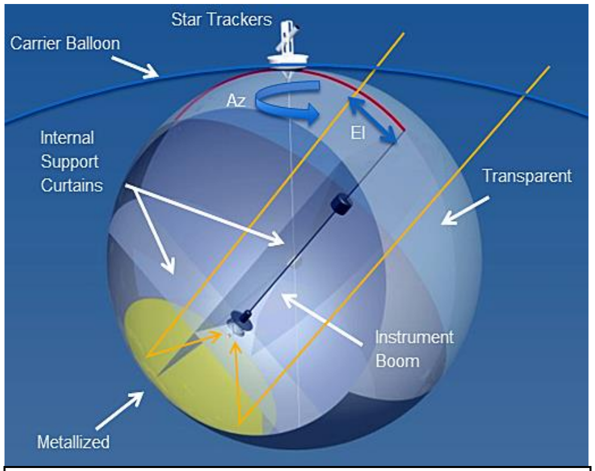

Figure IV.2: LBR Concept. The LBR spherical reflector resides within a transparent carrier balloon, which serves as both a launch vehicle and radome.

NASA's zero pressure or, more recently, super pressure balloons provide a means of transporting to and maintaining payloads of 2-3 tons in near space (see Figure IV.1). With this lift capability it is perhaps possible to construct a 10 meter carbon-fiber telescope and launch it to near space. However, the combination of stratospheric winds over such a large dish surface and pendulation at the end of a long balloon tether will make pointing the telescope at the required arc second levels problematic or impossible.

Figure IV.3: Echo 1 Satellite during tests in 1960: 30.5 m in diameter, 0.5 mil Mylar.

Instead of attempting to maintain the pointing of a large telescope at the end of a tether, we propose to deploy a telescope in the benign, protected environment ***within*** the carrier balloon. The telescope is itself a balloon, spherical in shape, metalized on one side and anchored to the top of the carrier balloon via a rotating azimuth plate (see Figure IV.2). The carrier balloon serves as both a stable mount and a radome for the inner balloon reflector. Light from space (or the atmosphere or ground) first passes through the ~2 mil thick polyethylene skin of the carrier balloon and then through the ~1 mil thick Mylar side of the inner balloon. Together these layers have < 8% absorption at the wavelengths of interest. The incoming light then encounters the aluminized, spherical, back surface of the inner balloon and is then focused into a receiving system. To achieve the performance of a 10 meter parabolic reflector, a 20 meter diameter inner balloon can be used with a modest size (~1 meter) spherical corrector. For acceptable aperture efficiency, the inner balloon needs to hold its spherical figure to $\leq \lambda/16$ of the wavelength being observed. The surface roughness should be $\leq \lambda/30$. As an example, the ground state transition of water has a wavelength of 538 μm (557 GHz). At this wavelength the LBR surface roughness needs to be ~ 21 μm and the spherical figure held to 40 μm. The required surface roughness is achievable for Mylar under pressure (see Echo I balloon, ca. 1960 in Figure IV.3). The spherical figure specification is more challenging and will require a combination of surface monitoring and active feed focus/positional control to achieve. Telescope pointing is accomplished by rotating the azimuth ring and the LBR sphere in elevation, together with tip/tilt adjustments of the corrector. Attached to the rotating azimuth plate on the outside of the balloon are star cameras to determine absolute position on the sky and gyroscopes to maintain pointing knowledge as the telescope slews. The telescope's power system and command and control unit are housed in a conventional gondola service module hanging below the carrier balloon. Low-loss power and fiber optic data cables connect the service module to the telescope and instrument. The `Top Hat' Long Duration Balloon (LDB) experiment launched in 2001 had a similar payload configuration, but with a 1 meter aluminum telescope mounted to the top of a

Figure IV.4: Top Hat Balloon Launch in 2001.

rotating azimuth plate. During the launch (see Figure IV.4) a tow balloon is used to lift the telescope/rotating plate up while the carrier balloon is being inflated underneath.

V DETAILED DESCRIPTION OF CONCEPT

V.A Spherical Reflectors

V.A.1 History

At the heart of LBR is a spherical reflector. Spherical reflectors have a long history in astronomy. This is due in part because a spherical shape is a "natural" result of different types of surface grinding processes. It is also an easy form to measure since all points are at a single distance, the radius of curvature, from the center of the curvature. It has been recognized for several centuries that a spherical reflector is an imperfect focusing element. As shown in Figure V.A.1 a spherical reflector unlike a parabola, does not bring a plane wave (parallel rays) to a point focus. Radiation from a small section of a sphere (discussed further below) is brought to the paraxial focus denoted F, located at a distance equal to half the radius of curvature from the surface of a sphere. As one uses more and more of the sphere, the initially parallel rays are focused to a line extending away from the center of curvature (towards A).

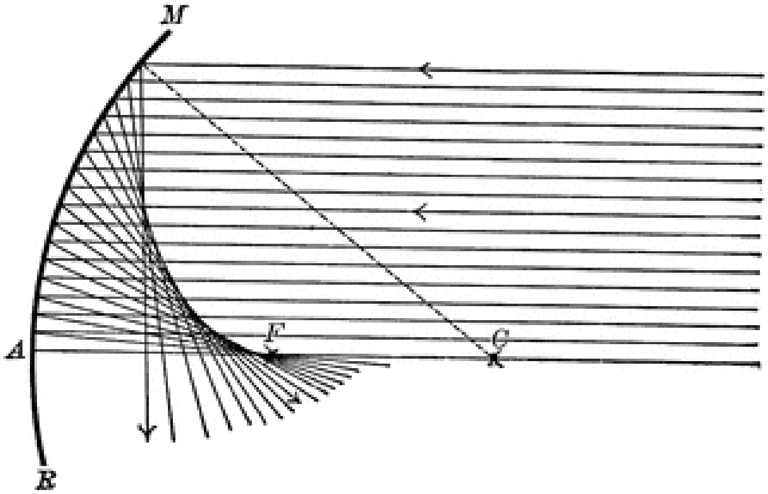

Figure V.A.1: Schematic of spherical aberration from a spherical reflector. The rays passing close to the center of curvature (C) are brought to the paraxial focal point (F), while parallel rays incident at greater distances from C cross the C-F axis closer to the reflecting surface.

Thinking reciprocally, radiation reflected from a large section of a sphere is not transformed into a perfect plane wave having uniform phase perpendicular to its direction of propagation; there is a significant phase error that results in an imperfect beam, and which is referred to as spherical aberration. However, unlike a parabola of revolution, which does have the desired property of bringing parallel rays to a point focus, a spherical reflector has no axis of symmetry.

Radiation incident from different directions is focused to lines parallel to the direction of incidence, but rotated around the paraxial focal point. Thus, whatever be its imperfections in focusing, a spherical reflector has an essentially unlimited field of view. This property of spherical antennas has led to their use in a variety of systems for which the large field of view compensates for imperfect focusing ability.

The large field of view of a spherical reflector means that to point the beam in different directions, one need only move the feed/receiver in a circular arc centered on the center of curvature of the sphere and having a radius approximately equal to half the radius of curvature of the sphere. The reflector surface, if made larger than the portion utilized at any moment, does not need to move at all. This important advantage was one of the motivations for the design of a 1000 foot diameter radio telescope; steering such a large structure to point in different directions would be difficult (to say the least) but as conceived (Gordon and LaLonde 1961) the Arecibo telescope's spherical primary is held above the surface of a natural bowl-shaped depression. The radius of curvature of the primary reflector of the Arecibo telescope is 870 ft., and the feeds thus move along an arc approximately 435 ft above the spherical surface, as seen in Figure V.A.2.

Figure V.A.2: The Arecibo radio telescope. The spherical primary reflector is 1000 ft in diameter. A line feed for 400 MHz operation can be seen hanging below the platform and track. The tip of the line feed is at the paraxial focal point of the spherical primary.

In order to achieve the desired large collecting area for the Arecibo telescope, a spherical cap having a radius of 500 feet is illuminated by the feeds, which definitely does not result in anything like a point focus; in fact, the length of the focal line is 96 feet. To couple to this, waveguide "line feeds" were developed based on waveguides with multiple radiating slots. These require accurate phase control, which greatly limits their instantaneous bandwidth, and the loss increases rapidly with frequency, which limited their maximum frequency to less than 2 GHz.

The limitations of line feeds led to the development of a two-element off-axis reflective corrector for Arecibo, which corrects the spherical aberration and brings rays to a point focus (Kildal, Baker, and Hagfors 1991). Referred to as the "Arecibo Gregorian" as it incorporates concave surfaces, this system operates at frequencies up to 10 GHz with broad bandwidths, limited by the receiver systems, which employ standard types of feedhorns (Goldsmith 1996).

The design of a spherical-primary radio telescope for operation at millimeter wavelengths incorporating a single surface corrector was built in Armenia (Herouni 1989). Its surface accuracy is specified to allow operation to frequencies up to 100 GHz. The spherical primary is 54 m in diameter, but only 32 m is illuminated at any one time. This allows pointing the beam over a very wide range of angles, which is achieved by rotating the corrector and receiver around the center of curvature. This is accomplished by mounting an arm on a large spherical bearing at the center of curvature, with the bearing being supported by a tripod structure as shown in Figure V.A.3. Scanning over 45° from zenith without spillover is possible, as compared to approximately 20° for Arecibo.

Figure V.A.3: View of 54m diameter spherical primary reflector of millimeter-wavelength radio telescope in Armenia. The on-axis corrector is seen mounted at the end of a pivot arm supported by a tripod structure.

The Hobby-EberlyTelescope (HET) is an optical analog of the Arecibo Gregorian system in the sense that it employs a 11.1 x 9.8m diameter spherical primary and a corrector system. The primary reflector of the HET is fixed in elevation but rotates in azimuth while the corrector and instruments move in elevation in order to point at an arbitrary direction. The HET corrector consists of multiple refractive elements, but achieves an impressively large FOV for an optical telescope with a spherical primary. A second optical telescope based on the same design is the SALT telescope in South Africa.

V.A.2 Using LBR as a Parabola

An LBR of diameter, D_{SPH}, can serve as a parabolic mirror with effective diameter $D_P \sim 0.25\ D_{SPH}$ with good beam efficiency without the use of a spherical corrector.

V.A.2a Analytic LBR Performance Description

As mentioned in the preceding section, one can take advantage of a spherical primary in two ways. The first is simply to use a relatively small section such that the spherical aberration is acceptable, while the second is to construct a corrector. Each of these has advantages and disadvantages, which we now discuss.

A sphere centered at y = R with radius R passes through x=y=0. The equation for this sphere is

$$y1 = R - (R^2 - x^2)^{0.5}\ . \qquad (1)$$

The Taylor's series expansion for this sphere (or circle, more accurately; the sphere is formed by rotation about the y axis) is

$$y2 = x^2/2R + x^4/8R^3\ . \qquad (2)$$

The equation for a parabola of focal length f with same the location and orientation is

$$y3 = x^2/4f. \qquad (3)$$

By comparing equations (1) and (3), we see that the focal length of paraxial section of the sphere is

$$f = R/2. \qquad (4)$$

The paraxial focal point of the spherical antenna is thus half way between the surface and the center of the sphere.

The three curves and differences are plotted in Fig. V.A.4. The error in the 2-term approximation is an order of magnitude smaller than the difference between parabola and sphere. If we take the units to be meters, we see that an edge sphere-parabola different of 1 mm occurs at a radius of 2.8 m. Thus, it would seem that a 5.6m diameter spherical antenna would work reasonably well at a wavelength of a few mm.

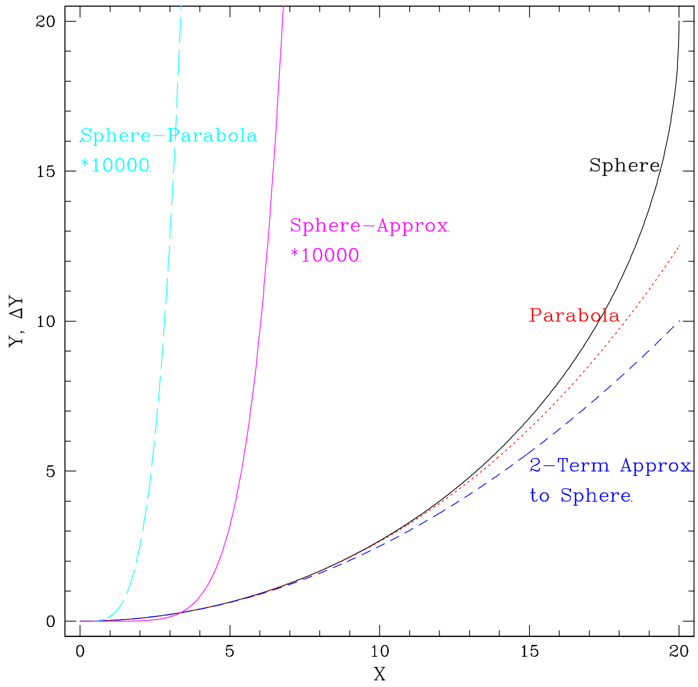

Figure V.A.4.: Comparison of shapes of cuts through spherical and parabolic reflectors having same focal lengths and locations.

The expressions for circle and parabola (equations 2 and 3 above) are both even functions of x. Thus, the coefficients of odd powers of x in the expansion are zero. The first two nonzero terms give the expression

$$f(x) = x^2/2R + x^4/8R^3 . \tag{5}$$

Substituting R = 2f yields

$$f(x) = x^2/4f + x^4/64f^3 . \tag{6}$$

The difference between the surface between the parabola and the sphere is

$$\Delta = x^4/64f^3. \tag{7}$$

At the edge of the antenna of diameter D, the radius x = D/2, and the surface deviation is given by

$$\Delta = D^4/1024f^3. \tag{8}$$

This can also be expressed as

$$\Delta = f/1024(f/D)^4 . \tag{9}$$

Thus, if we have a maximum acceptable fractional wavelength deviation and the telescope focal length, we can solve for the allowed focal ratio yielding

$$f/D = [f/1024\Delta]^{0.25} . \tag{10}$$

For example, if λ = 2 mm, and we want a $\lambda/10$ maximum error, Δ = 0.1 mm. This yields f/D = $[f(mm)/102.4]^{0.25}$. If R = 5 m, so that f = 2.5 m = 2500 mm, f/D = 2.22 so that D = f/2.22.

In the case of LBR a 10m diameter balloon with f = 2.5 m operates as a parabola with an equivalent diameter of 1.13 m. It is thus appropriate to ask what a realistic limit on the maximum surface error is. This question is considered in a pioneering article by T. Li (Li, 1959). He considers moving the feed away from the paraxial focal point to introduce a path error across the aperture such that the path error at the EDGE of the reflector is zero. Li states that this gives the minimum error over the whole dish, but does not state what this minimum is! The zero error at the antenna edge condition results in his equation 5, which can be written

$$f/D = [f/941\Delta]^{0.25} . \tag{11}$$

This gives only a very incrementally larger f/D ratio for given f and Δ and hence a slightly smaller diameter. However, one assumes that since Δ = zero at the center and at the edge, the RMS phase error will be less than for case where error is zero at the center and Δ at the edge. Assuming a uniformly illuminated aperture, the rms phase error is determined by integration of equation 7. We express

$$\Delta(r) = r^4/64f^3 \ . \tag{12}$$

If we integrate the square of this from 0 to R, and divide by the area of the antenna, and express the result in terms of the diameter, we find that rms surface error to be

$$\Delta_{rms} = f/2290(f/D)^4 \ . \tag{13}$$

This is a factor about 2.2 times smaller than from equation (9). The analog to equation (10) is

$$f/D = [f/2290\Delta_{rms}]^{0.25} . \tag{14}$$

If we naively adopted the requirement that the rms phase error should be $\lambda/16$, then for 2mm wavelength, Δ_{rms} = 0.125 mm. This gives f/D = $[f/286]^{0.25}$. Again for 10 m diameter balloon, R = 5 m and f = 2.5 m = 2500 mm, so f/D = 1.7 and D = 1.45 m. That is somewhat larger than the first cut value.

The next step is to include the illumination pattern of the antenna, which deemphasizes the outer parts. Thus, the condition of making the error zero at the edge may no longer appropriate. With a weighting function equal to the power pattern with 10.5 dB edge taper so that the Gaussian beam radius w = 0.455 D. The square of the path error at radius r is given by the square of equation (12), so that we have integral from 0 to R in the numerator

$$\int \exp(-2(r/w)^2 \ (r^8/4096f^3) \ 2\pi r dr, \tag{15}$$

while in the denominator we have just the integral of the power pattern. Converting this to function of a dimensionless quantity x = r/w gives limits 0 and 1.1 and the expression

$$\Delta^2_{ave} = \int x^9 \exp(-2x^2)dx/\int x\exp(-2x^2)dx \ . \tag{16}$$

The numerical integration gives (0.037/0.23), and the final result is

$$\Delta_{rms} = f/3736(f/D)^4\ . \qquad (17)$$

We thus get about half the rms as in previous calculation, and

$$f/D = [f/3736\Delta_{rms}]^{0.25}\ . \qquad (18)$$

Putting in the same value for rms surface error as in the example above, and for the same balloon parameters we find f/D = 1.52 and D = 1.64 m. However, a more detailed numerical analysis (see below) reveals that, with proper refocusing, the percentage of D_{SPH} that can serve as a parabolic reflector without the use of a corrector can be pushed up to ~25%.

V.A.2b Numerical LBR Performance Description

Let us consider a spherical reflector with a parent sphere diameter of D_{SPH} as shown in Fig. V.A.5. The actual reflector has a diameter A_P and is illuminated by an ideal Gaussian feed located at the sphere paraxial focal point $f_p=R_{SPH}/2$. We calculated the spherical reflector aperture efficiency at 450 GHz for a fixed parent sphere with the diameter of LBR (D_{SPH}=20 m) and different reflector apertures as shown in Table V.A.I. The Gaussian feed had a -10 dB edge taper at the different edge angles shown in the table.

As we mentioned in the previous section, by de-focusing the feed by a distance Δz along the optical axis we could reduce the overall phase error in the aperture. Fig. V.A.6 Shows the calculated aperture phased distribution in wavelengths at 450 GHz for the case of A_P=2.1 m with the feed at the paraxial focal point and after refocusing the feed by moving it towards the spherical reflector a distance Δz=+13.0mm.

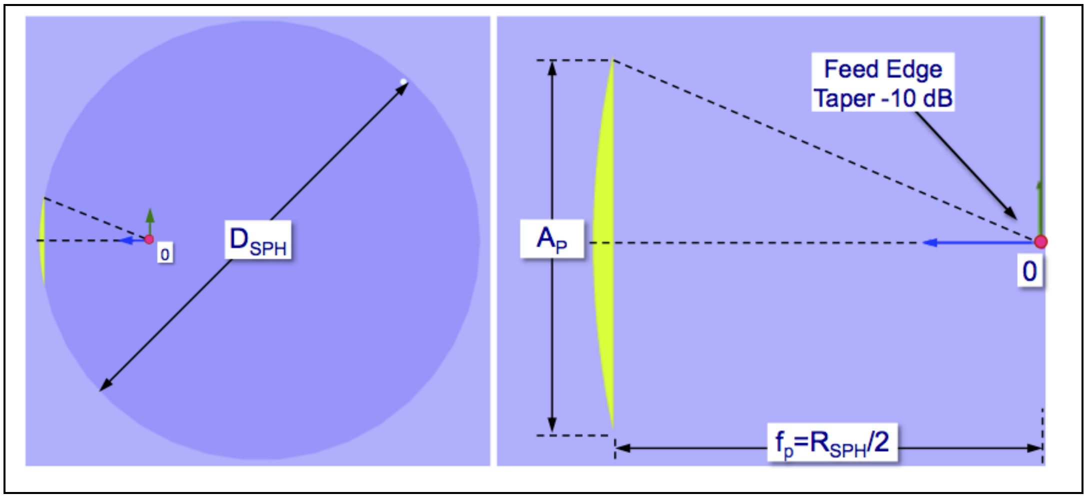

Figure V.A.5: Spherical reflector geometry with no corrector. *Left:* Parent sphere diameter. *Right:* Detail of the actual reflector aperture illuminated by an ideal Gaussian feed with an edge taper of -10 dB, located at the focal point f_p.

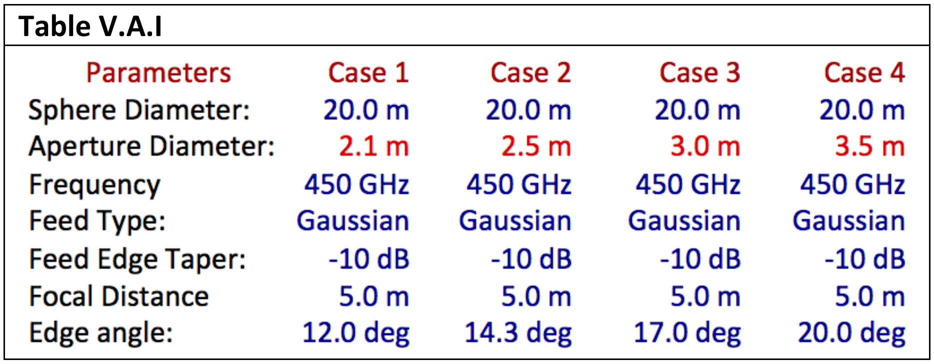

Table V.A.I

Parameters	Case 1	Case 2	Case 3	Case 4
Sphere Diameter:	20.0 m	20.0 m	20.0 m	20.0 m
Aperture Diameter:	2.1 m	2.5 m	3.0 m	3.5 m
Frequency	450 GHz	450 GHz	450 GHz	450 GHz
Feed Type:	Gaussian	Gaussian	Gaussian	Gaussian
Feed Edge Taper:	-10 dB	-10 dB	-10 dB	-10 dB
Focal Distance	5.0 m	5.0 m	5.0 m	5.0 m
Edge angle:	12.0 deg	14.3 deg	17.0 deg	20.0 deg

The spherical aberration is apparent in the left figure, with feed at the paraxial focal point, for which the overall aperture phase rms is ϕ_{RMS}= 0.063 λ. Refocusing by Δz=13mm, results in a reduction of the overall phase rms error, ϕ_{RMS}= 0.016 λ.

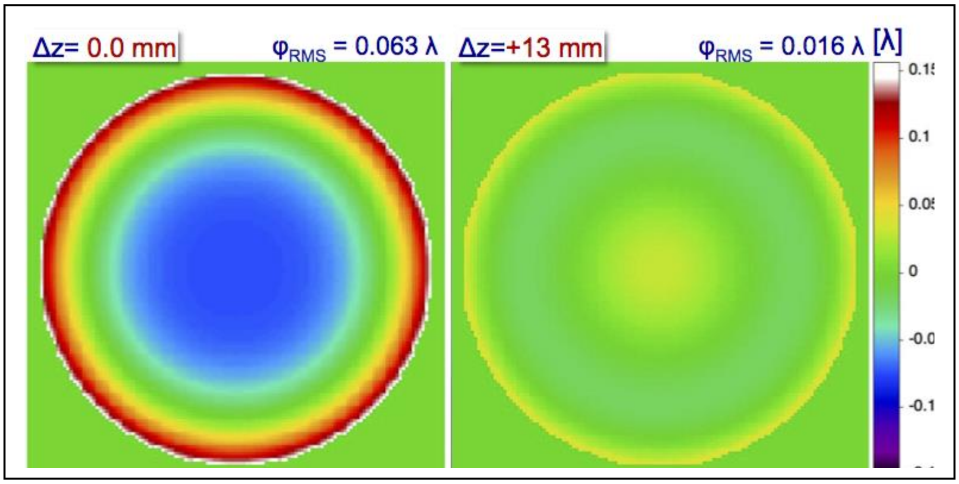

Figure V.A.6: Calculated aperture phase distribution in wavelengths, at 450 GHz, for a 20m parent sphere diameter and a reflector aperture diameter of A_P=2.1m, illuminated by a -10 dB edge taper Gaussian feed. *Left:* before and *Right:* after re-focusing by Δz=13mm.

Figure V.A.7 shows the normalized far field radiation pattern in dB, calculated at 450 GHz, for this case (A_P=2.1m), before and after re-focusing by Δz=13mm.

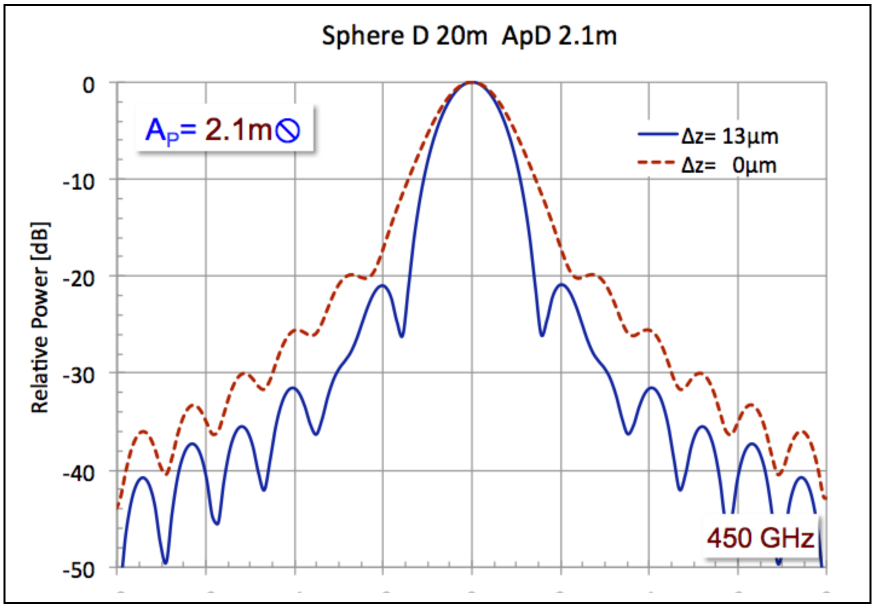

Figure V.A.7: Calculated far field radiation pattern, at 450 GHz, for a 20m parent sphere diameter and a reflector aperture diameter of A_P=2.1m, illuminated by a -10 dB edge taper Gaussian feed, before and after refocusing the feed by by Δz=13mm.

The aperture efficiency varies from 46% at the paraxial focal point to 78% after re-focusing. (no blockage was included in the calculation). Fig. V.A.8. shows the calculated aperture efficiency (at 450 GHz) as a function of feed de-focusing for various values of reflector diameters (fixed parent sphere D_{SPH}=20m).

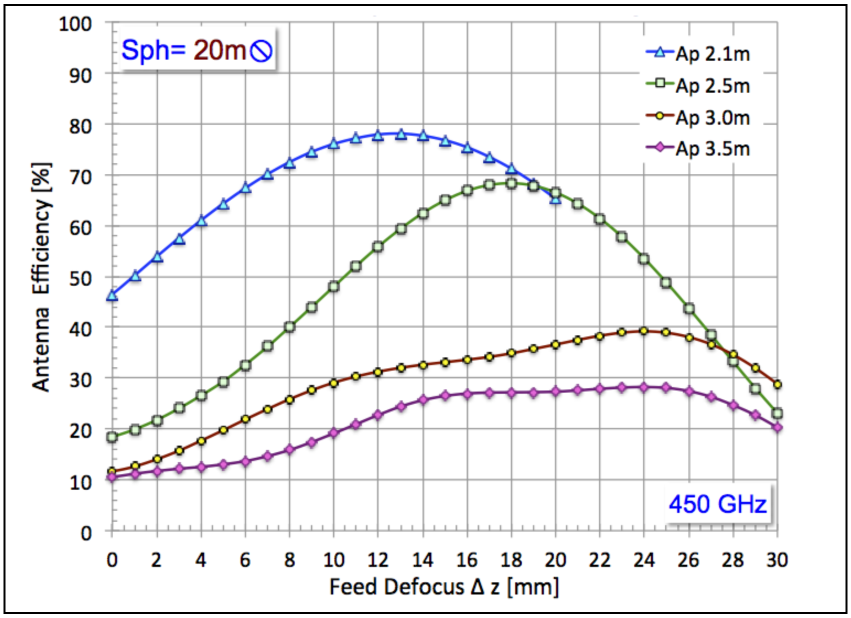

Figure V.A.8: Calculated aperture efficiency (at 450 GHz) as a function of feed de-focusing for various reflector apertures.

The numerical simulations show that with the proper use of focusing, an LBR of diameter, D_{SPH}, can serve as a parabolic mirror with effective diameter $D_P = 0.25\ D_{SPH}$ with good beam efficiency without the use of a spherical corrector.

V.A.3 Spherical Correctors

As discussed in the preceding section, it is possible to use a spherical reflector without any corrector, provided the f/D ratio is limited to a value determined by the allowable phase error. The result is that the effective diameter of the spherical primary is limited. It is thus appropriate to consider the use of a corrector for LBR. Correctors can be divided into two general classes – those which are axially symmetric, including those for HET and the Armenia Telescope, and off-axis correctors, such as that used for Arecibo. As is usually the case, each class has advantages and disadvantages. In the following, we discuss the modeling work on correctors we have performed in NIAC Phase I.

V.A.3.a On-axis Design

The on-axis spherical corrector design increases the fraction of the diameter of the spherical mirror that can be utilized by *a factor of two.* Changes in the reflector’s radii of curvature of 50 mm (or more with an active corrector) can be tolerated.

V.A.3.a.1 LBR 3 Meter Diameter Sphere Overview

The initial study of an on-axis design was conducted for the 3 meter diameter spherical balloon with the goal of making and eventually testing the spherical corrector system. This system is designed for a primary frequency of 115 GHz since for testing purposes we will be observing from the ground. The LBR 20 meter spherical balloon is discussed in the next section and addresses the details of designing for 557 GHz.

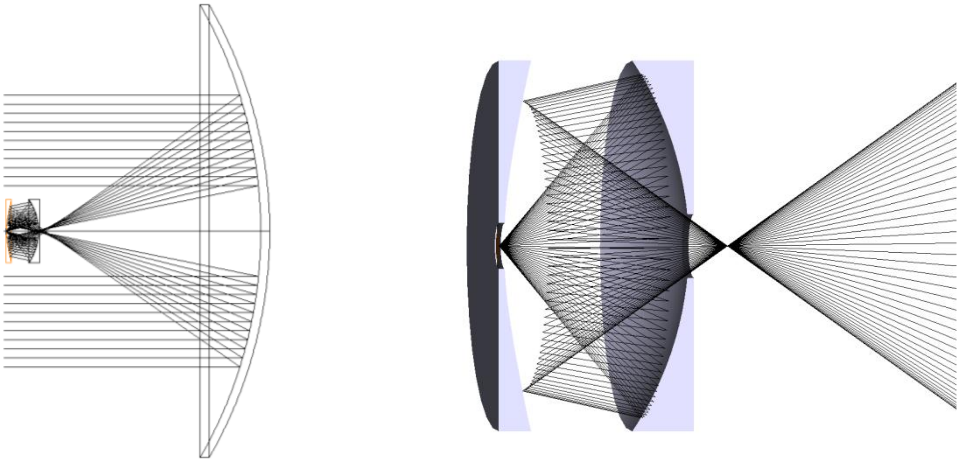

Figure V.A.9: Proposed On-Axis Spherical Corrector System Design for the 3 m diameter sphere. Left – Overall ray trace with adaptive secondary highlighted red. Right – 3D rendering of the secondary (left) and tertiary (right).

One of the main caveats in the on-axis design is minimizing beam blockage. In the case of a 3 m diameter sphere with a single secondary corrector, an issue arises with where to put the feed horn and instrument package. Due to the size of the package, putting them in front of the secondary would clip incoming beams from the primary mirror. A solution would be to position them near the primary surface, but for large primary spheres it is hard to correct the wavefront for aberrations with the focal plane at that location. Combine that with the logistics of supporting the optics within the balloon, a 2 mirror corrector system near paraxial focus was decided upon. The tertiary mirror would redirect the focus through the secondary mirror to allow for the feed horn to be behind the secondary mirror, Figure V.A.9 illustrates this concept. This also allows us to take advantage of the already existing blocking profile of the secondary, and we avoid adding any additional blockage. The driving limitations for the design of this on-axis 2 mirror spherical corrector become the clearance and proper sizing of the through holes in both the secondary and tertiary mirrors. To better visualize the optical ray paths the images in Figure V.A.10 illustrates step by step the ray path through the proposed system.

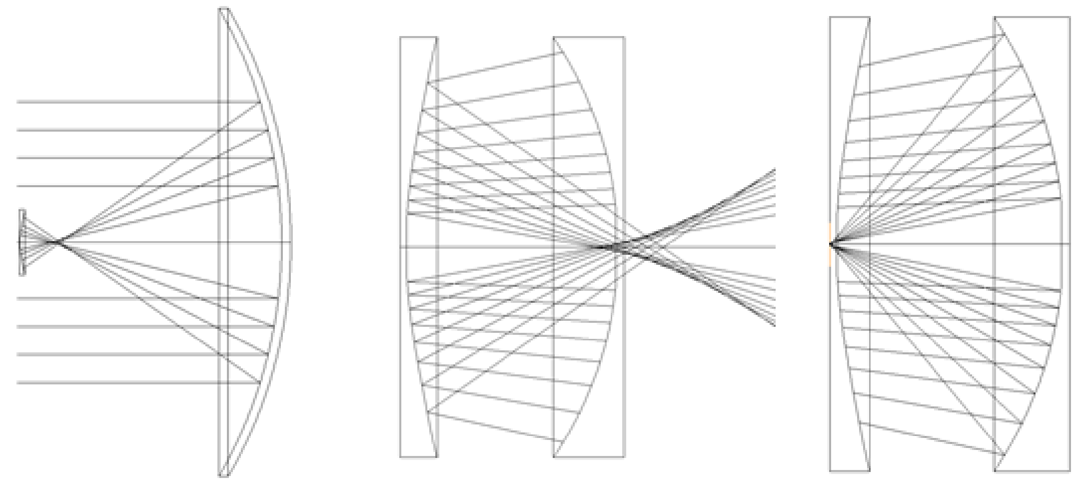

Figure V.A.10: Step by step ray trace. Left – Rays from infinity hit the primary, come to a focus range, the paraxial focus, diverge and hit the secondary. Middle – Incoming rays from the primary are visible on the right, they pass through the through hole, reflect off the secondary, and before coming to a focus hit the tertiary. Right – Rays from the tertiary focus down into the hole of the secondary mirror.

For our 3 meter prototype target wavelength of 2.7 mm, we must account for the Gaussian beam nature of the waves. In order to avoid significant clipping of the Gaussian beam, we require that the clearance, or diameter of the through hole, is 3*w(z), where w(z) describes the beam waist size at a specific distance of z, in this case the center of the through hole. Following the ray path trace within the optical design program Zemax, one needs to also have enough clearance there as well. This severely limits the entrance pupil diameter (EPD) of the incoming

Table V.A.II: General mirror properties			
	Primary	**Secondary**	**Tertiary**
Diameter	1.5 m	120 mm	120 mm
Radius of Curvature	-1500 mm	240 mm	-185 mm
Surface Type	Spherical	Even Asphere	Even Asphere
Through Hole Diameter	N/A	36 mm	26 mm
Distance from Primary	N/A	842 mm	736 mm

rays, since as you introduce more rays, the paraxial focus point continues to increase in diameter, as Figure V.A.11 illustrates for the 20 m sphere.

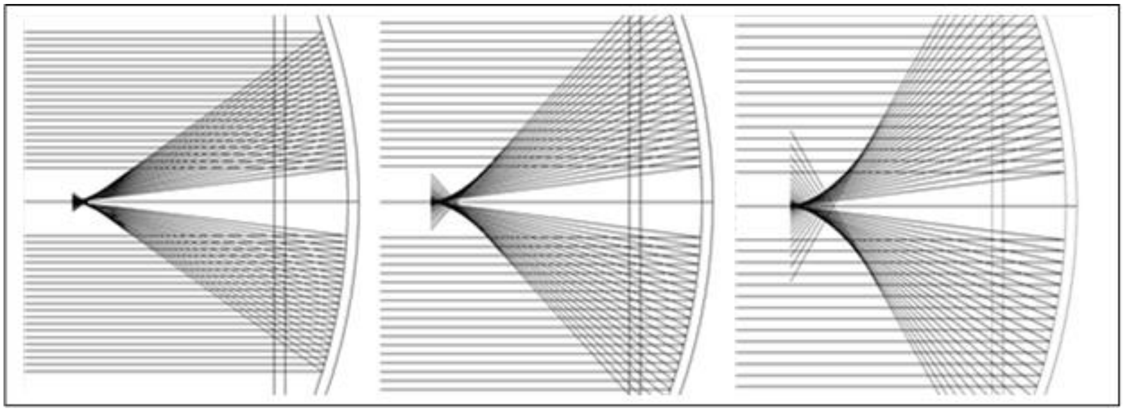

Figure V.A.11: Comparison of paraxial focus size for varying entrance pupil diameters. From left to right, 6.0 m of the primary illuminated, 8.0 m and 10 m.

For the 3 m diameter sphere we target a diameter of 1.5 m of the parent sphere to act as the primary mirror. Ideally, we would like to illuminate the entire 1.5 m. With the known constraints however, we start by underfilling the primary and iteratively design and expand the EPD. The initial starting point in the design set the EPD to 0.75 m. Aspheric mirrors were then put in and optimized iteratively with adjustments being made on position and surface properties. The aspheric surface in Zemax is a departure from the typical spherical surface generally referenced. These aspheric surfaces depart from a standard definition of a spherical surface, in such that they are not representable as spheres, parabolas, hyperbolas, or ellipses. The asphere is defined in terms of the deviation from the radius of curvature from a perfect circle and a series of exponents. In Zemax, the even asphere surface is used, defined by z, the sag of the surface,

$$z = \frac{cr^2}{1+\sqrt{1-(1+k)c^2r^2}} + \alpha_1 r^2 + \alpha_2 r^4 + \alpha_3 r^6 + \alpha_4 r^8 + \alpha_5 r^{10} + \alpha_6 r^{12} + \alpha_7 r^{14} + \alpha_8 r^{16} \quad (19)$$

where c is the curvature term (inverse of R, the radius of curvature), r is the radial distance from the optical axis, k is the conic constant, and alpha r^2, alpha r^4…etc, represent the even order aspheric terms. The two even asphere surfaces created for this model go up to the sixth order even asphere. Through optimization of the corrector surfaces and the distances between surfaces, the EPD was increased in the final design to 0.90 m.

The final optimized design for the LBR 3 m sphere, is summarized in Tables V.A.II & V.A.III. Due to constraints of the EPD, the primary mirror has 0.90 m out of the target 1.50 m illuminated. The size of the secondary and tertiary lead to aperture blockage of 28%. The Gaussian beam size, w(z), at the detector plane is 3.1 mm, which matches close to the desired 3.3 mm required by the feed horn of the system.

Table V.A.III:	
Focal Length	729 mm
F/#	0.81
Entrance Pupil Diameter	900 mm
Max Wavefront Error	0.062 waves
RMS Wavefront Error	0.013 waves
Gaussian Beam Waist (w_0)	3.0 mm

Figure V.A.12 shows the wavefront error of the system, with the maximum wavefront error on-axis at 0.062 waves. The effect of the large secondary obscuration size can be seen as the OPD is missing at the middle of the plot. We were able to correct the spherical wavefront with aspheric surfaces for both the secondary and the tertiary. Both surfaces are even aspheres defined and optimized out to the 6th order.

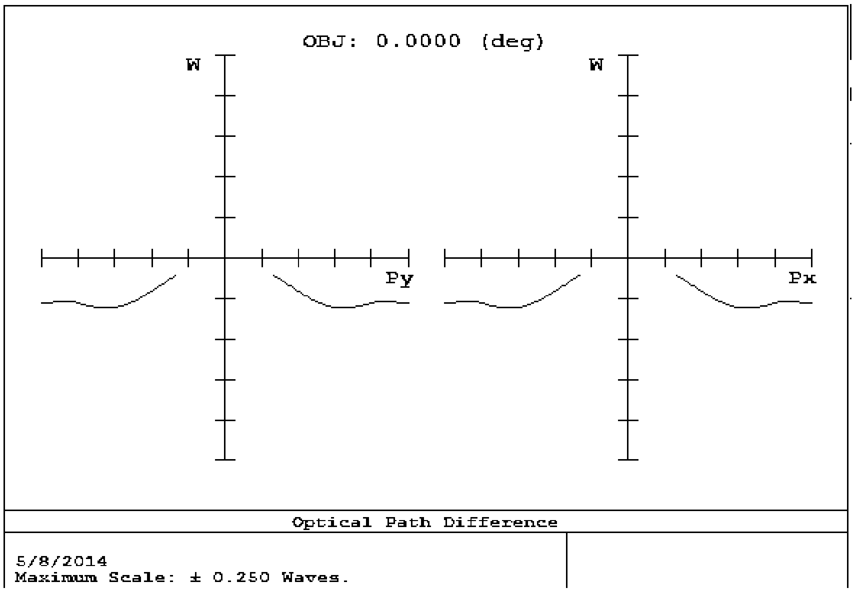

Figure V.A.12: The optical path difference, or wavefront error, measured in waves for the 3 m sphere design.

V.A.3.a.2 Gaussian Beam Analysis

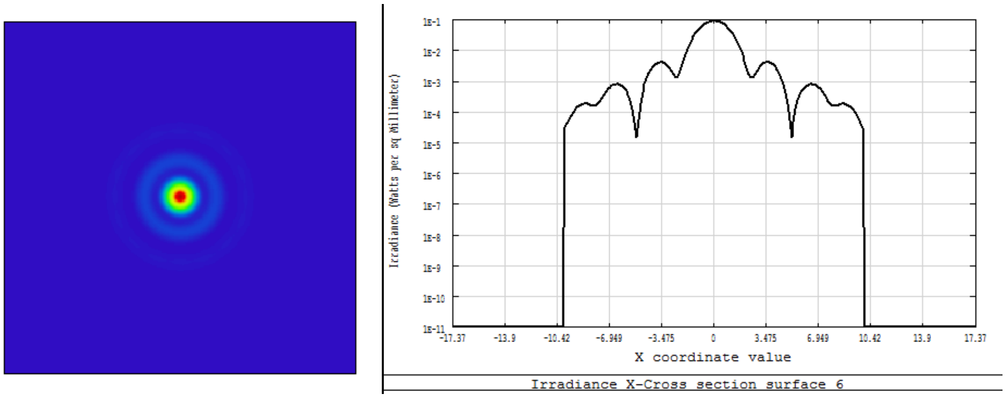

Figure V.A.13: Left - False color profile of the propagated beam pattern at the focal plane of 3 meter LBR. Right – Cross section of the irradiance profile in the far field. Note the x-axis is in terms of the image plane dimension (mm).

In dealing with radio and Terahertz frequencies, the properties of the projected beam pattern in the far field and the phase error are important properties to model. Generally, we want to limit the maximum phase error to $\pm$ λ/16. Zemax offers the Physical Optics Propagation tools for further Gaussian beam analysis, however these are a rough baseline in the case of the LBR design. This comes about as a caveat to the routine and complexity with which Zemax calculates the propagation of waves. It is cautioned that the results for fast beam systems, i.e. under F/# may not be as accurate due to the scalar diffraction theory Zemax employs. For far-field results, this can lead to inaccuracies of diffraction around apertures, which we are extremely interested in. That being said, as order of magnitude model, we can look into the Zemax results for some insight. Further detailed analysis can and will be made within a physical optics dedicated software, such as FRED by Photon Engineering, or ideally one of the standards for radio telescope analysis, GRASP by TICRA, in NIAC Phase II.

Figure V.A.13, shows the Irradiance beam profile and a cross section of the beam profile as well. These reflect an initial Gaussian beam waist radius of 450 mm propagated through the system, which simulates the limit to which we can illuminate the dish (EPD of 900 mm), due to constraints on the through holes.

V.A.3.a.3 3 Meter Tolerancing

The biggest optical challenge for this project is dealing with the surface irregularities and deformations of the primary mirror that result out of having a Mylar balloon for the primary. Zemax's tolerancing tools were used to characterize the system. The tolerance routine allows for one to set values and compensators to determine statistically how a system of errors will affect the performance of the design. By trial and error and further optimization using the results, the system tolerances for manufacturing, alignment, and other errors can be determined. Tolerances can be defined with minimum and maximum values of departure from the nominal. These include such things as the radius of curvature of each surface, distances between surfaces, decentering and tip, tilt of elements, and surface irregularity (Spherical Aberration and Astigmatism). Certain compensators are available to attempt to correct for the errors introduced. The primary compensator used in these types of systems is changing the focal point of the system. Other compensations include changing the radius of curvature, conic section, and surface variables in the case of polynomial or aspheric surfaces.

For the 3 m system, the analysis occurred on two levels. First we use the previously mentioned variables and no compensators. The second iteration looks at mimicking the effects of a corrective deformable secondary along with an adjustable focus, by varying the surface parameters of the aspheric mirror and adding a moveable detector plane. The main variable tracked for system performance on both runs was the RMS wavefront error, as well as the Monte Carlo results for the overall wavefront error plot. The goal was to minimize the RMS wavefront error.

Analysis started with default Zemax tolerances, which are fairly loose, but initially set for visible wavelength systems. This first analysis started with a long observational wavelength of 2700 microns, so our tolerances could be more relaxed. For example, the manufacturing RMS surface roughness tolerance of λ/10 for these mirrors is 61 microns. A summary of the final tolerances that were determined to keep the RMS wavefront error low and all wavefront errors below a quarter of a wavelength can be seen in Table V.A.IV for a Monte Carlo simulation of 1000 runs.

For a system with no focus adjustment or adaptive optics secondary, the nominal RMS wavefront error for the system is 0.0136, while the average of the Monte Carlo runs is 0.0228. Yet, with the introduction of compensators, tolerances can be relaxed and the nominal RMS wavefront error of the system improves to 0.0042 waves. As can be seen in Figure V.A.14, where the left plot represents the no compensator system, the wavefront error was kept just below 0.25 waves. The right plot shows the full run of 1000 Monte Carlo simulations for the system with compensators. The adaptive secondary leads to much better control of the wavefront error with larger tolerances.

Table V.A.IV Tolerancing Results

	No Compensators	**Compensators**
	Tolerance (+/- mm)	*Tolerance (+/- mm)*
M1 – *Radius of Curvature*	1.00	50.00
M2 – *Radius of Curvature*	0.05	0.05
M3 – *Radius of Curvature*	0.05	0.05
M1– *Distance relative to M2*	1.00	10.00
M2 – *Distance relative to M3*	0.50	0.05
M3 – *Distance relative to Focal Plane*	0.50	0.50
M2 – *Decenter X/Y*	0.10	0.10

M2 – *Tilt X/Y*	0.10	0.10
M3 – *Decenter X/Y*	0.10	0.25
M3 – *Tilt X/Y*	0.10	0.25
M1 – *Surface Irregularity (SA & Astig)*	0.50 waves	2.00 waves
Nominal RMS Wavefront	0.0136	0.0042
1000 runs - Best RMS Wavefront	0.0098	0.0035
1000 runs – Worst RMS Wavefront	0.0669	0.0707
1000 runs – Mean RMS Wavefront	0.0223	0.0270
1000 runs – Stnd Dev RMS Wavefront	0.0093	0.0174

Taking a look at Table V.A.IV, we can see that tolerances could actually be somewhat loose when it comes to the positioning of the system. The biggest positive insight was seeing that surface irregularities of 2 waves were tolerable in combination with 50 mm of departure from the radius of curvature of the primary mirror. The surface irregularities correspond to 50% spherical aberrations and 50% astigmatism, not easily correctable by focus shifts. Slow deformations of the primary balloon surface should therefore be tolerable if they are not too extreme.

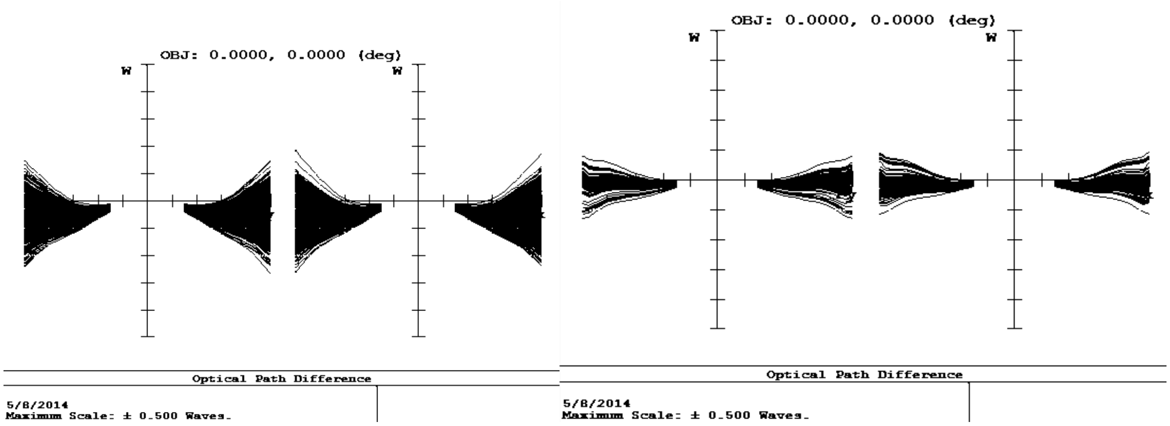

Figure V.A.14: Left – Plot of the optical path difference for 1000 Monte Carlo runs with no compensators. Right – Plot of the optical path difference for 1000 Monte Carlo runs with adaptive secondary and focus compensation.

Additional study into the deformation of the balloon can lead to even better analysis and tolerancing of what we would expect to see in flight. As part of the on-axis design it would be critical that the secondary and tertiary were built as one unit, positioned against each other such that we can get at least 250 microns accuracy between the centering and tip/tilt of the tertiary relative to the secondary. If these parameters are bettered, the amount of primary deformation the LBR could handle could be even greater. It is important to keep in mind that for this 3 m model, the wavelength is a factor of 4.5 times greater than the 20 m version, so the tolerances in certain aspects are more forgiving. An analysis of the tolerancing of the 20 m balloon follows in Section V.A.3.b.6.

V.A.3.a.4 Implementation & Future Work

The real 3 m model, as described in Sec. VII.A, is a custom 3 m plastic sphere that was successfully setup with a feed horn and measurements of a simulated source and the Sun taken. An aluminum machine mill was used to manufacture the corrector system. The mounting and installation of the corrector system has yet to occur. Continuing work on the system this summer should lead to a trial run with the corrector system that was described in this section. As a follow up in parallel, a deformable silicone based secondary mirror was investigated to replace one of the aluminum mirrors, detailed in Sec. V.B.6. This experiment placed 12 actuators behind a molded cast of the asphere design for the secondary, allowing for a deformable mirror to take shape. Measurements need to be conducted on the closeness of this surface to the design surface, which will utilize a CMM machine and or Faro arm. Both these systems could be tested with near field sources, and the appropriate response modeled in GRASP or FRED to serve as a model for comparison.

V.A.3.a.5 20 Meter Diameter Balloon Design

The proposed flight LBR design utilizes a 20 m diameter balloon, half of which is aluminized or designated for use as the primary mirror. As opposed to the 3 m diameter design, the flight LBR will be observing at frequencies of 557 GHz, or a wavelength of 538 microns. At this shorter wavelength, a simple scaling of the 3 m version provides a good foundation, but ultimately lacks the correcting power needed for the larger primary and hence larger spherical aberration. Unmodified, the scaled up version of the 3 m design leads to a wavefront error on the order of 5 waves as opposed to 0.05 waves.

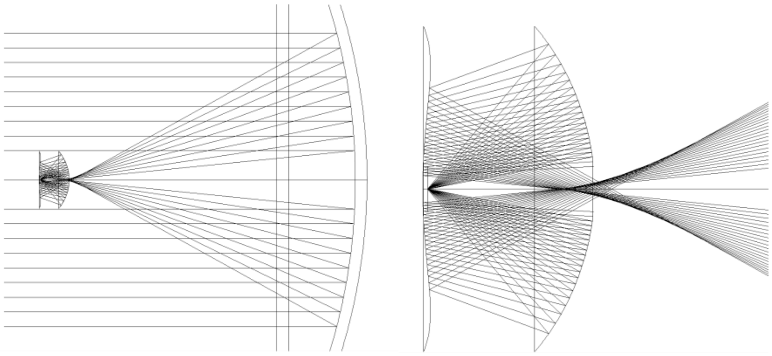

Figure V.A.15: Left – Ray Trace of 20 m system. Right – Close-up of corrector system for 20 m.

The same constraints for design apply for the 20 m diameter versions as did in the 3 m, with regards to beam clipping in the through holes, and the expansion of the paraxial focus as the entrance pupil increases, see Figure V.A.15. With an EPD of 10 m, the positioning of an on-axis tertiary mirror at paraxial focus of 5 m leads to the ray paths covering a diameter of 2.6 m.

Positioning the tertiary in such a location that minimizes the diameter of the optical ray path diameter to 1 m, leads to the tertiary being 4.5 m from the primary. But when needing to satisfy the Gaussian beam waist clipping requirement of 3w(z), a through hole of 0.75 m in diameter is needed at this location. Neither case is desirable so we are left with the task of starting off with an EPD of 5 m or smaller and optimizing the design.

In the end, sacrificing the amount of the primary that is illuminated was necessary to create a well toleranced and low wavefront error system. A ray trace of the under illuminated 20 m diameter LBR can be seen in Figure V.A.15.

While making final optimizations to the 10 m aperture design, it was found that minimizing the wavefront error lead to a sacrifice of the beam waist size at the detector plane. Tables V.A.V & V.A.VI detail system properties. However a simple lens with the appropriate focal length can be designed to expand the beam to the proper waist size for the feed horn.

Table V.A.V

	Primary	**Secondary**	**Tertiary**
Diameter	20.00 m	.972 m	.972 m
Radius of Curvature	-10000 mm	1354.6 mm	-792.8 mm
Surface Type	Spherical	Even Asphere	Even Asphere
Through Hole Diameter	N/A	65 mm	172 mm
Distance from Primary	N/A	5400 mm	4888 mm

Due to the relatively small through hole on the Tertiary, 172 mm, only 5000 mm of the primary could be illuminated. From detailed study of the on-axis design, we conclude that excellent performance can be achieved from these on-axis systems in terms of image quality, i.e., wavefront errors below 0.05 waves, however this is at the sacrifice of being able to use the full primary aperture.

Table V.A.VI

Focal Length	3671 mm
F/#	0.73
Entrance Pupil Diameter	5000 mm
Max Wavefront Error	0.038 waves
RMS Wavefront Error	0.0007 waves
Gaussian Beam Waist (w_0)	0.92 mm

As detailed in section V.A.3.A, a 20 m diameter sphere with ~2.5 m illumination can be an acceptable baseline for our telescope with no corrector. With this on-axis design we can increase that to a diameter of 5 m with a F/# of 0.73. While this is approaching our design goals and utilizing more of the sphere, the need to get close to an EPD of 10 m is paramount. Section V.A.3.c addresses the next steps towards achieving that goal. Figure V.A.16, shows the irradiance beam profile and a cross section of the beam profile for 20 m diameter LBR with an effective aperture diameter of 5 meters.

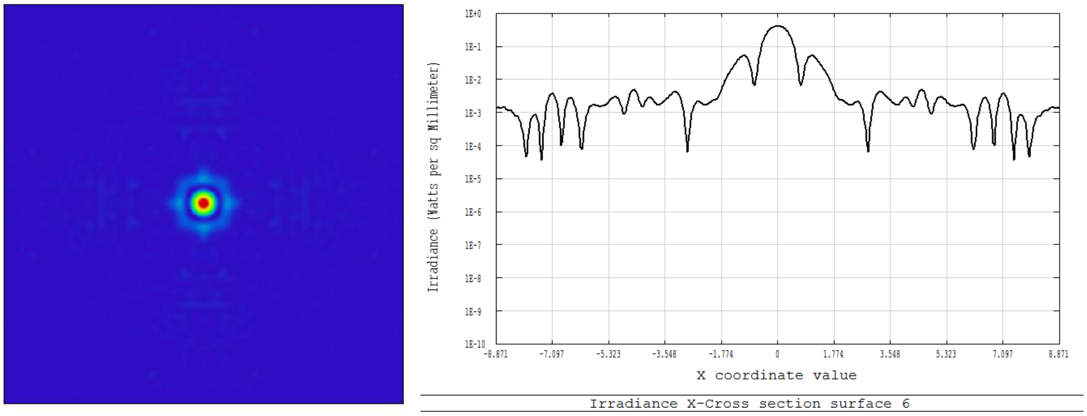

Figure V.A.16: Left - False color profile of the propagated beam pattern at the focal plane of 20 m LBR. Right – Cross section of the irradiance profile in the far field. Note the x-axis is in terms of the image plane dimension (mm).

V.A.3.a.6 20 Meter Tolerancing

With the 20 m on-axis design finalized, a tolerancing run was completed on the system using the same process as described in the 3 m section (see Table V.A.VII and Figure V.A.17). Not surprisingly, with the smaller wavelength system, we saw tighter tolerances were needed for the decenter and tilts of M2 and M3. Provided these requirements could be met, the amount of surface irregularity and radius of curvature variations remain comparable to the 3 m results.

V.A.3.a.7 Conclusion

The main drawback found with the on-axis designs are limitations imposed by the through hole on the tertiary mirror. Due to Gaussian Beam constraints based on locations, the illumination of the primary spherical mirror is limited to about half of its radius with the proposed designs. Nonetheless, the introduction of the spherical corrector system allowed for excellent performance, minimizing rms wavefront error of the system. A study of tolerancing showed that both the 3 m and 20 m systems would benefit greatly from having an adaptable secondary. The on-axis spherical corrector design increases the amount of the primary mirror that can be utilized by *a factor of two*. The corrector system design is scalable with some optimization. A quick study showed that the 20 m corrector system could be scaled up to a 40 m diameter system that would achieve the 10m primary illumination originally targeted. However we realize that the practicality of implementing such a large diameter balloon would pose some challenges, so we propose to look at off-axis designs for the corrector system as addressed in the next section.

Table V.A.VII	
	Compensators
	Tolerance (+/- mm)
M1 – *Radius of Curvature*	30.00
M2 – *Radius of Curvature*	0.05
M3 – *Radius of Curvature*	0.05
M1– *Distance relative to M2*	50.00
M2 – *Distance relative to M3*	0.05
M3 – *Distance relative to Focal Plane*	0.10
M2 – *Decenter X/Y*	0.400
M2 – *Tilt X/Y*	0.050
M3 – *Decenter X/Y*	0.075
M3 – *Tilt X/Y*	0.025
M1 – *Surface Irregularity (SA & Astig)*	2.50 waves
Nominal RMS Wavefront	0.0033
1000 runs - Best RMS Wavefront	0.0040
1000 runs – Worst RMS Wavefront	0.0647
1000 runs – Mean RMS Wavefront	0.0270
1000 runs – Stnd Dev RMS Wavefront	0.0135

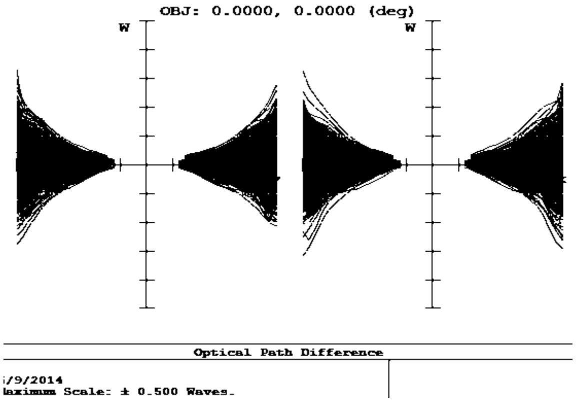

Figure V.A.17: 20 M Tolerancing Run showing the optical path difference of 1000 Monte Carlo simulations with the adaptive secondary and adjustable focus

V.A.3.b Off-axis

> Scaling from the Arecibo design, an off-axis corrector system for LBR should permit the realization of a 10 m telescope aperture to be realized with a ~20 m diameter balloon.

The off-axis corrector used at the Arecibo radio telescope is a dual shaped reflector system, see Fig. V.A.18. The figure show a ray-tracing of the spherical corrector system, on the left, the overall geometry, and on the right a detail of the ray-tracing of the secondary and tertiary shaped reflectors. The final focal point has a subtended illumination half-angle of 60° (f/D=0.43)

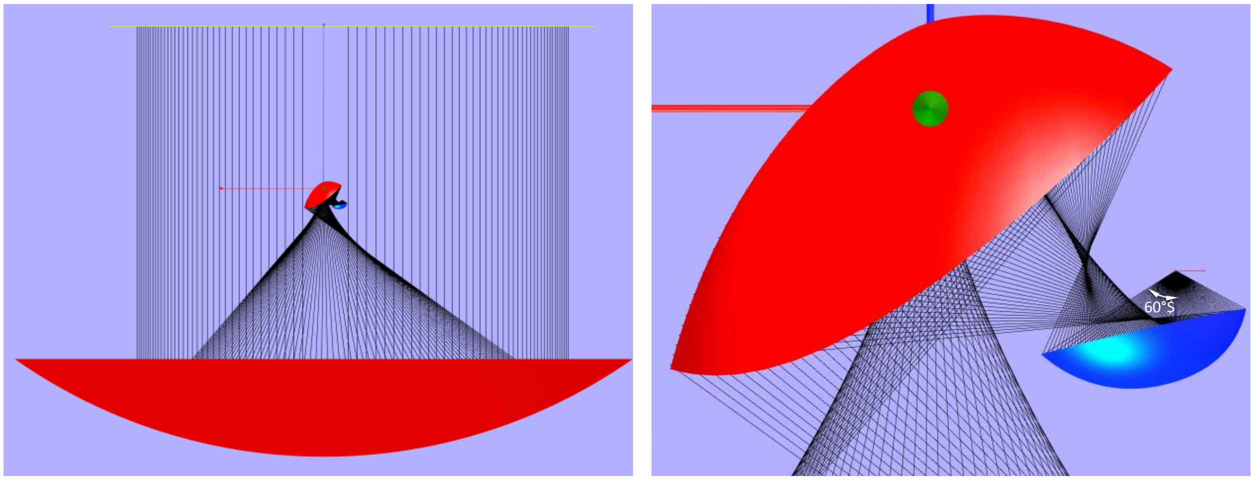

Figure V.A.18: Off-axis spherical corrector used in Arecibo radio telescope. *Left:* Ray-tracing including blockage. *Right:* Detail of the ray-tracing on secondary and tertiary shaped reflectors, and final focal point.

The corrector system corrects for the spherical aberration and provides an elliptically shaped aperture illumination, with nearly uniform distribution. The corrector illuminates only partially the 305m available aperture; this allows to point the telescope, by moving the whole corrector system on an on the elevation track (1° to 19.7°) centered at the center of the main reflector parent sphere, without spillover. Figure V.A.19 shows, on the *left*, the elliptically shaped aperture illumination (size (236m x 206m) of the Arecibo's optics, and on the *right*, the corresponding far field radiation pattern at L-Band. The Arecibo's beam is elliptical, with a size 3.8' x 3.3' at L-band.

Scaling from the Arecibo design, the off-axis corrector system for LBR should permit the realization of a 10 meter telescope aperture to be realized with a balloon diameter of ~20 meters. The detailed design of an optimized off-axis corrector will be a performed in NIAC Phase II.

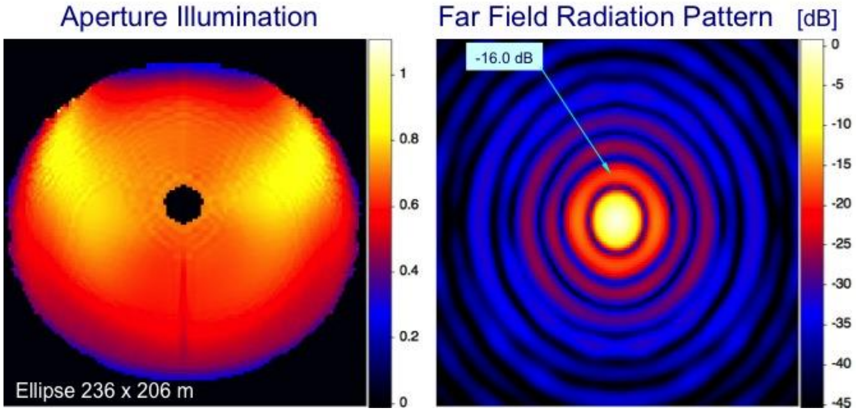

Figure V.A.19: Arecibo radio telescope corrector. *Left:* Aperture illumination. *Right:* Far field radiation pattern at L-Band. Elliptical beam width is 3.8' x 3.3' at L-Band.

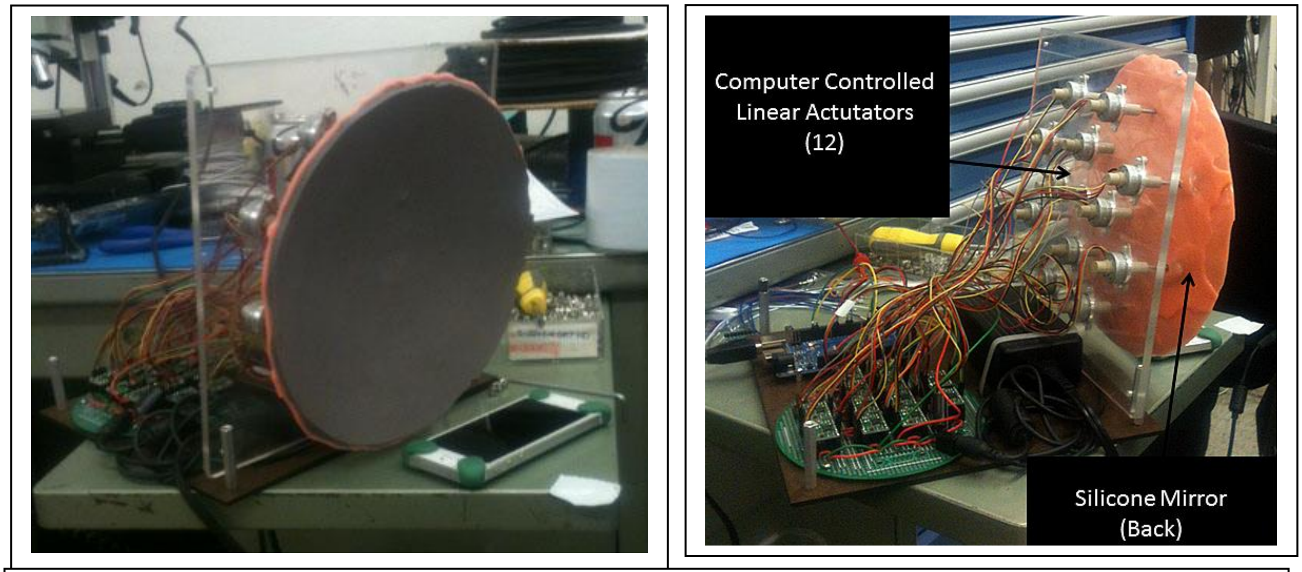

Figure V.A.20. Adaptive corrector prototype. The LBR spherical reflector requires a spherical corrector to bring converging rays to a single focus. The spherical corrector must be adaptive to compensate for nonspherical distortions in the balloon reflector surface. Pictured is an 8 inch scale model prototype of a computer controlled, flexible corrector.

V.A.3.c Adaptive Corrector

An adaptive corrector can be constructed that neutralizes the effects of unwanted, nonspherical distortions in the reflector surface. The corrector can be constructed for use with either the on-axis or off-axis spherical corrector system.

The On and Off axis correctors described in the previous two sections assume incoming rays from an ideal spherical surface. However, even with the proper choice of materials and careful manufacture, nonspherical distortions due to a combination of gravity and differential pressure will inevitably lead to nonspherical distortions. The analyses of these forces over the course of a flight suggest the distortions will occur over large physical and temporal scales (>1 meter and ~0.5 to 12 hours) with peak amplitudes of between 25 and 50 mm. The shape of the LBR sphere will be measured optically (see Section V.B.6) and deviations from an ideal sphere computed every few seconds. The shape of the spherical corrector will then be adjusted to compensate for these deviations.

The diameter of the LBR corrector will be ~1 meter. To provide a conjugate match to the distortions, the mirror surface must be extremely flexible and adjustable under computer control. In order to investigate the feasibility of such a structure, we constructed an 1/6th scale model of an adaptive corrector (see Figure V.A.20) out of silicone with 12 linear actuators. To make the mirror, a high quality negative of the ideal corrector surface was first made out of plaster. While the silicone was still in liquid form, it was loaded with fine grain aluminum powder. The aluminum powder is used to make the final mirror reflective at the frequency of interest. The silicone/aluminum powder mixture is then poured over the plaster mold and allowed to cure. Attachment points for the linear actuators are embedded in the back of the mirror while it is still in the curing process. The mirror is indeed quite flexible, allowing displacements of at least 15 mm (the maximum displacement of the available actuators). A movie showing the actuator in action is can be viewed at http:soral.as.arizona.edu. To provide ~1 meter spatial resolution on the LBR surface, ~80 actuators will be required across the back of the full-size adaptive corrector. The M-227 linear actuator from Physik Instrumente has up to 50 mm travel and more than meets the repeatability and accuracy requirements for the LBR spherical corrector.

V.B Large Balloon Reflector (LBR) Design

V.B.1 Materials

There are several materials that can be used for the fabrication of the LBR sphere. There are four major factors which affect the surface figure of the LBR sphere: 1) differential pressure and therefore skin stress, 2) coefficient of thermal expansion, 3) any localized stiffening due to reinforcements or seams and 4) gravitational effects distorting the spherical shape. Considering these 4 design considerations, it encourages the use of relatively stiff (Young’s modulas) materials with balanced mechanical properties. Potential homogenous materials include such films as Nylon®, Mylar®, LaRC-CP1® Polyimide. These base materials can also be tailored to adjust for these effects by the use of scrims or weaves mechanically bonded to a base film to tailor the mechanical stiffness orientation. This is exemplified by the NASA DP6611-0.25-0.25 which is a woven 30 Denier, high tenacity polyester fiber adhesively bonded to a layer of 0.25 mil polyester film bonded to a 0.25 mil balloon grade linear low density polyethylene (LLDPE) . This composite has been use for super-pressure balloons and stratospheric airships (Smith and Lee, 2007). The LBR requires a conductive surface therefore metallization of one hemisphere is required. The metallization of Mylar® and other materials has been successfully accomplished for decades as demonstrated by the ECHO satellites as well as other long duration scientific super-pressure balloons such as the GHOST and CARRIER balloon flights conducted by NCAR in the 1960s and 1970s.

The carrier balloon heat balance is typified in (Figure V.B.1) (Smith 2000) below. Fortunately the Antarctica flight environment is a fairly benign balloon environment (Figure V.B.2) (Farley 2010). During the launch and flight windows for scientific balloon flights from McMurdo Station, the balloon is exposed to constant daylight, although at a low elevation angle. The surface albedo also increases the heat load and can vary between ~0.5-~0.8. The LBR will end up being a subset of what the carrier balloon is seeing, but attenuated. A more detailed analysis will be performed with Thermal DeskTop® in Phase II to better predict the total, transient and localized heat loads on the LBR.

In the case of Tables V.B.I & II above, the numbers are based on the Room Temperature properties of Mylar®. This should be the worst case condition since the lowest strength and modulas occur at the warmer temperatures and should provide a conservative estimate for the deformations of the LBR. In reality the film temperature should be lower and as such, have higher stiffness, therefore lower deformations and thermal contractions. The LBR axial focus travel is adequate to correct for the changing LBR radius while the adaptive optics should adequately correct for any localized distortion of the surface.

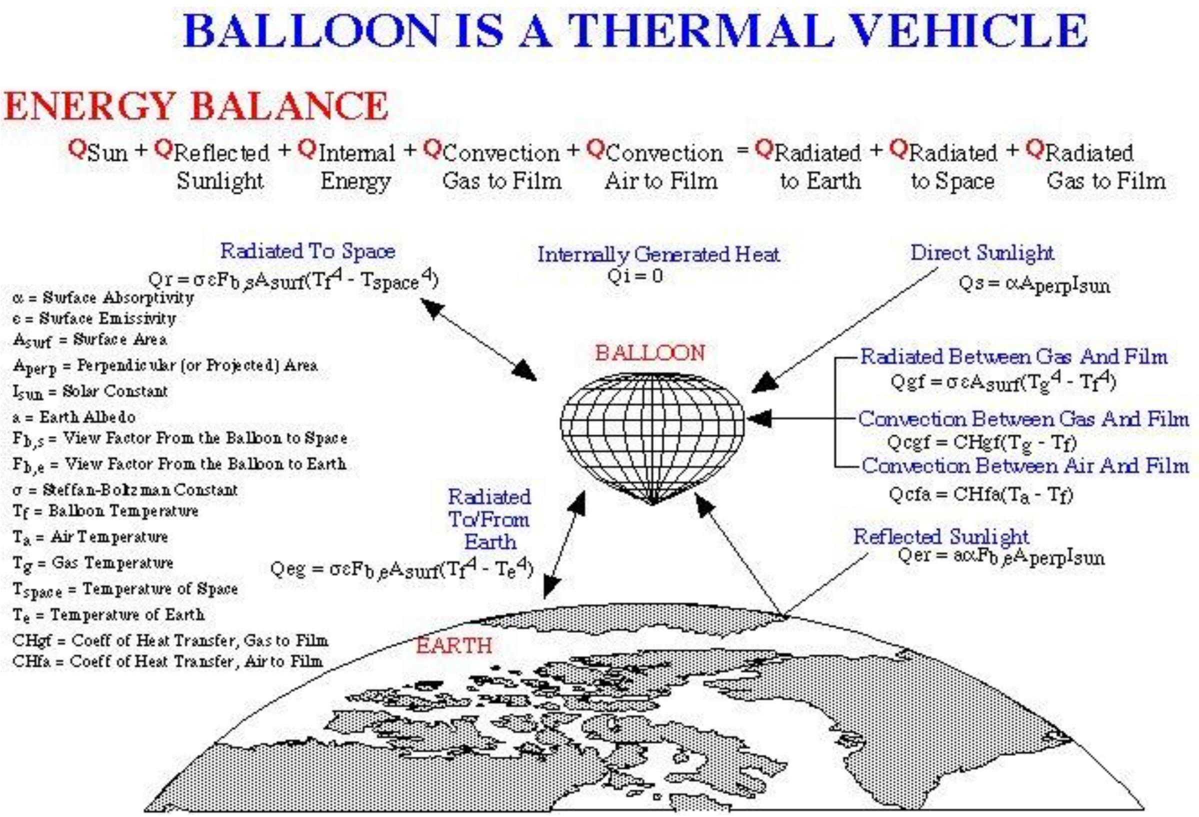

Figure V.B.1. Radiative thermal heat balance of a balloon.

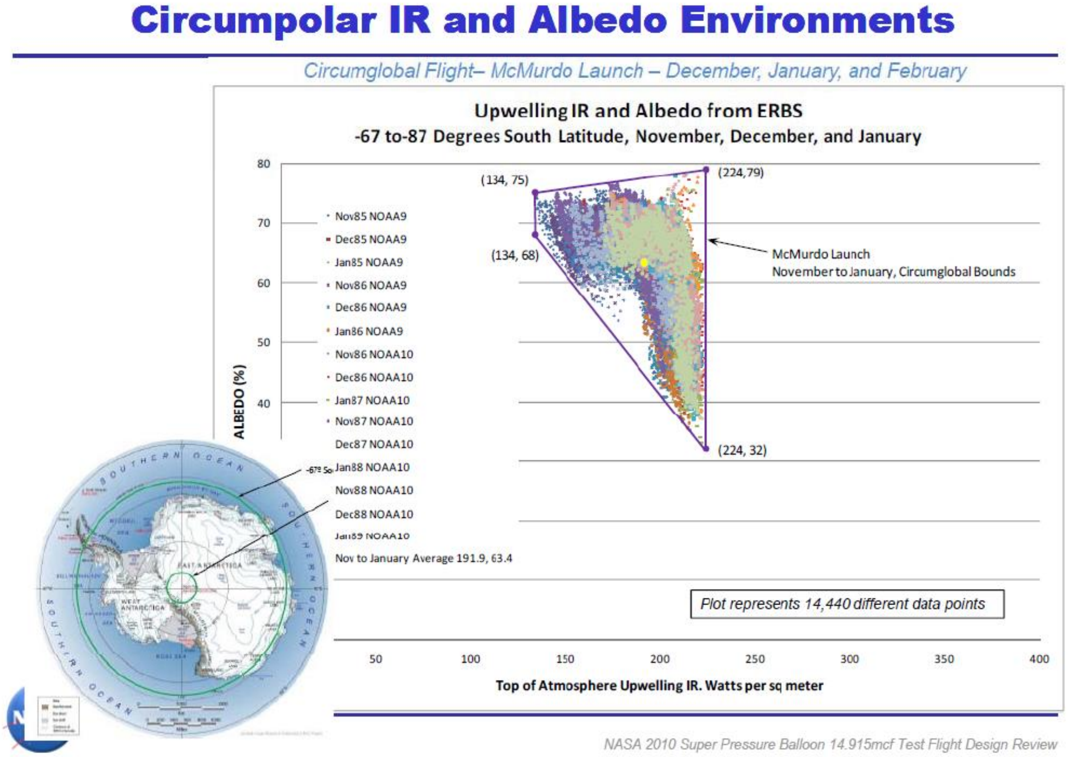
Circumpolar IR and Albedo Environments

Circumglobal Flight– McMurdo Launch – December, January, and February

NASA 2010 Super Pressure Balloon 14.915mcf Test Flight Design Review

Figure V.B.2: Antarctic flight environment: albedo and upwelling IR flux.

It is desired to minimize the expansion and contraction due to increases and decreases of internal differential pressure (Table V.B.I) and thermal contraction and their influence on surface figure and LBR radii (Table V.B.II).

Table V.B.I: Change in LBR radius as a function of deviation in stress level

Change in Stress: psi	**10000**	**8000**	**6000**	**4000**	**2000**
E (Modulas-RT): psi	700000	700000	700000	700000	700000
Change in Radius (cm)	**14.3**	**11.4**	**8.6**	**5.7**	**2.9**

Table V.B.II: Contraction in radius due to cooling

Change in Temp.	Change in Radius (cm)
-10.0	-0.18
-20.0	-0.36
-30.0	-0.55
-40.0	-0.73
-50.0	-0.91
-60.0	-1.09
-70.0	-1.27
-80.0	-1.45
-90.0	-1.64

The distortion due gravitational effects and rotation in the elevation control of the LBR are minimized by the use of the 3 planes of the internal curtains. The internal curtains (center of FO2) provide additional radial stiffening in the 3 axes in addition to the mountings for the receiver hardware. However, it will provide some localized stiffening due to their attachment to the skin. The adaptive optics should be more than adequate to correct for these with real time mapping of the surface serving as the feedback to the system's axial and adaptive optics. A more detailed thermal and finite element analysis will be performed in Phase II to quantify distortions due to the four (4) major factors that will influence the spherical LBR surface figure.

Stratospheric Long Duration Balloon with LBR Instrument FO1

Reflector Assembly

Internally Mounted Deployed during Ascent

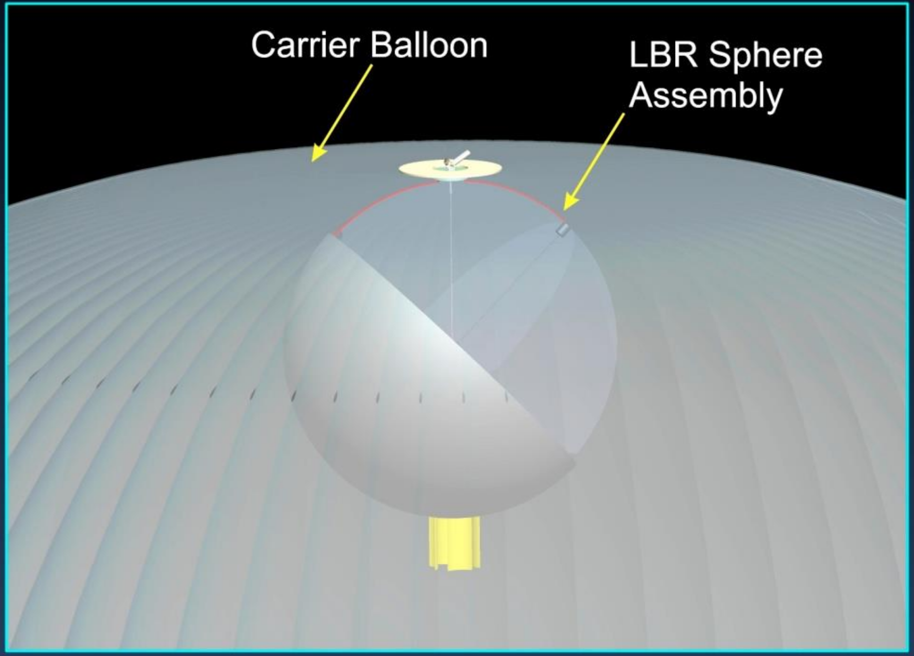

LDB Balloon with LBR

Volume: 29.7 mft3
Height: 335 ft. (103m)
Diameter: 424 ft. (129m)
Lifting Gas: Helium
Dual Caps

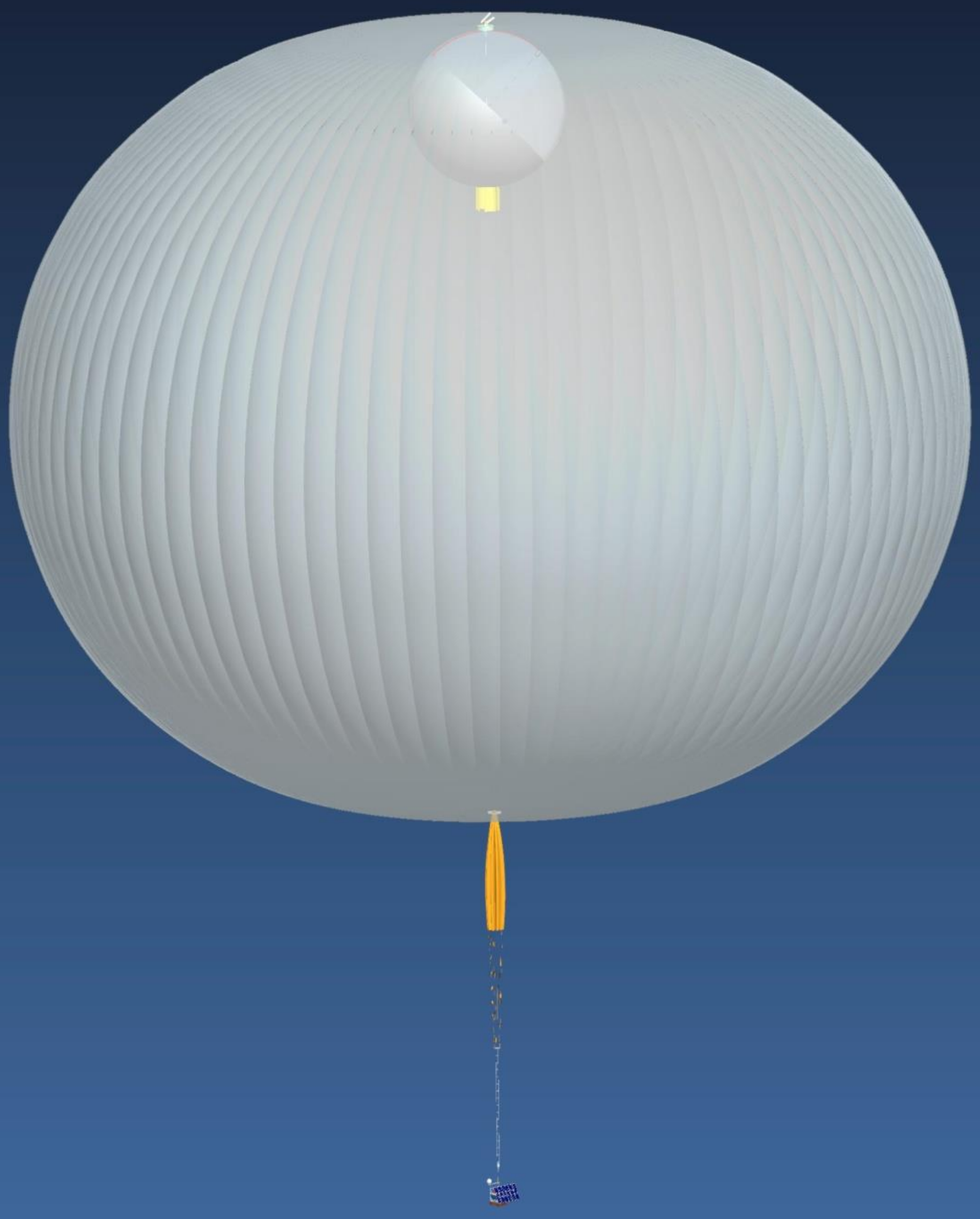

LDB Balloon with LBR

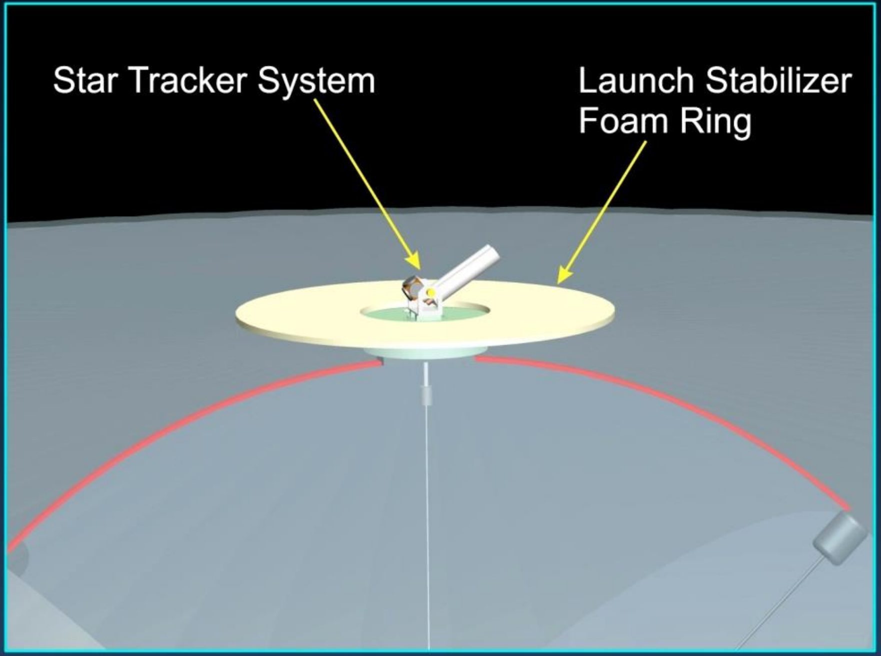

Parachute & Payload

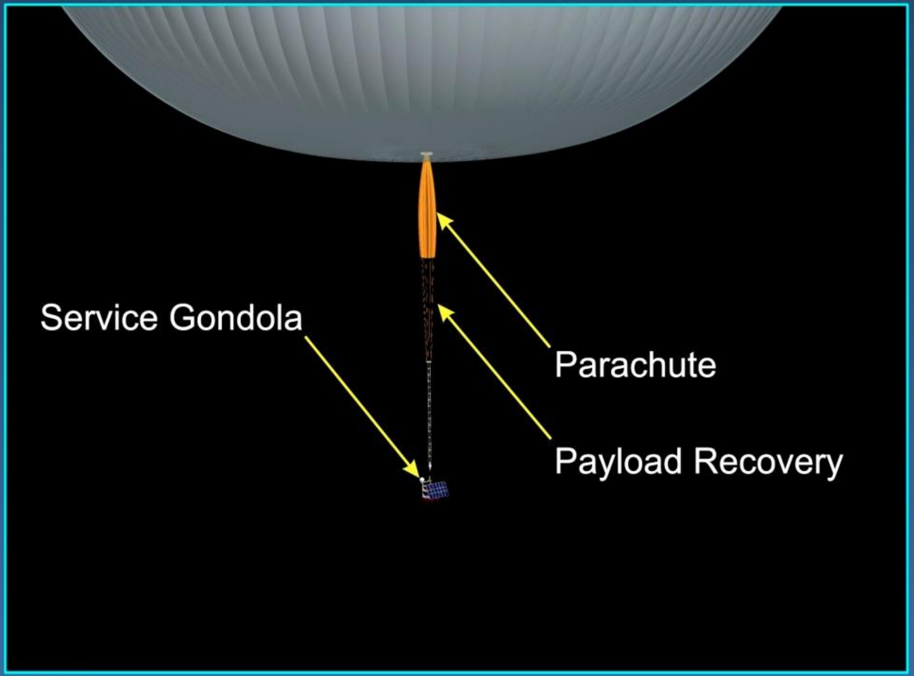

Service Gondola

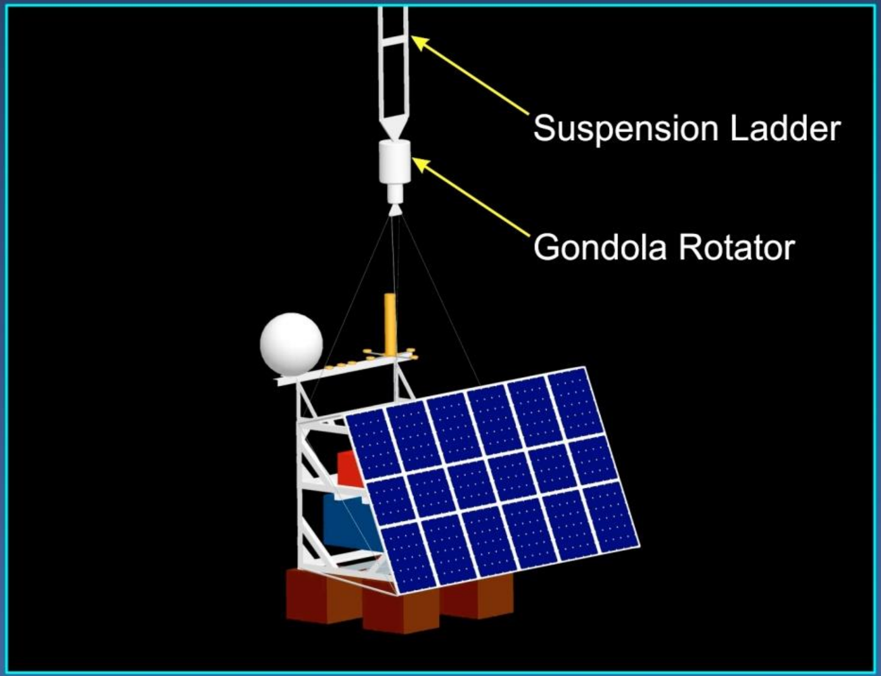

TA008788_Perry

THz Sub-Orbital Large Balloon Reflector (LBR)

FO2

Top Plate Assembly

Mounts to the Carrier Balloon Top Ring

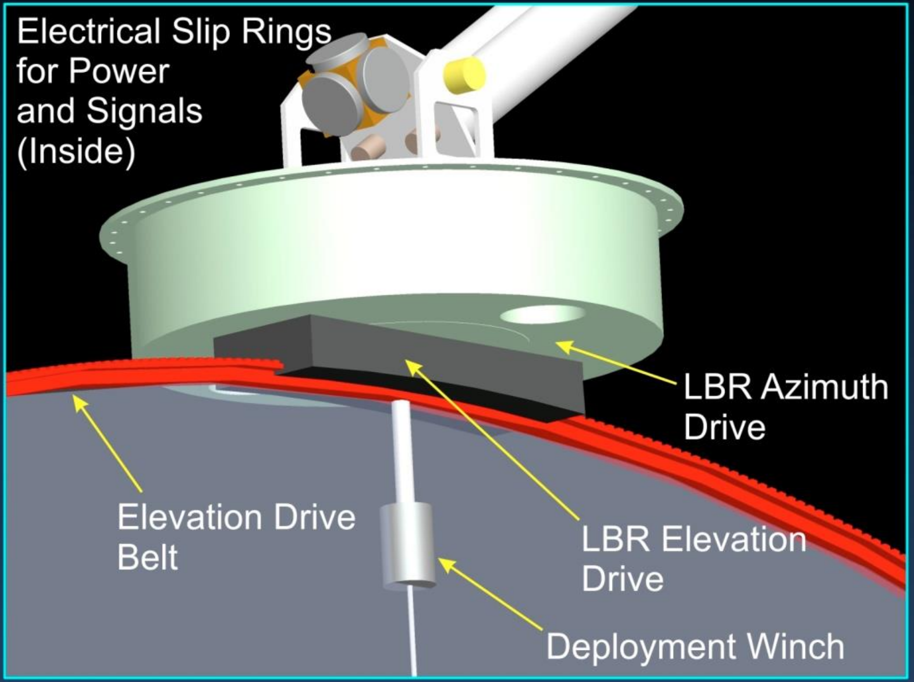

Corrector and Receiver Assembly

Adaptive Optics Axial Focus Control

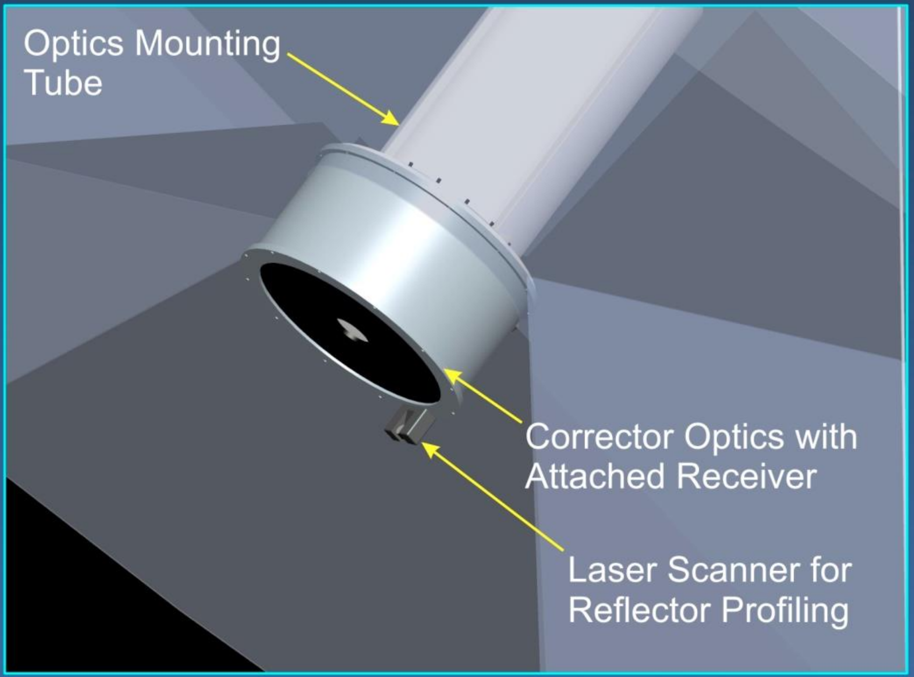

Spherical Reflector Assembly

20 Meter Diameter
Pressurized to 1 mbar with Helium
Azimuth Range : Unlimited
Elevation Range: -10° to 70°

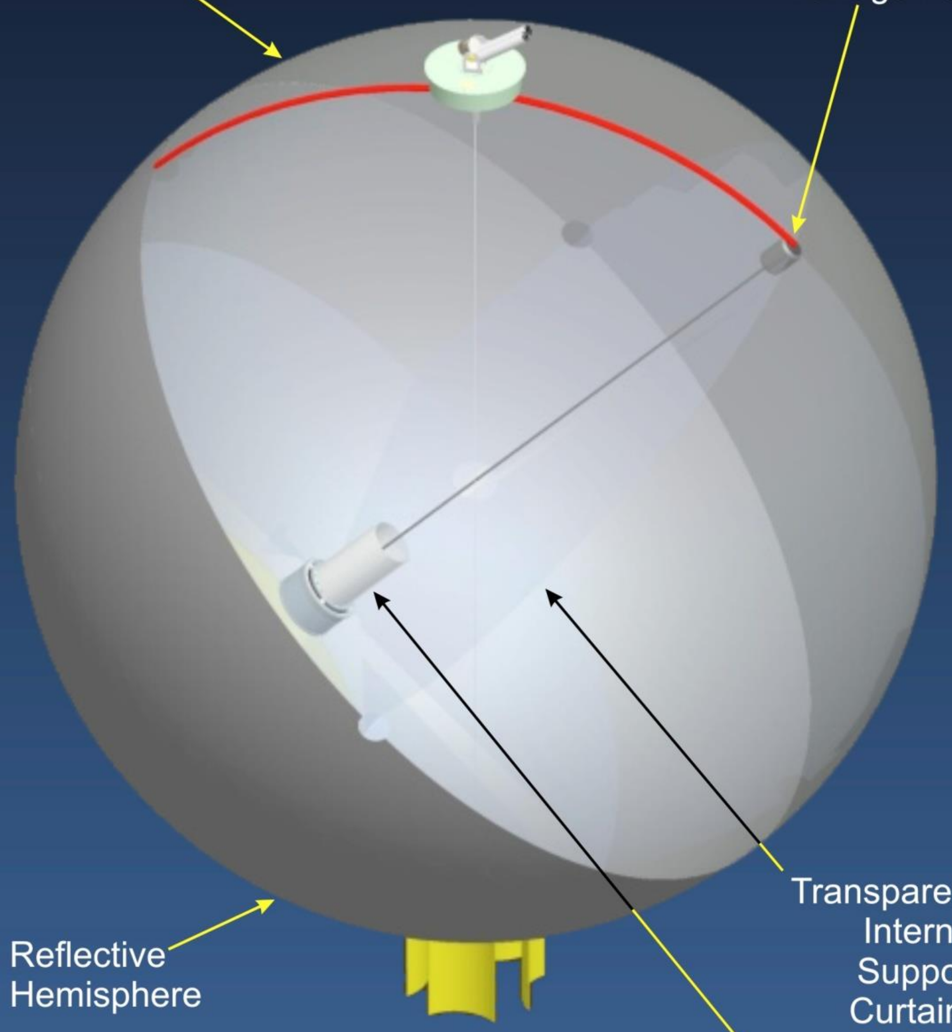

Top Plate Assembly

Diameter: 2m Depth: 0.75m

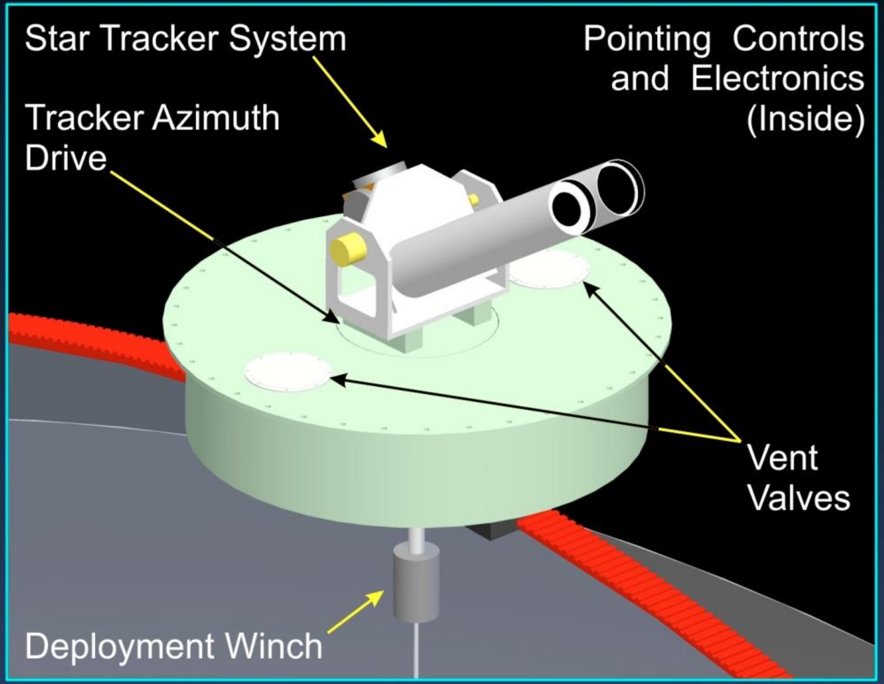

Pressure Management

Constant Differential Pressure
Redundant Blowers and Relieve Valves

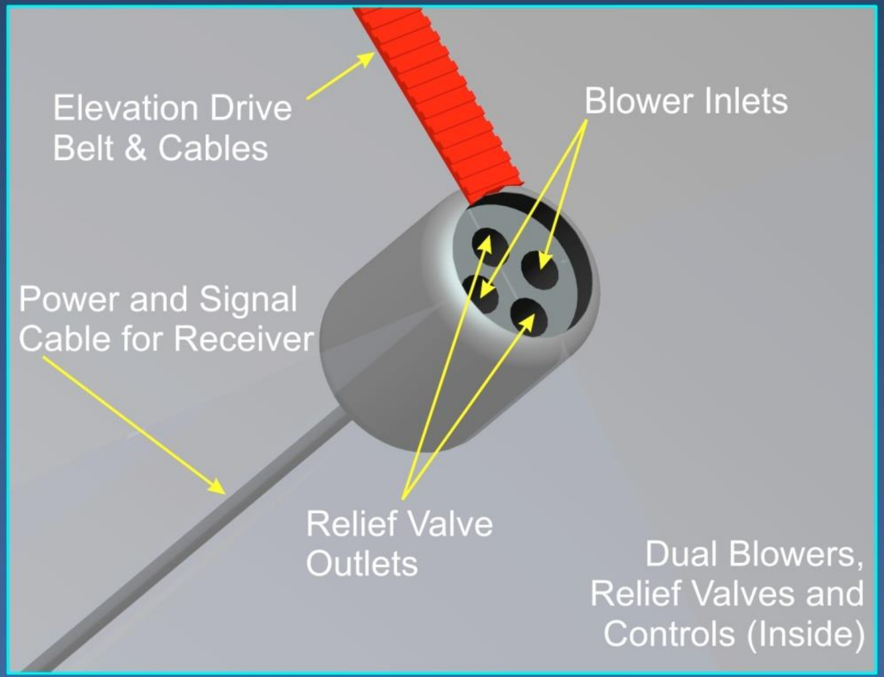

TA008787_Perry

V.B.2 Fabrication methods

Several approaches to the fabrication of a 35m inflatable antenna were investigated as part of the NEXRAD in Space (NIS) antenna concept. This also included many fabrication methods with a wide variety of materials have been investigated over the years (Thomas and Veal 1984; Chodimella, Surya, et al 1984). The ideal material would consist of a balanced film, where the mechanical properties are the same in all directions. Additionally, it would be preferable to have the antenna fabricated of a single 3 dimensional shaped membrane. If that were not possible, then 3 dimensional segments joined by edge fused interface of adjoining segments. The material would also have a coefficient of thermal expansion (CTE) equal to 0, such that it is stable under all temperatures. Unfortunately, the real world does not cooperate that easily.

Fabrication methods of inflated structures using the mechanically "stiffer" materials such as Mylar®, Kapton® or composites (e.g. the NASA developed DP6611, etc.) have long been established. Scientific balloons and other inflatables have been fabricated from these materials for decades. A lap tape seam can be used, but often results in a seam failure due to the bending moments induced by the asymmetrical circumferential loading of the seam thereby causing the seam to peel. Normally a heat and pressure activated adhesive bi-tape seam has been proven to effectively seam a butt joint where the seam has to fail in shear. This has been successfully demonstrated on both free-flight scientific super-pressure balloons, as well as stratospheric airships. For this application, we would employ the bi-tape seam.

V.B.2.a Gore method (Balloons)

Three different approaches to seaming of the LBR have been preliminarily investigated. The first approach was the typical "gore" technique (Figure V.B.3) (i.e. banana peel) employed in the fabrication of large scientific balloons. The "gore" technique makes use of flat sheets of film cut into a pattern and then sealed together to create a 3 dimensional (3D) structure. For a small number of gores under low pressure the volume looks faceted. This then requires higher pressures to stretch or deform the material into the more spherical shape. If too few, it will exceed the structural limits of the material and fail, often catastrophically. This can be remedied by increasing the number of gores but this further creates an undesirable stiffening of the structure at the apex and nadir of the sphere due to converging seam tapes. The structure thus has a variable structural stiffness along its length which has to be accounted for in the structural analysis such that the final shape will be the desired spherical shape. Whereas this is usually fine for large scientific balloons using large deformation polyethylene, it presents more difficulty for the stiffer materials and smaller volumes associated with the LBR. Another approach that can be used is seaming together of latitudinal bands of flat material. More structural analysis and testing are required to define the influence on the LBR surface figure.

Figure V.B.3. Typical “gore” pattern sections used in most scientific balloons

Spherical: ECHO **Oblate: ULDB Pumpkin**

Figure V.B.4. Examples of inflatables using “gore” technique

V.B.2.b Polyhedron (Soccer Ball)

Another construction method is similar to that employed in soccer balls (and geodesic domes), where hexagonal and pentagonal sections are seamed together into a Goldberg polyhedron (Figure V.B.5). This approach could provide more uniform loading over the “gore” approach but may be more costly to fabricate   The polyhedron can be constructed from an icosahedron with the 12 vertices truncated such that one third of each edge is cut off at each of both ends. This creates 12 new pentagon faces, and leaves the original 20 triangle faces as regular hexagons. Thus the length of the edges is one third of that of the original edges. A similar technique can be applied to construct polyhedra with tetrahedral symmetry and octahedral symmetry. These polyhedra will have triangles or squares rather than pentagons.

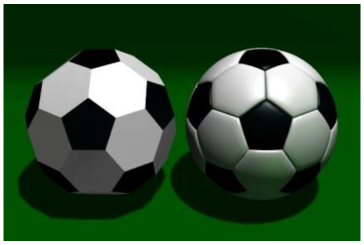

Figure V.B.5. Example of a Goldberg polyhedron

A sphere fabricated this way would offer a more uniform structural stiffness distribution. However, the fabrication of such a sphere may be more difficult from a production standpoint due to the size of the inflatable and possibly be more costly. More structural analysis and fabrication investigation is required and will have to be conducted under Phase II.

V.B.2.c 3 Dimensional Fabrication (Sails)

The ideal way of designing and fabricating the LBR would be to cast it in the correct spherical shape. Several methods were investigated, such as blown extrusion, casting, etc. None of the approaches investigated appeared very feasible for our application based on complexity, required environmental controls and equipment availability. As such, we investigated other ways of obtaining a 3D shape rather than trying to deform flat panels into a 3D shape. A leader in this field of sail making is North Sails North America located in Minden, Nevada with their 3DL® sail making process (North Sail 2014).

Most modern sails achieve their three-dimensional shape through the contour of numerous panels of sailcloth sewn together in a process called broadseaming. 3DL® takes this process to the next step. Instead of relying on flat cloth with curved edges, the 3DL® process molds the entire sail over a three-dimensional mold (Figure V.B.6). Programmable molds are draped with Mylar film and then a computer-controlled system applies precisely tensioned yarn over the Mylar. 3DL may offer up to 20% savings and deform less. 3DL more efficiently utilizes each individual yarn because it is laid smooth and continuous - with no breaks or bending at seams - in the same shape that it is expected to take when sailing. The molds can be adjusted to shape sails of widely varying cambers. Sewing or seaming is limited to the corners, edges or attachment points of the sails.

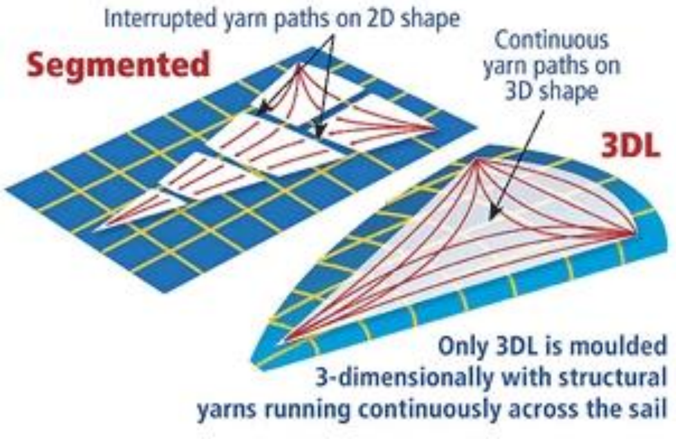

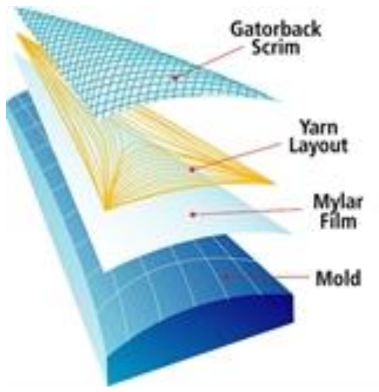

Figure V.B.6. Northsail 3DL® Process. The 3DL® process molds the entire sail over a three-dimensional mold.

This same process can be applied to the LBR fabrication. It uses many of the same materials that have been used in ballooning for decades. In discussions with the North Sail, their table molds are not large enough to cast one single LBR. However, we should be able to make large sections of the LBR and later seam the larger sections together. The process will have to be modified to minimize areal densities.

V.B.3 Internal structural supports

The LBR sphere is an inflated structure as shown in FO1. The structure is made of two hemispherical hull sections, one that is transparent and one that is metalized to be reflective to the THz signal. Three internal orthogonal curtains will provide shape stability and serve as mount for the adaptive corrector and science receiver. This whole structure will be folded and packaged in a container for installation in the carrier balloon. The packed LBR remains in this protective container during launch. During ascent the container will be slowly lowered using an internal winch. Once the flaccid LBR is completely extended from the container, the blowers will pump helium from the carrier balloon in to the LBR sphere. The two blower assemblies will maintain the selected differential pressure to provide the optimum shape and stability. The LBR hull and internal curtains will be made of very thin film and scrim that have been selected to be almost completely transparent to the target signal.

V.B.4 Instrument Unit integration

The LBR Instrument Unit (IU) includes 1) the adaptive spherical corrector, 2) the surface measurement system, and 3) the THz receiver system. This IU will be mounted inside the sphere at the intersection of three orthogonal support curtains. Rigidly fixed at the focus point of the spherical reflection surface, the IU mount will include a gross focus motion that can move the whole assembly axially, while an array of actuator will warp the secondary reflector to fine tune the focus while correcting for any distortion in the reflector surface. The complete deflated LBR sphere assembly will fold in to a soft container (shaped bag) about 1.9m diameter x 3m long. The packed LBR will be suspended from the "Top Plate assembly" attached by an internal winch and cable. The Instrument Assembly of the Top Plate and packed LBR (FO1) will be installed in the field after the carrier balloon layout prior to inflation. The balloon top ring will be supported about 4m off the ground by a stand. A crane will lower the Instrument Assembly into the balloon via the opening at the top. Once in place the unit will be secured with screws, connectors carrying electrical power and signals will be connected. After the unit is mated with the balloon communications with and the status of the LBR will be verified during preflight checks.

V.B.5 Steering mechanisms

The LBR instrument is pointed by rotating the whole spherical reflector in elevation and azimuth. The azimuth rotation range will be unlimited. The elevation range will be -10° to 70°. Wireless communications will be used for the processed signals and instrument control. A slip ring assembly will be used to provide electrical power to the LBR. The azimuth rotator will be powered by a direct drive servo motor with a high resolution encoder, while the elevation change will be accomplished by driving a toothed belt that is secured to the circumference of the LBR sphere.

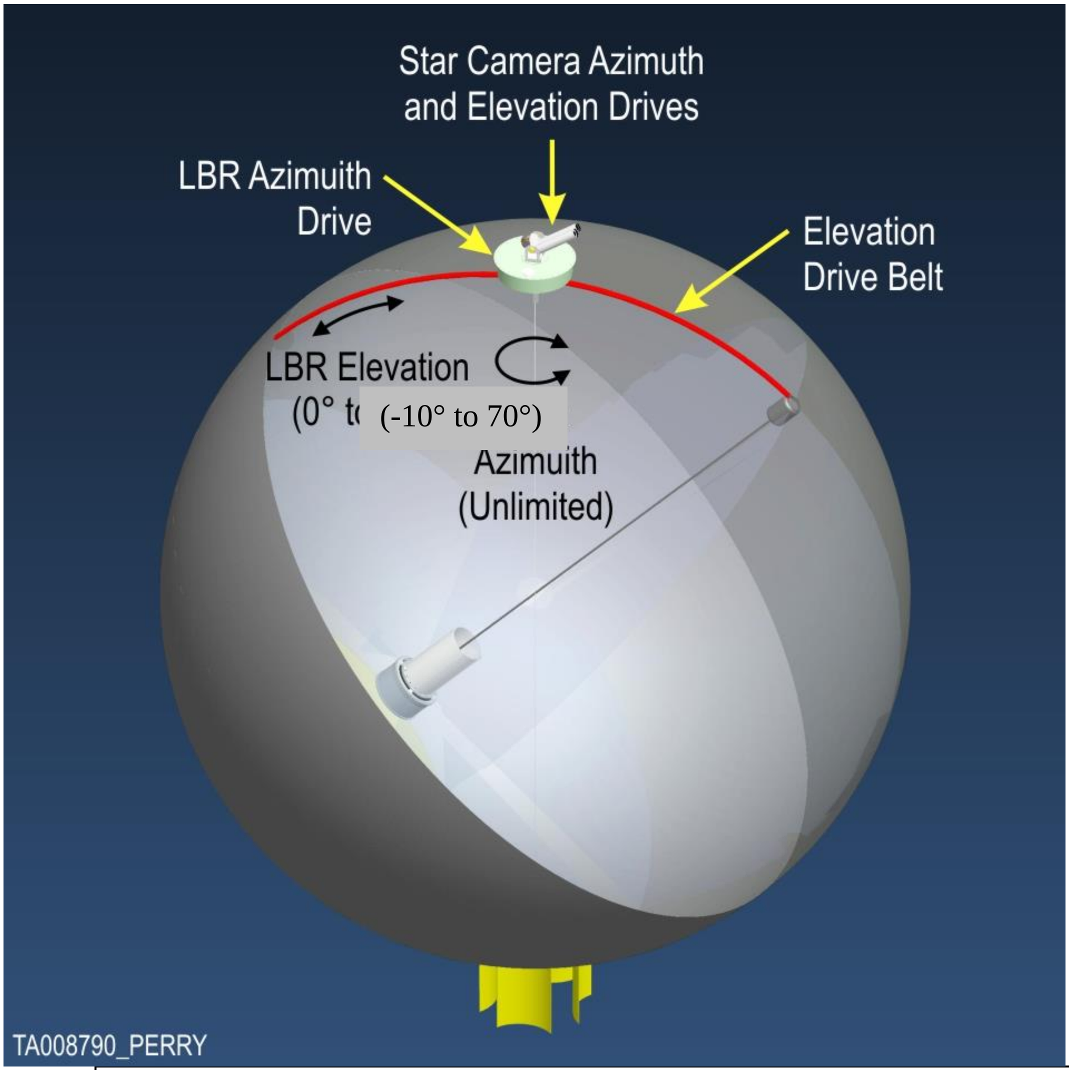

Figure V.B.7: Cutaway view of LBR interior. Coarse steering is achieved by rotating the LBR balloon in azimuth and elevation. Fine pointing is achieved by controlling the tip and tilt of the spherical corrector.

This belt will be driven by a servomotor powered anti-backlash gear arrangement. A linear high resolution encoder will provide accurate elevation positioning. These drive systems will be housed in the bottom of the carrier balloon’s top plate assembly along with the azimuth drive for the star camera telescope that will be mount on the top of the top plate assembly. Figure V.B.7 shows the proposed arrangement. The star camera will lock on to a reference star and provide offsets to the elevation and azimuth drives to keep the LBR reflector pointed to within +/- 0.5° of the target position. Fine pointing will be performed using the tip-tilt controls of the adaptive corrector. A similar approach has been used by our team members on the BRISSON gondola, where pointing accuracies of <5" were achieved. This measured performance more meets our pointing goal of ~5", corresponding to ~1/3th our diffraction limited beam at our target observational frequency of 557 GHz.

V.B.6 Surface figure measurement system

A key to the successful operation of LBR will be the ability to measure its surface figure during flight and compensate for nonspherical distortions that may occur. The surface figure of the inflated reflector will be determined by an optical instrument mounted to the front surface of the corrector housing. The instrument will measure the surface figure by determining the location of several million positions on the reflector surface in 3 dimensional space. Each measured position will serve as a control point in a non-uniform rational basis spline (NURBS) model fit to the reflector surface (see Figure V.B.8). Such fits are in common used in computer graphics and CAD programs. The NURBS model of the reflector surface will then be used to determine the deviation from an ideal spherical surface. This information will be used to calculate the amount of adjustment for the gross focus actuator, along with the adjustments needed for the array of adaptive optics actuators on the secondary reflector. The performance of the system will be periodically checked by measuring the main beam efficiency of the reflector/telescope on compact astronomical sources, e.g. the Sun, Moon, and planets.

Several different types of ranging devices have been under consideration; these include a time of flight (TOF) infrared laser ranger, an infrared parallax range finder, and an optical parallax range finder.

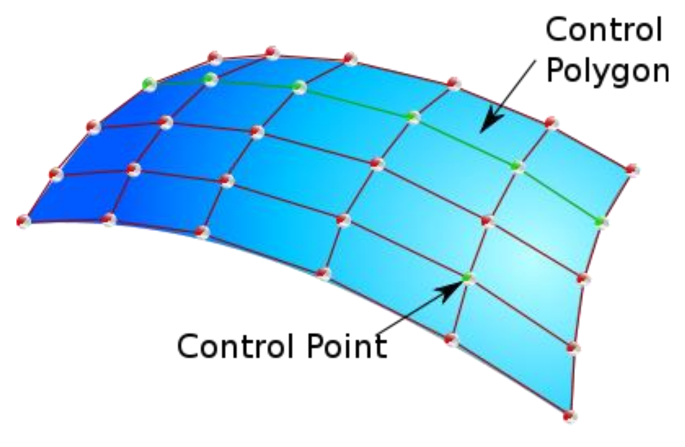

Figure V.B.8. NURBS surface model fit. Each point measured on the reflector surface serves as a control point for a spline surface fit.

As part of our Phase I study we gained access to the FARO Focus 3D laser ranger (TOF) system. Figure V.B.9a shows the laser ranger is being operated from inside our 3 meter LBR prototype. The ranger uses a single 905 nm laser to scan across the balloon surface using two rotating mirrors. A full image of the balloon (see Figure V.B.9b) can be made to ~ 1 mm accuracy in just a few seconds. The sphere surface is formed from 0.8 mm thick thermoplastic polyurethane (TPU) gores. The TPU material was found to be largely transparent at the laser frequency, yielding only a small percentage of returns. However, when covered with aluminized

Mylar (the reflecting surface material for the flight version of LBR) strong reflections and accurate surface determinations could be made. Figure V.B.10 shows the surface fit to returns from a section of the sphere where a sheet of aluminized Mylar was attached. Gaps in the coverage are due to small scale wrinkles in the sheet. The system has a ranging distance of ~25 meters, making it a good match to the 20 meter diameter LBR.

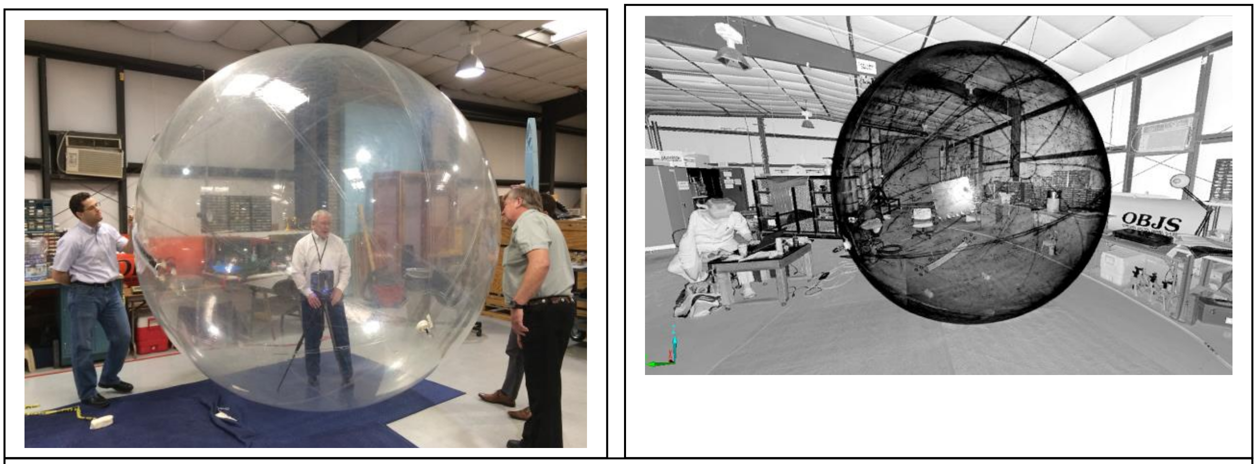

Figure V.B.9. Left: FARO TOF ranger (and operator!) within 3 meter prototype LBR plastic sphere. Right: TOF ranger image of full sphere in lab.

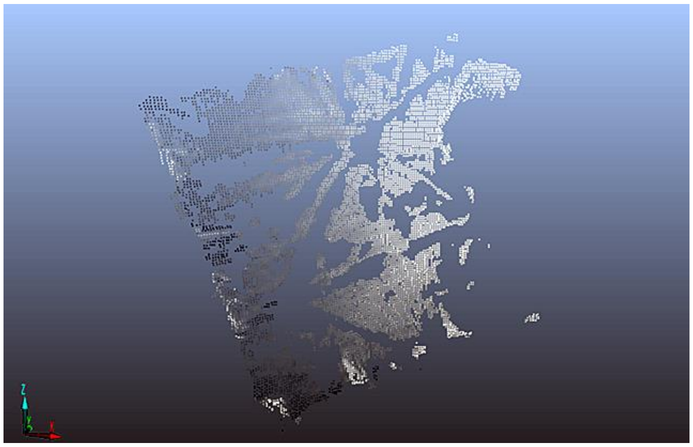

Figure V.B.10. FARO TOF ranger image of aluminized Mylar covered section of 3 meter sphere.

The two other surface measurement approaches studied in Phase I use a parallax based approach to determine distances to targets on the sphere's surface. The first of these employed a `Kinect' system from a Microsoft X-Box gaming console to project 1000's of infrared laser dots onto the balloon surface. The Kinect system uses two IR cameras located several inches apart to determine the parallactic angle and distance to each spot. This system was also able to measure distances to an accuracy of ~ 1 mm with no moving parts. The gaming system used here has a range limit of ~3.5 m. Non-gaming versions with larger range limits are available. Images from within the balloon made using the Kinect system are shown in Figure V.B.11.

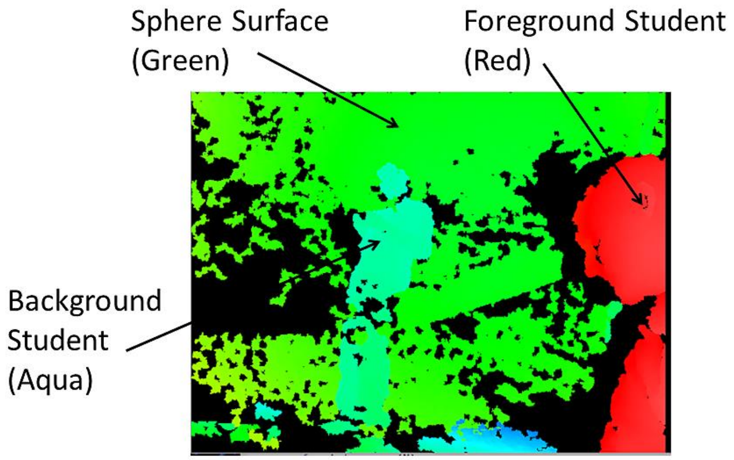

Figure V.B.11. "Kinect" parallax ranger image taken from within LBR 3 meter sphere.

Testing with the rooftop version of LBR showed that the Kinect system can be blinded by infrared radiation emitted by the aluminized Mylar surface when illuminated by the Sun. A solution to this problem is to utilize an optically based parallax ranging system. Here, instead of using infrared laser dots projected onto the reflector's surface for parallax measurements, a regularly spaced array of small (~5 mm diameter) optically reflective dots are printed on to the gore surfaces from which the LBR sphere is formed. Parallax measurements of the dots are made by two high definition optical cameras, one mounted on each side of the corrector assembly. By combining the parallax measurement with the location of the dot on each camera's CCD, it will be possible to locate the dots in x, y, z and generate a 3-D image of the reflector surface (e.g. Figure V.B.12). From this image the displacements on the corrector's actuators needed to achieve optimum performance can be calculated. Small, high definition cameras, such as the Nikon D800 DSLR, are available with more than enough pixels and field of view to measure the reflector surface to the level of accuracy needed for a flight version of LBR. Ultimately, LBR will be flown in the Antarctic summer from McMurdo, where the Sun is up 24 hours. However, for a test flight, it will likely be flown from Ft. Sumner, NM, in which case it can encounter night. At such time a light will be turned on inside LBR to provide the necessary illumination of the surface.

During Phase II we will perform extensive testing of the optical parallax and FARO 3D laser ranging system with LBR's surface in full sunlight. Commercially available software will be used to convert the test measurements into a 3-D model of the reflector's surface. From this model corrections to the secondary's surface figure will be determined.

V.B.7 Pressure/thermal management system

The LBR is a sphere that will be pressurized at a constant differential pressure to produce a rigid, stable structure. The carrier balloon will be launched with LBR not inflated, stowed in a

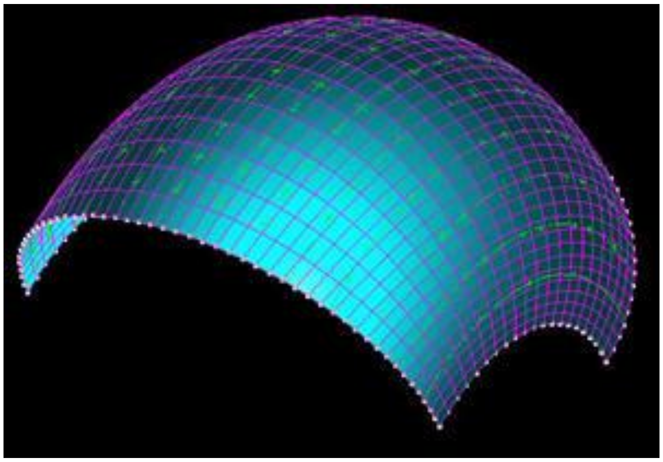

Figure V.B.12. Example NURBS surface model fit to a spheroid.

canister suspended from the top plate. The top plate assembly of the carrier balloon with Instrument Unit installed will be supported during launch by a small tow balloon. After launch the tow balloon, along with the protective cone covering the Star Tracker Telescope, will be release and will separate from the carrier balloon. When the system ascends to an altitude of 12km, the LBR will be deployed by slowly winching down the storage container and extending the flaccid LBR sphere.

Once completely extended, the dual blowers will inflate the sphere with helium drawn from the carrier balloon. Once inflated the blowers will pressurize the sphere to 1 mbar differential pressure, then turn off. As the balloon continues to ascend and the pressure in the balloon drops, relief valves in the pressure management system will open to allow excess helium to move from the sphere back into the carrier balloon. The system will use a combination of pumping and venting of the sphere to maintain a target differential pressure during the flight. This pressure management system will automatically compensate for gas expansion changes resulting from thermal variations.

Thermal management will be passive, using a combination of surface coatings and thermal radiators to manage the heat produced in the sphere by Sun loading and power dissipation. The internal electronic systems will be designed to minimize waste power. All exposed hard surfaces on the LBR will be white for heat management.

V.B.8 LBR control computers

The LBR control computer will be housed in the “Top Plate Assembly”. It will use wireless communications to send and receive control data from the instrument control computer inside the sphere. WiFi will also be used to send and receive data from the service gondola computer. The LBR control computer will control the LBR from prelaunch through termination, managing the tow balloon release, LBR deployment sequence, pressure management and pointing control. The instrument computers mounted in the LBR receiver assembly will provide focus and fine pointing control via the adaptive corrector optics. The received signal will be processed and digitized and the results passed to other computers via the local WiFi connection. The LBR control computer will also monitor the sphere pressure and temperature. Based on this information the computer will control the blowers and vent valves in the pressure management system.

V.C Instrument Unit (IU) Design

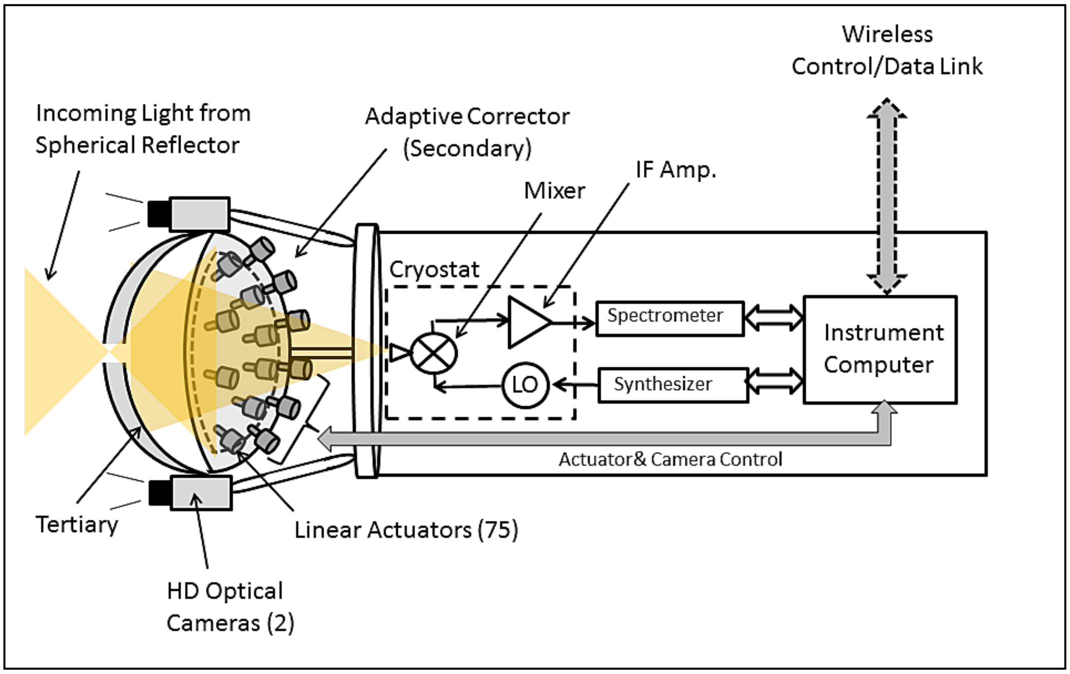

Figure V.C.1. LBR's Instrument Unit (IU). THz light from the 10 meter reflector enters the optical system which corrects for spherical aberration and focuses it into a low-noise THz receiver system. The receiver produces a power spectrum of the THz light which is passed on to the instrument computer and wirelessly to the telecommunications system. The instrument computer also produces a real time fit to the primary reflector's surface using parallax measurements from two optical cameras. The computer reshapes the corrector using actuators to compensate for nonspherical distortions.

A Block Diagram of the Instrument Unit (IU) is shown in Figure V.C.1. LBR's optics are designed to provide a 13" full-width-half-maximum (FWHM) diffraction limited beam at the frequency of the astrophysically important ground state water line (557 GHz). LBR's optical system consists of a 10 meter spherical reflector (primary), an adaptive correcting secondary, and a tertiary. In this on-axis design, THz light from the spherical reflector forms a focal line at the entrance window on the back of the tertiary. The beam then re-expands onto the adaptive secondary and is then focused and allowed to re-expand. The THz light is then reflected by the surface of the tertiary and comes to a focus at the feedhorn of a mixer. The mixer down-converts the THz sky signal to microwave frequencies; multiplying the incident sky and LO signals together. The product of the multiplication contains sum and difference frequencies. Filtering permits only the difference (*i.e.* intermediate frequency (IF)), signal to appear at the mixer output. From there coax conveys the downconverted sky signal to a series of low-noise microwave amplifiers. For optimum performance, the mixer and first stage amplifier reside in a cryostat where they are cooled to cryogenic temperatures by a closed-cycle refrigerator. The amplifiers boost signal levels to where they can be digitized without increasing the noise. A digital spectrometer is used to produce a power spectrum of the amplified signal. The instrument computer 1) reads-out the spectrometer, 2) models the shape of the spherical primary from parallactic surface measurements, and 3) adjusts the secondary's shape to produce a conjugate match to nonspherical surface distortions (see Sections V.A.3d and V.B.6). During flight the LBR beam quality will be routinely measured and optimized on a strong calibration source (e.g. Moon and planets).

V.D Pointing Control System (PCS)

The Pointing Control System for LBR will be based on the PSC that APL has developed for the STO and BRRISON balloon missions. Its basic components are a guidance package mounted on the carrier balloon top plate and a PCS computer housed in the Avionics Computers Box installed on the service gondola suspended from the carrier balloon.

V.D.1 LBR Guidance Package

The guidance package shown in Figure V.D.1 provides accurate attitude knowledge of the entire balloon and sensor system. The package consists of a gimbal mount carrying two star cameras and an inertial measurement unit (IMU). The star cameras and IMU are mounted to a common precision plate that can pivot in pitch (elevation) via a direct motor drive mechanism. The guidance package is attached to the azimuth rotator plate on top of the carrier balloon,

The expected absolute accuracy will be < 10 arcsec over 10 minutes (the time between two star fixes obtained by the star cameras, see below).

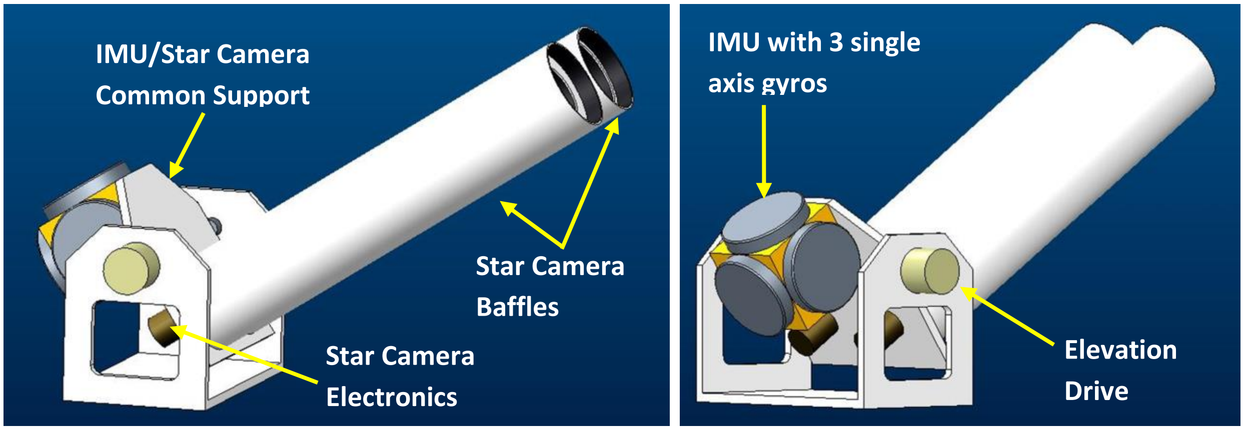

Figure V.D.1: Two views of the LBR Guidance Package on top of the carrier balloon.

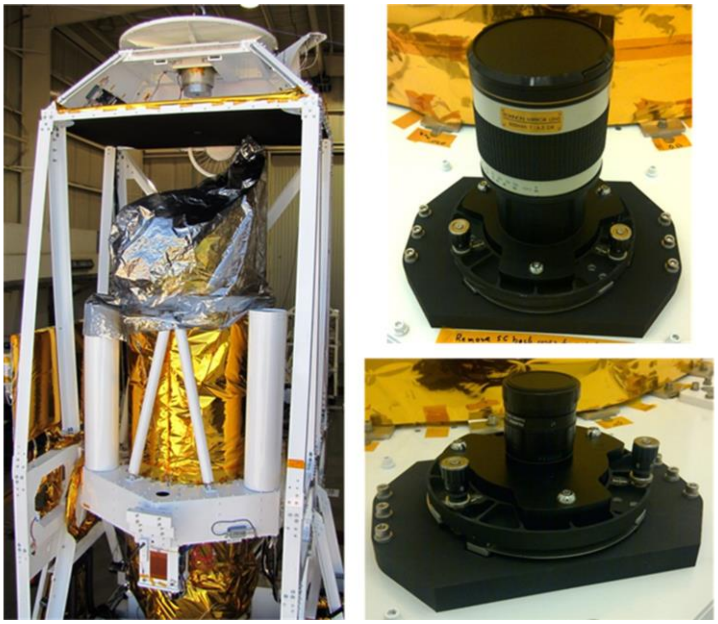

Figure V.D.2 Star Cameras installed on the BRRISON gondola. Left the 4.5 ft long baffles. Right top the NFC lens system. Right bottom the WFC lens system.

V.D.1.a Star Cameras

For precise absolute attitude knowledge LBR will carry on the GNC top assembly two star cameras very similar to the ones that APL developed for STO, and were successfully flown on STO, and BRRISON (see Figure V.D.2), balloon missions. Each star camera is mounted on a precision tip-tilt adjustment plate that allows arcsecond-level angular adjustment of the aim direction. These plates are designed for high thermal stability of the aim direction.

One star camera is configured with a 50mm focal length f/2.4 lens and red filter. This wide-field camera (WFC) has a ~7° FOV and is capable of detecting magnitude 6.8 (and dimmer for very red stars) stars at 120 kft altitude during daylight conditions with a ~350ms exposure time. The camera's FPGA is loaded with a custom configuration that performs flat fielding of the image as well as computing statistics for dynamic thresholds used for bright spot identification. The camera's processor computes spot centroids from each image and provides a timestamp. The results are sent via Ethernet interface to the PCS computer that performs star identification and calculates the aim point. This is the primary star camera used for absolute pointing knowledge. Its expected instantaneous pointing knowledge accuracy is about 5 arcsec. The expected time between two star fixes is every 10 minutes, but it could be run as fast as every 5 seconds.

LBR's second star camera is identical to the WFC except that the lens is a 500mm mirror lens. This narrow-field star camera (NFC) has a ~0.5° FOV and is capable of imaging faint stars down to magnitude ~10 during daylight at 120 kft altitude. It is used to establish absolute error limits on the WFC pointing solution and verification of low jitter and proper slew scans. During commissioning, live video from this narrow field of view camera can be sent over the LOS video link to the ground. It can also be used to provide absolute position references in the event of a problem with the WFC, provided that rough pointing is known.

The two star cameras have 4.5 ft long baffles to baffles designed to reject all stray light that could reach the star cameras lenses from outside the cameras field of view. At the balloon float altitude of ~ 120,000 feet the sky brightness in day-light is much reduced with respect to the ground but still considerable. Therefore, a well baffled optical system is needed to permit the star cameras acquire faint stars also during the day.

V.D.1.b Inertial Measurement Unit (IMU)

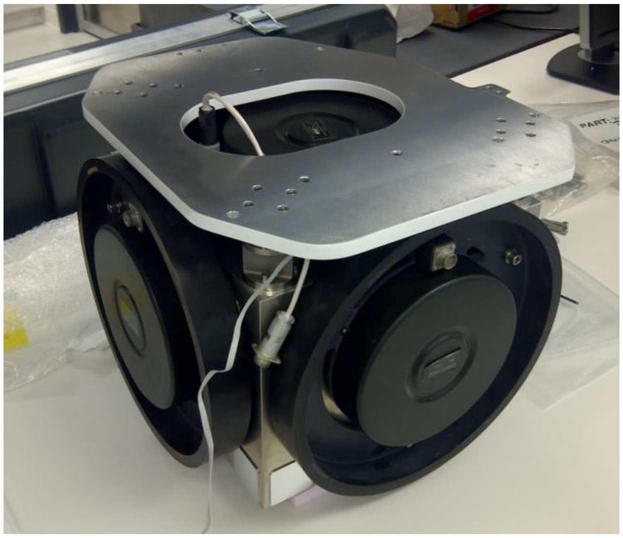

Figure V.D.3: IMU Developed by APL for BRRISON. The 3 single axis optical gyroscopes are visible (one is partially hidden behind a mounting plate). The entire assembly approximate size is 1 ft x 1 ft x 1 ft.

While the star cameras provide instantaneous absolute attitude knowledge the relative attitude will be measured by an inertial measurement unit (IMU). The LBR IMU will be nearly identical to the one that APL has developed and successfully flown on BRRISON in 2013. The IMU is made from three orthogonal Optolink SRS-2000 high-precision low-drift fiber optic gyroscopes (FOGs) mounted on 3 orthogonal faces of a diamond turned Gossamer Cube (see Figure V.D.3). The gyroscopes are relatively insensitive to magnet fields (less than 3 arcsec/min/gauss), but we will use a three-axis magnetometer located in the IMU cube to subtract the magnetically induced bias drift. The IMU is mounted on a common plate with the star cameras and moves together with them (Figure V.D.2). The attitude is computed and maintained in inertial coordinate space. Since the gyroscopes only measure relative attitude the star camera system is used to reestablish the absolute telescope attitude periodically (typically every 10 minutes).

V.D.2 PCS Computer

The PCS computer will essentially be the same that APL has developed for the STO, and BOPPS balloon missions. It is housed inside the top plate assembly on top of the carrier balloon. It is composed of PC104 COTS boards vacuum compatible and with industrial operating temperature range between -40 and +85 degrees C. The components are: a CPU board, two digital acquisition cards for the digital and analog input/outpus of the PSC computer with the various sensors and motors, a power supply, and a WiFi router. Via the WiFi router the PCS computer can communicate with both the LBR instrument computer inside the LBR balloon and the Command & control computer housed in the service gondola. Figure V.D.4 shows a block diagram of the guidance and control package installed on the top plate assembly.

The software that the PCS computer for LBR will run is basically the same as the software run on STO and BRRISON. The PCS computer receives the sensor data from the IMU and star camera and computes the balloon and instrument absolute attitude in azimuth, elevation, and rotation. A real time process samples and stores data from all of the analog sensors, performs integration of the FOG signals, implements the control equations for the azimuth, elevation, reaction wheel braking, and telescope balance servo loops, and calculates the telescope aim position.

The PCS computer runs a process that commands the star cameras. It commands the WFC to acquire a star field image. The WFC identifies potential stars on the image and forwards to the PCS computer a table with information of the location and relative brightness of the identified bright spots on the star field image. The PSC computer then performs star recognition by comparing star positions and relative brightness with a star catalogue. It computes a rotation matrix that aligns the telescope's reported aim point to the observed aim-point of the WFC. This matrix is used it to update the IMU and telescope vectors.

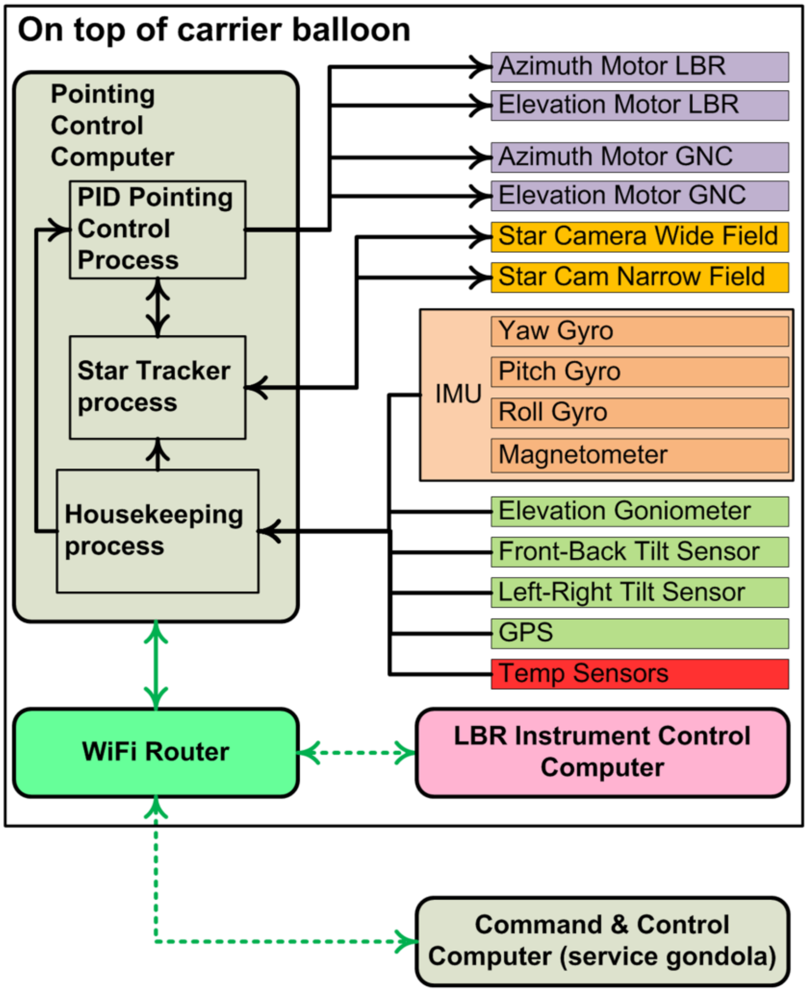

Figure V.D.4: Block diagram of the LBR Guidance and Control system. The pointing control computer resides inside the top plate assembly.

The digital control system to maintain pointing will be the same successfully used for STO and BRRISON. It uses sophisticated Proportional-Integra-Derivative (PID) controller to determine the azimuth and elevation motors drive current entirely from the position error delivered by the IMU. This PID controller was developed and refined by APL over the past 15 years of scientific ballooning.

V.E Service Gondola

The Service Gondola carries and protects the avionics computers, the power system, and the balloon control and telecommunication systems, which are necessary to support the LBR instrument and mission. It is suspended from the bottom of the carrier balloon, underneath its parachute like any other conventional stratospheric balloon gondola. Its conceptual design is based on the heritage of several gondolas built and flown by CSBF as well as subsystems built and flown by APL. The service gondola and all its subsystems will be designed built and tested at APL, with the exception of the balloon control and telecommunications package which is provided by CSBF.

V.E.1 Structure

The gondola structure is essentially a frame composed of several 3x3 inches aluminum channels bolted together to form a box with two decks and painted with a white thermal coating. Its basic design is shown in the Foldout FO3. Its basic dimensions are 5.5 ft x 5 ft x 5.5 ft (WxDxH). The top of the two decks carries the avionics computers box, the Power Distribution Unit (PDU) and a box containing the rechargeable batteries bank. The lower deck carries the CSBF provided Support Instrumentation Package. This is a basic design used in several CSBF and other institutions gondolas for stratospheric scientific balloon missions.

Below the bottom of the gondola hangs a CABF provided ballast hopper that carries ballast that is dropped in flight to maintain the balloon altitude over the course of the mission. Also underneath the gondola are attached crush pads that cushion the impact of the gondola with the ground at landing.

On top of the gondola structure is attached an antenna boom carrying several antennas for receiving GPS signals and to communicate with relay satellites like TDRSS and IRIDIUM. The gondola is suspended by 4 steel cables at its four top corners. The cables connect to the CSBF provided rotator assembly (see Section V.E.6 for details on the rotator) which in turn is connected to the suspension flight train, the in-line parachute, the CSBF provided termination assembly, and the carrier balloon.

The gondola mass is shown in Table V.E.I.

V.E.2 Avionics Computers

The entire command and control system for LBR design is shown in a simplified block diagram in Foldout FO3. We heavily base our design on the STO, BRRISON and BOPPS system developed by APL. In particular for LBR we plan to use nearly the same design for the avionics computers that now APL is building and testing for the upcoming BOPPS 1-day balloon mission from Fort Sumner (New Mexico). The computers and their peripherals are composed of mainly commercial off the shelf (COTS) electronics boards in PC-104 format with industrial temperature operating temperatures from -40 to +85 degrees C. All the components are capable of operating in vacuum thus not requiring the need of a pressurized vessel to house them. This has a significant mass savings advantage. LBR will carry two computers: the pointing control computer (described in SectionV.D.2) residing in the top plate assembly on top of the carrier balloon, and the Command and Control (C&C) computer installed on the service gondola. The two computers communicate between each other with the Instrument Computer via WiFi Ethernet. A WiFi capable Ethernet hub also vacuum compatible and capable to operate between -40 and +85C is housed inside the avionics box, and one is housed in the top plate assembly. Finally a COTS PC-104 format power supply within the avionics box powers all the components within.

V.E.3 Command & Data Handling

Command and data handling is managed by the C&C computer system. It interfaces to the other subsystems via Ethernet and connects to the SIP and associated radio links for communications with the ground (see block diagram in Foldout FO3).

Table V.E.I: Estimated LBR System Mass Summary	Mass	
	lbs	kg
Service Gondola		
Frame	536	243
Avionics	25	195
LBR Power	525	238
Harness	20	9
CSBF provided equipment:		
Rotator	150	68
SIP	350	159
SIP Power	100	45
Antennas	46	22
Ballast Hopper	23	10
Crush Pads	80	36
Total Service Gondola (without ballast)	**1855**	**841**
Flight Train (CSBF provided equipment)		
Parachute Assembly	543	246
Standard Flight Train Components	215	98
Total Flight Train	**758**	**344**
LBR Spherical Telescope		
Sphere Structure	397	180
LBR Elevation Drive Assembly	30	14
LBR Azimuth Drive Assembly	23	10
Balloon Top Plate Assembly	61	28
LBR Harness	20	9
LBR Deployment System	55	25
LBR Sphere Pressurization Assembly	14	13
Total LBR Spherical Telescope	**600**	**272**
GNC Package on Top of Balloon		
IMU	43	20
Star Cameras	22	10
Mount and Elevation System	27	12
Harness	5	2
Total GNC Package	**97**	**44**
Total Carried Mass (without ballast nor balloon)	**3310**	**1501**
Launch Stabilizer (Ethafoam Ring on top of Balloon)	**40**	**18**
Balloon, Raven W29.47-2x-P (LDB: Zero Pressure)	**3675**	**1667**
Total Mass Including Balloon (without ballast)	**7025**	**3186**

The C&C computer runs the Linux operating system. Its mode of operation is the same successfully employed on STO, BRRISON and BOPPS. The OS, library, and C&C software are placed on independent partitions that are mounted read-only. Logs, saved state, parameters, configuration, and temporary data are written to separate partitions that are read-write.

Two independent serial ports provide the command uplink from the two independent command ports on the SIP. Commands can originate from either port but contain a serial number that prevents duplicate and out-of-order command execution. Ground commands are sent to the C&C computer via the SIP telecommunication system described in Section V.E.6.

Housekeeping data is received from the PCS computer and instrument computer via TCP/IP sockets. Additional housekeeping generated within the C&C computer is added to it then sent to the FPGA on the CPU board for forward-error-correction (FEC) coding and transmission to the Line-Of-Sight (LOS), TDRSS, or IRIDIUM-dial-up downlink paths supplied by CSBF.

Science downlink data from the instrument computer also flows through the C&C computer. The instrument computer writes compressed science data to a disk partition (10MB) located on the C&C computer. The C&C computer packetizes the science data and sends it to the FPGA for FEC and downlink. Downlinked data is erased from the C&C disk partition after it has been sent. The C&C computer commands the instrument to stop writing science data to the downlink directory when the disk partition reaches near capacity and commands it to resume when the partition is < 50% full. The instrument has a random-access data store capable of storing all of the science data throughout the mission.

V.E.4 Power

The LBR power system design is heavily drawn from the APL power system successfully flown in several past scientific balloon missions the last of ones are STO, and BRRISON. It is composed of three main sub components: the Solar Arrays, the Power Distribution Unit, and the Rechargeable Batteries Bank.

For the initial LBR design we assume a Long Duration Balloon (LDB) flight from Antarctica during the Antarctic summer. The flight duration could be of up to 50 days and the Sun will always be above the horizon. This assumption simplifies the design.

Table V.E.II: Summary Estimated LBR System Power

		Average [w]	Peak [w]
Instrument			
	Receiver Module	260	260
	Optics Module	30	630
	FARO Laser 3D Scanner	80	80
	Total Instrument	**370**	**970**
Gondola and G&C			
	Pointing	30	150
	Avionics	50	80
	Total Gondola and G&C	**80**	**230**
LBR			
	Pointing	50	150
	Pressurization System (2 each)	20	200
	Total LBR	**70**	**350**
	Total Power	**510**	**1510**

The solar arrays we baseline are composed of 480 cells single-junction mono-crystal, back aluminized SunPower C60 cells. The total size of the arrays is about 7ft x 13ft. They are attached to the front side of the gondola at an angle of 22 degrees with respect to the vertical. This angle is the optimum angle to generate maximum power for flight out of Antarctica, but it can be adjusted/optimized depending on the launch site (Antarctica, mid-latitudes like New Zealand or Australia, ...), flight duration (2 days to 100+ days), predicted flight trajectory, and flight time of the year. The CSBF provided rotator provides sufficient azimuth attitude to maintain the solar arrays always facing the Sun, in day-time, to within 1 degree throughout the entire flight, thus guaranteeing maximum power generation. This design is nearly identical to the solar array system s successfully flown on STO in 2011. Foldout FO3 shows the currently planned configuration of the solar arrays.

The maximum power delivered by the arrays is about 1200 W, while the current estimated total LBR average power requirement will be only about 510 W (see power estimations in Table V.E.II). This gives a margin of 690 W.

The PDU is responsible to distribute the loads across the panels, ensures that the system's battery stacks are maintained at near full charge, sunlight permitting, and provides on/off power switching capability to the various LBR subsystems from ground commands. It will be in design very similar to the one used for STO.

The battery stack that we plan to initially use is composed of 4 sealed lead-acid ODYSSEY PC1700 rechargeable batteries connected two pairs in series and each pair in parallel. With a capacity of 130 Ah the battery stack will guarantee full power delivery for an entire Antarctic flight with 100% instrument and subsystems duty cycle. The bus voltage delivered by the power system to all subsystems is 24V.

This design can also be adapted for an Ultra Long Duration Balloon (ULDB) flight of 100+ days where the flight will include multiple day-night cycles. In this case the gondola will have to carry additional rechargeable batteries to allow operation of the instrument during the nigh time. A larger number of solar cells will also be needed to allow simultaneous operation of the instrument and recharging the batteries during the day time.

V.E.5 Thermal Control

Thermal control for the service gondola as well as of the GNC package on top of the carrier balloon will be done mainly using passive means. The main means are use of Multi-Layer-Insulation (MLI) thermal blankets made of Mylar, or thermal shorting with the service gondola aluminum frame. Most of the electronics used has a wide operating temperature range from -40 to +85 degrees C which in itself is normally within the temperatures routinely experienced by balloon payloads flying in Antarctica at 120 kft altitude during the Antarctic summer when the Sun is always above the horizon. Typically the only single phase when very cold temperature down to -50 degree C can be experienced is right after launch when the payload flies through the tropopause. Heaters with thermostats have been routinely used to warn sensitive electronics or components during this phase of the flight. A detailed thermal analysis will determine on a case-by-case basis what best method to use for thermal management.

V.E.6 Balloon Control and Telecommunications

The LBR Balloon Control and telecommunications system for will be the same that was succesfully used for several LDB balloon missions like STO and BRRISON. We will rely entirely on the NASA-CSBF provided Support Instrument Package (SIP) for remote link between the gondola and the ground. The block diagram in Foldout FO3 shows how the LBR computer systems interface with the SIP, while the ground segment is depicted in Figure V.F.1. The SIP has three available channels to/from the ground. For the first ~24 hours the gondola will be in Line-of-Sight (LOS) to the launch station in Antarctica and will use a UHF radio link at a data rate of 1 Mb/s. During LOS operations ample amounts of housekeeping data will be available for analysis of both science and gondola performance. After loss of the LOS radio link, communications will be maintained via a 92-Kb/s TDRSS satellite relay and a lower rate IRIDIUM relay (one 255 byte packet every 15 minutes). Another option we are investigating for the high speed over the horizon data link is to use IRIDIUM next. A 6-Kb/s TDRSS link is also available and is used as backup. TDRSS and IRIDIUM signals will be received at CSBF's Operations Control Center (OCC) in Palestine (TX) and sent to a local STO ground support computer that will redistribute the data packets to other STO ground stations at APL, the University of Arizona and to the team in Antarctica. About 90% of the science data acquired during the flight will be downlinked using the TDRSS link and will be sufficient to meet the scientific goals in the case of payload loss. The ground support computers will use the same software package GSEOS, by GSE Software, Inc., that was previously used for STO-1. The telecommunication ground system is described in Section V.F.6.

The SIP is also used by CSBF to control the balloon operations and altitude. Via the SIP ground controllers can command ballast dropping to regain altitude or if also Helium venting if necessary. Via the SIP CSBF also commands the termination procedure which is described in Section V.F.8.

V.E.7 Distribution on LBR

Our concept approach for the power and data link between the service gondola and the LBR system and GNC package on top of the carrier balloon is shown in Figure V.D.5. Power and telecommunication links will be accomplished using two separate approaches.

For communications link we are base lining to use a Ethernet WiFi system with a WiFi router on the service gondola communicating to another WiFi router on top of the balloon. The top WiFi router is responsible to perform networking connections between the WiFi on the service gondola, the PCS computer (to which it will be connected via hard Ethernet wire) and the Instrument Control Computer inside the LBR balloon which it also has WiFi capability. This way we will not have to send the data signals from the LBR instrument control computer to the service gondola C&C computer via an extremely long (up to 1000 feet) Ethernet cable, two slip-ring assemblies and a set of bulkhead connectors, which could likely cause signal degradation.

For the power distribution we will utilize a minimum of two long power cables of equal length running from the top of the service gondola through the rotator assembly (via slip-rings), along the furled parachute and the sides of the carrier balloon, to reach the LBR on top. The two power lines will be stitched along the carrier balloon support guy lines at opposite sides of the balloon. This balances the mass of the wires and prevents the balloon to list on one side causing the top assembly and the LBR to be off center.

The challenge for the power lines is how to minimize the power wires mass and voltage loss along the cables since the cable length will be on the order of 850 to 900 feet. However, the TopHat balloon mission launched from Antarctica in 2001 was able to accomplish this. To prevent imbalance on the carrier balloon we plan to run two sets of equal mass cables along opposite sides of the carrier balloon.

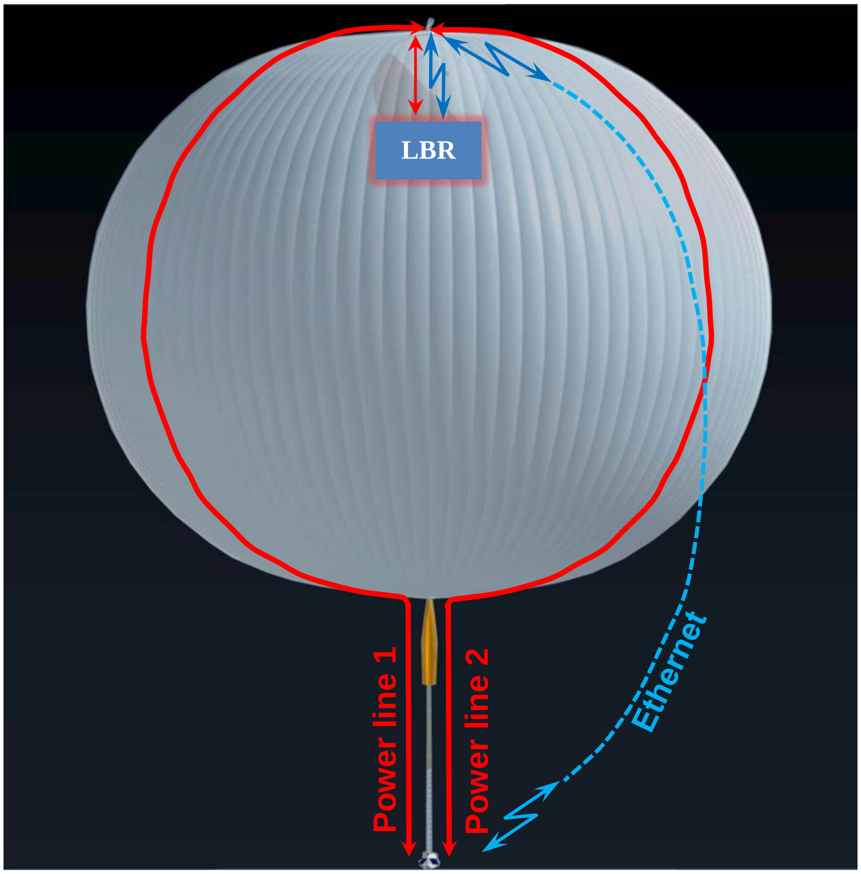

Figure V.D.5: Power and telecommunications from the service gondola to the LBR system on top of the balloon.

LBR Service Gondola

FO3

Back View

Front View (always facing the Sun)

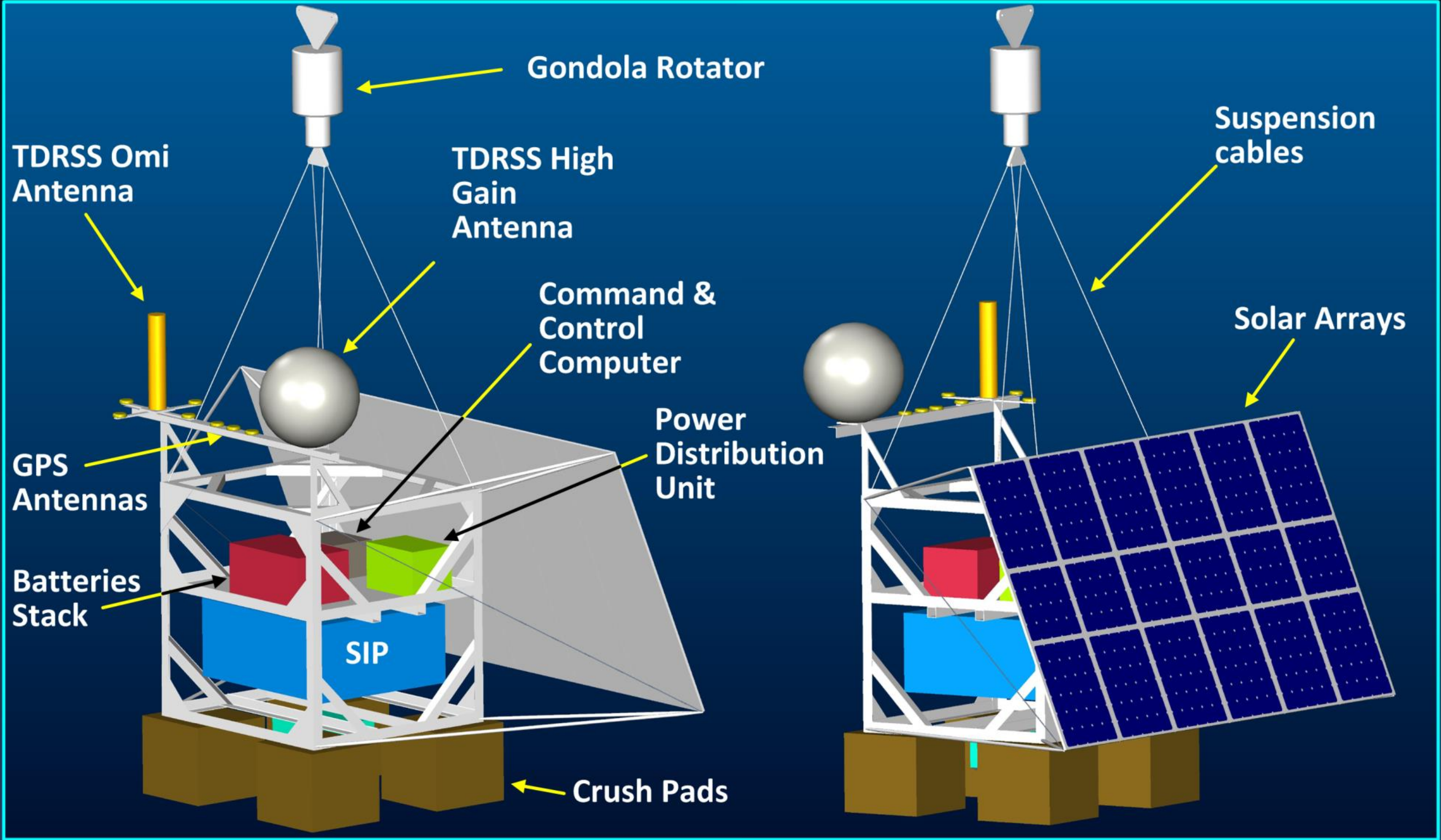

LBR Systems Block Diagram

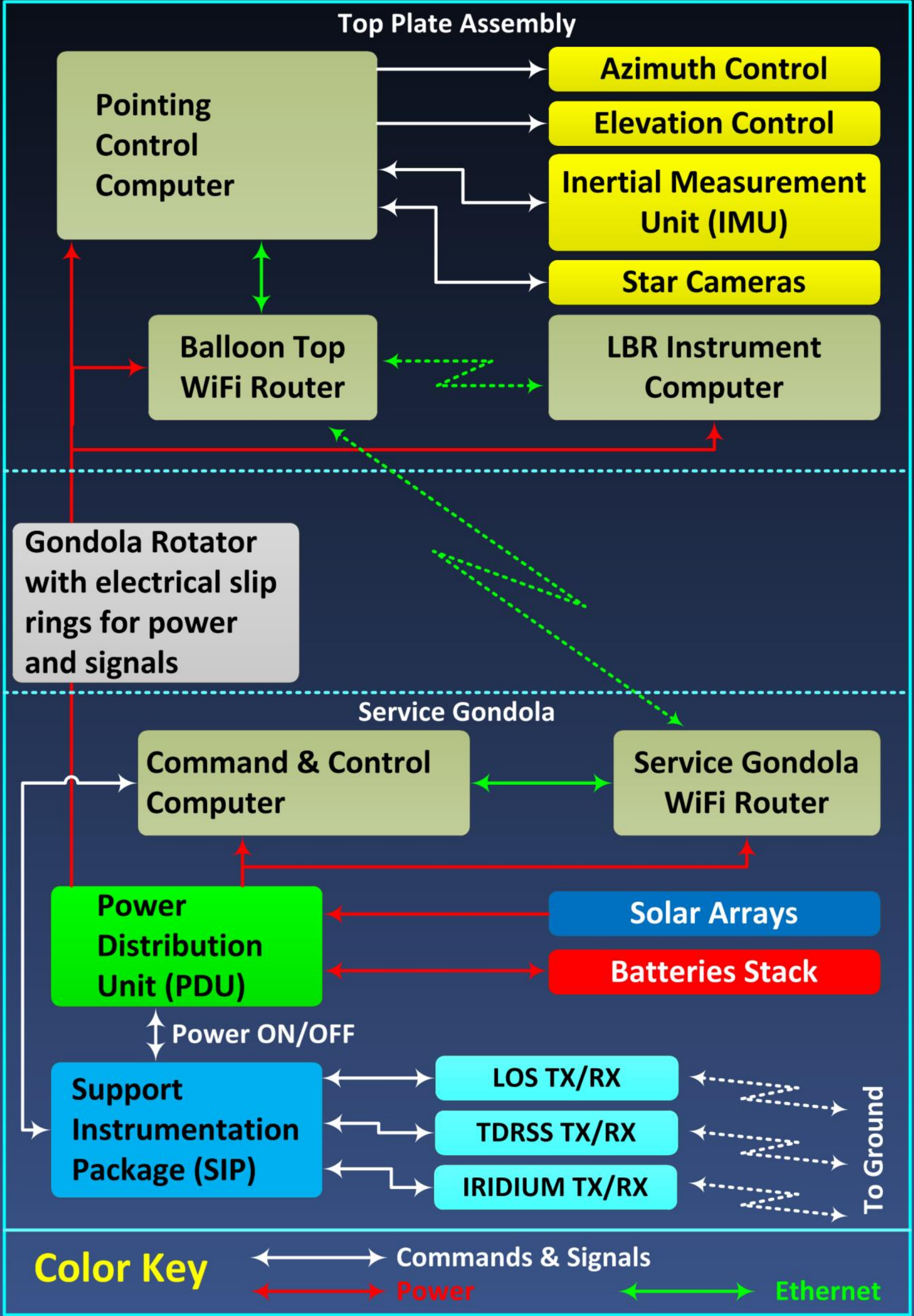

Service Gondola Stats

Frame dimension: 5.5 x 5 x 5.5 ft (WxDxH)

Mass (as shown without ballast): 841 kg

Solar arrays dimension: 13.5 x 7 ft (WxH)

Solar arrays power generation: 1200 W

Batteries capacity: 130 Ah

Heritage

The LBR service gondola and subsystems draws heritage from the STO gondola flown in Antarctica for 14 days in 2011

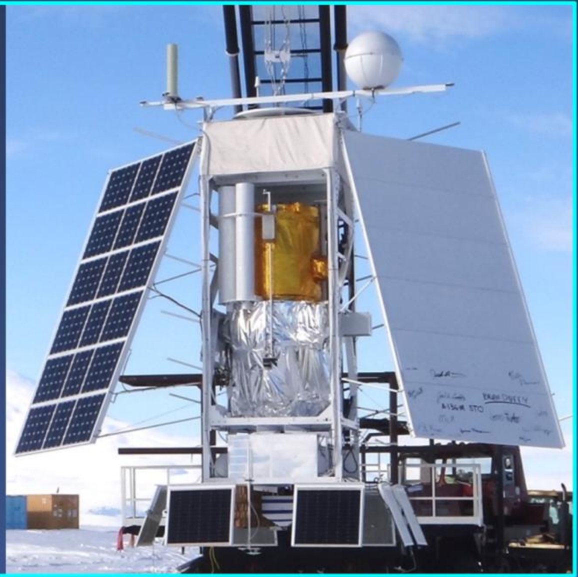

V.F **Mission Profile**

Mission operations for LBR will mostly follow the paradigm successfully implemented for various balloon mission carried out by JPL, APL, and UofA. Over the years the mission operations plan has been refined and improved.

LBR is baselined to be launched and flown from McMurdo (Antarctica) during the Antarctic summer. NASA's Balloon Program Office (BPO) has a long history of launching stratospheric balloons from McMurdo station. LBR can also be launched from other locations like Alice Springs in Australia, New Zealand or Kiruna Sweden.

V.F.1 Ground System

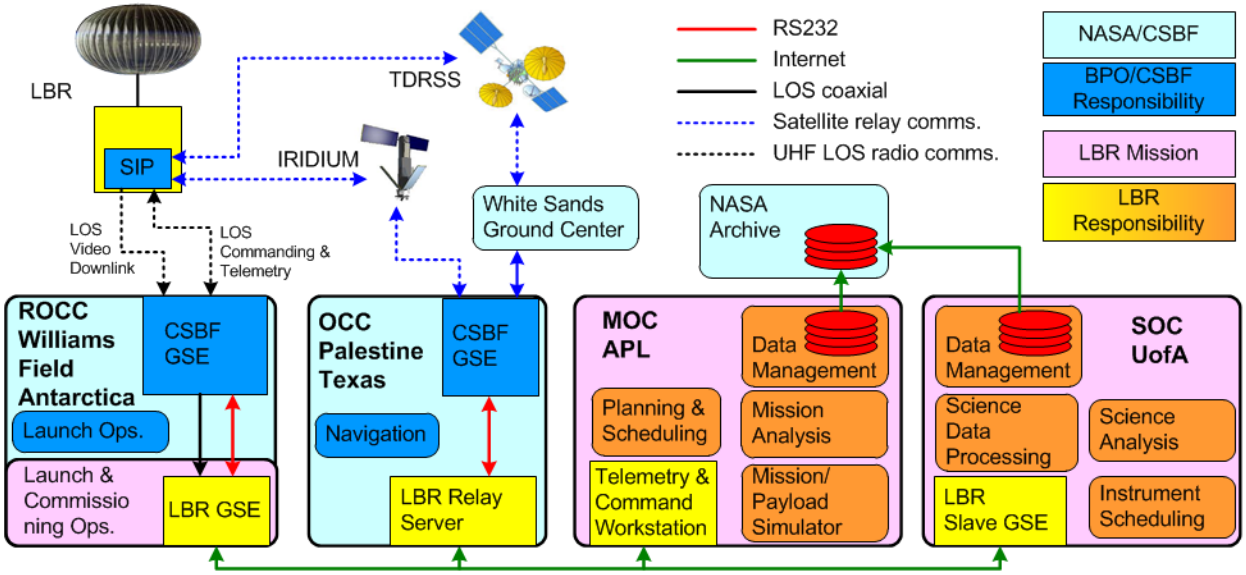

Figure V.F.1: LBR Ground Segment design

LBR ground segment design is shown in Figure V.F.1 and will be the same APL, and UofA developed for the STO balloon mission. While the payload is in LOS with the Remote Operations Control Center (ROCC) in Antarctica the control of the gondola is handled by personnel in Antarctica. Following loss of LOS, control is handed over to the Mission Operation Center (MOC) at APL. The MOC interfaces via a virtual private network (VPN) Ethernet connection to a LBR fully autonomous relay computer server located at the Operations Control Center (OCC) in Palestine (TX) which connects to CSBF's ground computers via serial interfaces. The OCC is the station receiving the TDRSS and IRIDIUM relay data from gondola's SIP. It is operated and continuously manned by CSBF personnel. LBR's OCC server's sole purpose is to relay telemetry and science data from the OCC to the MOC and the SOC, and to retransmit the commanding packets from the ground to the payload. It stores all telemetry and science data on a data storage bank.

The ground support computers at the ROCC, OCC, MOC, and SOC use the software package GSEOS, by GSE Software, Inc., that was previously used for the STO and BRRISON balloon missions. This package is widely used at APL to interface with space missions like e.g. MESSENGER and New Horizons.

V.F.1.a Mission Operation Center

The MOC will be located at APL. It interfaces with LBR's relay server at the OCC. It is the primary station handling all communications to and from the balloon payload. The MOC is continuously manned during the science flight(s). APL provides gondola operations and subsystems health monitoring; a gondola engineering team for early operations payload checkout, mission termination, anomaly investigation, and mission operations management. APL engineers also review, and certify observing program changes submitted by the science team to ensure payload safe operations, and upload certified updated operations to the C&C computer. The MOC stores all downlinked telemetry and science data on a data storage bank.

V.F.1.b Science Operation Center

LBR SOC is located at the UofA, it interfaces directly to LBR's relay server at the OCC via a VPN Ethernet connection. The SOC receives the same telemetry information and has the same commanding capability as the MOC. All MOC functions are transferrable to the SOC if Ethernet connectivity is lost at the MOC.

V.F.2 Flight Line Integration & Test

The LBR flight line procedures evolved from the heritage procedures conducted for the Top Hat payload (Figure V.F.2) successfully launched from McMurdo Station, Antarctica. The packaged LBR will be connected to the large apex fitting plate that has been previously fit checked with the apex balloon fitting back at the balloon plant. All electrical connections will be mated and electronic functional checks will be performed while the carrier balloon is still at the McMurdo staging buildings.

Figure V.F.2. TOPHAT payload prior to mating to balloon apex and after, with Tow balloon attached.

On the day of the launch, the entire system, balloon, LBR, Service Gondola will be taken to the launch site (Figure FO4-a). The balloon will be laid out normally with the apex of the balloon suspended via scaffolding in the air. The LBR container will be hoisted via small crane over the open balloon apex fitting and slowly lowered into the balloon and the LBR Plate will be bolted to the balloon apex fitting. The star tracker assembly will then be attached to the apex fitting. All mechanical attachments will be double checked and end to end electronic systems functional checks will be performed with the Service Gondola. Once complete, a tow balloon will be inflated with enough lift to suspend the star tracker and LBR. It is attached to the apex of the balloon via a special mechanical connection around the star tracker. The tow balloon is slowly hoisted higher until the bubble balloon is fully extended (Figure FO4-b). One quick final LBR functional check will be performed and then balloon inflation can commence.

V.F.3 Launch Sequence

Balloon inflation proceeds normally with the Operations Crew controlling the apex and tow balloon during the process. Once inflation is complete, the normal final pre-launch procedures are completed and the balloon with the LBR inside and the tow balloon are released from the launch spool. The mushrooming of the balloon is minimized by the ethafoam disk (Figure FO1) mounted to the top of the balloon for stability as well as the extra lift provided by the tow balloon. Once the balloon system is standing over the launch vehicle, the Service Gondola is released just like any normal scientific balloon. As the balloon rises and stabilizes, usually within 1000’ AGL (Figure FO4-c), a command will be issued to cut the tow balloon free of the apex of the balloon to float away.

V.F.4 Ascent

Normally the balloon is inflated with approximately 12% free lift. As such the initial ascent rate should be approximately 1000 ft/min. For this calculation a 29.47 mcf Zero-Pressure balloon is assumed. At approximately 60,000 ft altitude the balloon bubble has expanded to a point where the LBR deployment can be initiated. This is based on a Gross Load of ~7438 lb (payload of 3763 lbs+ balloon mass of 3675 lbs) for an equivalent SIGMA shape of ~0.2 (Smalley 1966). The top of the balloon at this altitude is ~543 ft, with a bubble radius of ~54.9 ft. The base of the bubble confluence should be at the ~266 ft. level, or 277’ below the top. Allowing for a total LBR deployed length of ~140 ft, adequate balloon bubble size should provide plenty of clearance for the LBR and balloon wall.

V.F.5 LBR Deployment

When the LBR deployment has initiated (Figure FO4-e), the LBR is slowly winched down in it protective bag until it is completely deployed. At this point, the “blowers” are turned on and inflation of the LBR commences by pumping He from inside the balloon to inside of the LBR. This allows for the initial injection to commence at the higher densities of the lower altitudes and the LBR inflation can make use of the adiabatic expansion of the gas due to decreasing altitude density. The LBR inflation continues during the rest of the ascent of the balloon until the balloon reaches its float altitude (Figure FO4-g).

V.F.6 Science Mission Operations

Once the balloon, LBR and Service Gondola have come to equilibrium, Science Operations can commence (Figure FO4-h). Initial checkout of all systems will be performed while the LBR comes to a stable pressure and dynamic oscillations dampen out. Synching and calibration of the star tracker and the LBR will commence. The LBR is going to be pressure limited control. Our preliminary estimates are to control the skin stress levels between 2000-4000 psi to minimize LBR size changes due to changing differential oscillations in the LBR due to radiative effects and their associated changes in temperature. The initial settings of the LBR receivers and adaptive optics will be biased for the operating skin stress levels and anticipated impact on LBR size of the coefficient of thermal expansion. Fortunately, the Antarctic environment is relatively benign on the balloon thermally.

V.F.7 Data Management

All science and flight data will be conveyed to the SOC through the CSBF telecom link and stored on solid-state flash drives in the service gondola.

V.F.8 Termination Sequence

At the conclusion of the mission, all systems will be “safed” and locked in their stowed positions. A command will be sent from the Palestine, TX LDB Flight Control Station to terminate, thus severing the parachute and Service Gondola from the balloon. At the same time it will initiate the deployment of a drogue chute from the balloon apex in an attempt to string out the balloon and LBR system.

V.F.9 Descent

The balloon will tend to wrap up around the LBR and the volume of the LBR will decrease with the increasing atmospheric pressure (Figure FO4-j). As such, the balloon and LBR should serve at a minimum as a “streamer”. Worst case would be it falling as a “clump”. Either way, some of the electronic systems may survive due to a slowed descent as well as the shock absorption of the balloon film balled up around the LBR. At this point we have no clear answer as to its overall survivability. However, the Service Gondola should descend the same as any scientific balloon payload on its own recovery parachute (Figure FO4-k).

V.F.10 Landing and Recovery

The Service Gondola will have a parachute sized for a 22 ft/sec terminal impact velocity which is standard for scientific balloon missions. The parachute will be cut away from the Service Gondola once it has been determined to be safely on the ground. Both the Service Gondola and the LBR/balloon will have location aids for the location and recovery of the systems. The Service Gondola will of course have the use of GPS and data passed thru TDRSS as well as an Iridium system. The LBR will also have GPS but its primary link will just be Iridium. A Twin Otter or Baesler aircraft will be dispatched to recover the Service Gondola, as well if at all possible, the LBR/balloon. After recovery, the hardware is returned to McMurdo for final recovery of data and readied for shipment back to the U.S.

Typical LBR Balloon Flight Profile

FO4

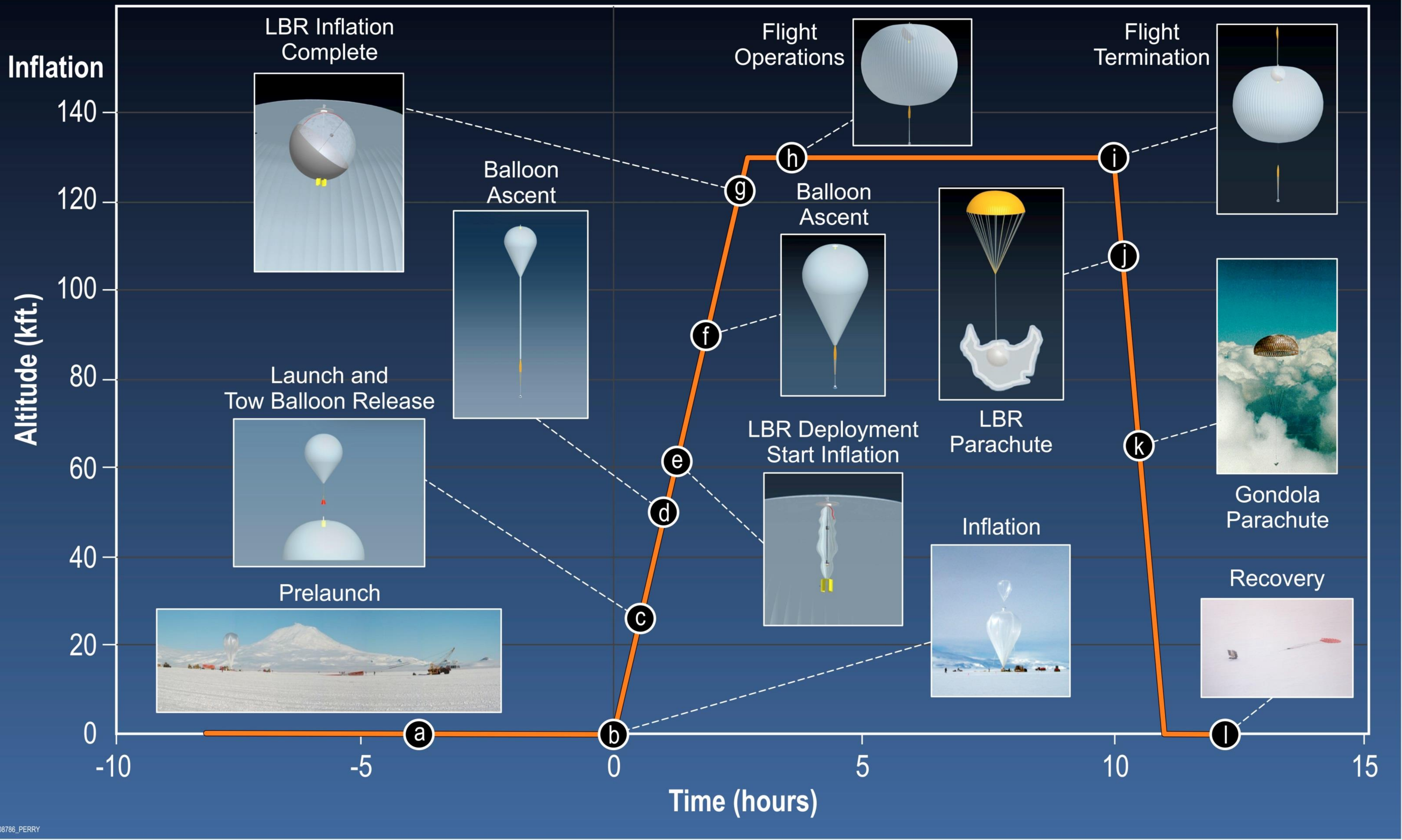

TA008786_PERRY

VI EXAMPLE APPLICATIONS TO NASA MISSION

VI.A Sub-Orbital 10 Meter THz Telescope

VI.A.1 Science Investigation

The terahertz (THz) region of the electromagnetic spectrum encompasses frequencies between 0.1 THz (100 GHz; λ = 3 mm) and 1 THz (λ = 300 µm). This range is of critical importance for astronomy because it includes the peak emission of blackbodies at characteristic temperatures between 10 K and 100 K. Thus, regions as diverse as Giant Molecular Clouds (GMCs) in which massive stars are forming, and which are the most massive molecular assemblages in the universe, and objects in the outer portion of our solar system, emit strongly at terahertz frequencies. Observations in this frequency range are severely hampered by the Earth's atmosphere, which generally becomes increasingly opaque as the frequency increases, and which completely blocks observations around the frequencies of strong atmospheric lines, notably of water and ozone. A suborbital platform is an effective way to circumvent this problem, and a large-area balloon-borne telescope will have a dramatic effect on many important areas of astronomy.

The astronomical signals in this frequency range are of two basic types. The first is broadband, or "continuum" emission from dust grains, which accompany the gaseous constituents of interstellar clouds. These grains radiate as a modified blackbody. That is, their emission can be described by a blackbody function multiplied by a frequency-dependent emissivity. The emission from planets and minor bodies in the solar system generally has a blackbody form. To study continuum emission, one can use fairly large fractional bandwidth $\delta f/f \approx 1$. To measure such signals efficiently, one generally uses direct detectors (bolometers or photon detectors) with the frequency discrimination being carried out by a simple filter.

The second type of signal is a spectral line, which can be emission or absorption (relative to the continuum) from an ion, atom, or molecule in a gas cloud, planetary atmosphere, or surroundings of a minor object in the solar system. A spectral line has a width determined by Doppler shifts due to motion within an interstellar cloud, or pressure broadening in a planetary atmosphere. The former are extremely small, with characteristic velocity dispersion ≅ 1 km/s. This corresponds to a fractional width $\delta f/f = \delta\lambda/\lambda$ = 3x10-6. Thus, to measure the profile of such lines, we require a fractional resolution $R = f/\delta f$ = 106. While the widths of pressure-broadened lines are greater, atmospheric line profiles also include a very narrow Doppler-broadened core. Extracting full information from spectral lines (whether from interstellar or solar system sources) requires coherent signal processing, which in practice means a heterodyne system.

The difference between these two types of observations and detectors is significant for LBR carrying out astronomical observations because for broadband continuum measurements, the emission from the essentially ambient temperature telescope can be the dominant source of noise. For very narrowband spectroscopic measurements, the contribution of the telescope noise is minimal. The only way to reduce the telescope's noise contribution for broadband measurements is to cool it; this is why the Herschel telescope was cooled to ~80K, JWST will be at ~ 40 K, and future space missions will have telescopes cooled to ~ 5 K. Since a large telescope at balloon altitude cannot be cooled, it can offer large collecting area for all types of observations, but there will be a noise penalty for broadband observations that will NOT be present for spectroscopy. Thus, while LBR can be used for continuum as well as spectral line observations, it is likely that its impact will be greater in the latter domain where its large collecting area, operating at wavelengths that are inaccessible from the ground, will enable a wide range of unique observations for astronomy and solar system science.

The situation is similar for studies of the Earth's atmosphere, but here it is the small beam width of the LBR that gives it unique capabilities. In a down-looking mode, the Earth's atmosphere and surface are in the near field of the antenna, so that the spot size will be close to 10 m diameter. And in a limb-sounder, the FWHM of LBR's beam will be ≈ 0.2' or 12" at 600 GHz, giving unprecedented vertical resolution in measurement of atmospheric constituents with spectral lines in the THz range.

VI.A.1.aSolar System

One of the most striking results from the Herschel Space Observatory has been the observation of water in a wide range of objects in the solar system. This has included planetary atmospheres, comets, and hugely surprising, in the asteroid (or dwarf planet) Ceres. While such bodies had been presumed to be "dry", spectroscopic observations of the ground state 556.9 GHz transition of ortho-H_2O revealed that significant outgassing of water vapor is occurring. The water vapor is seen in absorption against Ceres' continuum, as shown in Figure VI.A.1. The spectral resolution of the heterodyne spectrometer is 1.1 MHz. Since Ceres is an unresolved object, the signal from LBR will be approximately 8 times stronger than from Herschel due to the larger collecting area of the balloon-borne telescope. The water vapor appears to be time variable; there is considerable controversy if this is due to differing amounts of solar heating of the surface at different points in the asteroid's orbit, or localized cryovolcanism resulting in different observed water vapor signals as the asteroid rotates. Observations with LBR will be so sensitive that one could look at the variability on a time scale less than one hour, as well as searching for water vapor in other objects of this type to determine the distribution of water in the asteroid belt. A large balloon-borne telescope such as LBR is the only realistic possibility for pursuing this exciting result in the foreseeable future.

Another important category of solar system observation that could be carried out by LBR is the study of planetary atmospheres. Again, Herschel has had a major impact on this field, since with the high spectral resolution of the HIFI instrument; the vertical mixing profile can be obtained entire by remote sensing. Figure VI.A.2 illustrates this with a spectrum of molecular oxygen in Mars. Here again, the large collecting area of LBR compared to Herschel will give an

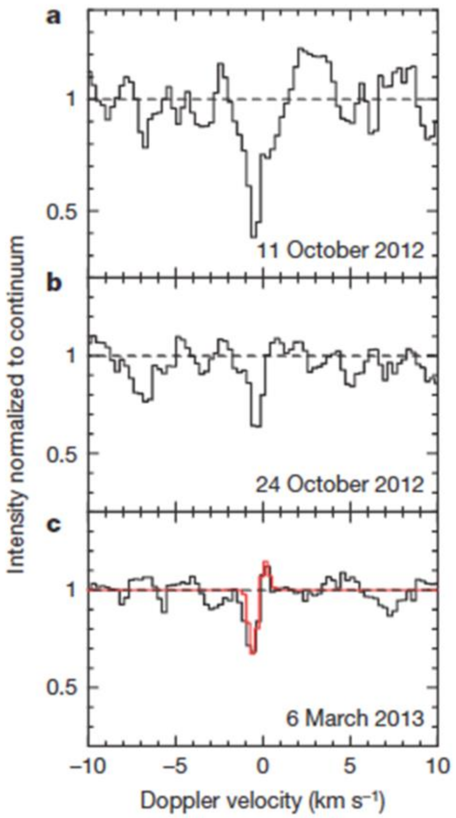

Figure VI.A.1 Spectra of water vapor absorption in Ceres at three different epochs taken with the HIFI instrument on the Herschel Space Observatory. The observed signals imply a minimum water mass sublimation rate of 6 kg s^{-1}. From Küppers et al. (2014).

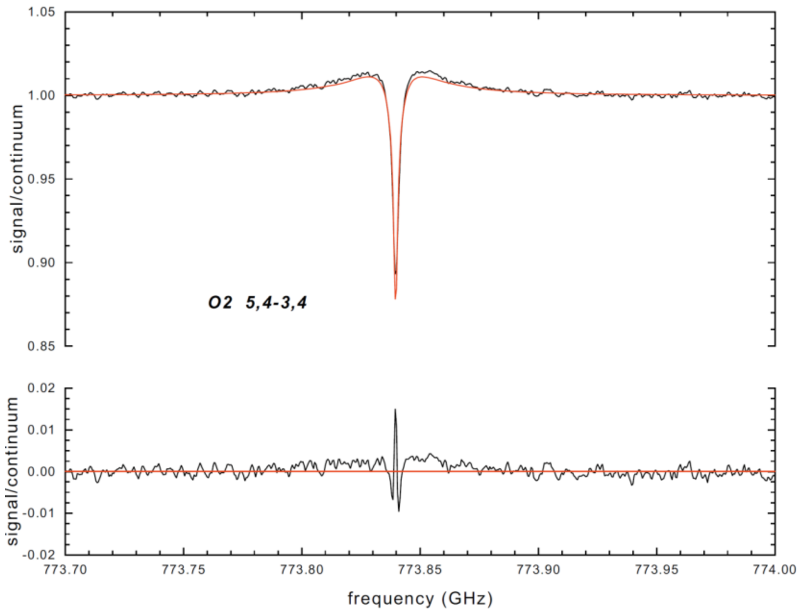

Figure VI.A.2 Observed and fitted line profile (top) of O_2 774 GHz line in the atmosphere of Mars. The signal is normalized to the planetary continuum. The residual from the best fit is shown below. A possibly even better O_2 transition is at 424 GHz, a frequency not covered by Herschel HIFI. From Hartogh (2014).

VI.A.1.b The Interstellar Medium of the Milky Way

The interstellar medium (ISM) is the material between the stars, and is the reservoir of material from which new stars are formed. Studies at millimeter and submillimeter wavelengths over the previous decades have revealed that the ISM is impressively rich in structure and composition. In particular, a complex chemistry operates in both the relative less-dense portions of the ISM (diffuse clouds) as well as in the colder, denser portions (molecular clouds). One of the current challenges is to understand the relationship between these two phases, as it appears that molecular clouds form from the diffuse ISM, and that the rate at which matter is transformed from its diffuse to its dense phase may control the rate of star formation in a galaxy. However, the processes responsible for this transformation (turbulence, shocks, thermal instabilities) are not well understood. Thus, studies of both phases of the ISM are being actively pursued.

Observations of the diffuse ISM can take advantage of the fact that regions of massive star formation, distributed throughout the Milky Way, can act as background sources for absorption studies. Thus, material all along the line of sight to a distant background source can be analyzed, and in general the differential rotation of the galaxy means that different regions show up at different velocities. Figure VI.A.3 illustrates the situation schematically.

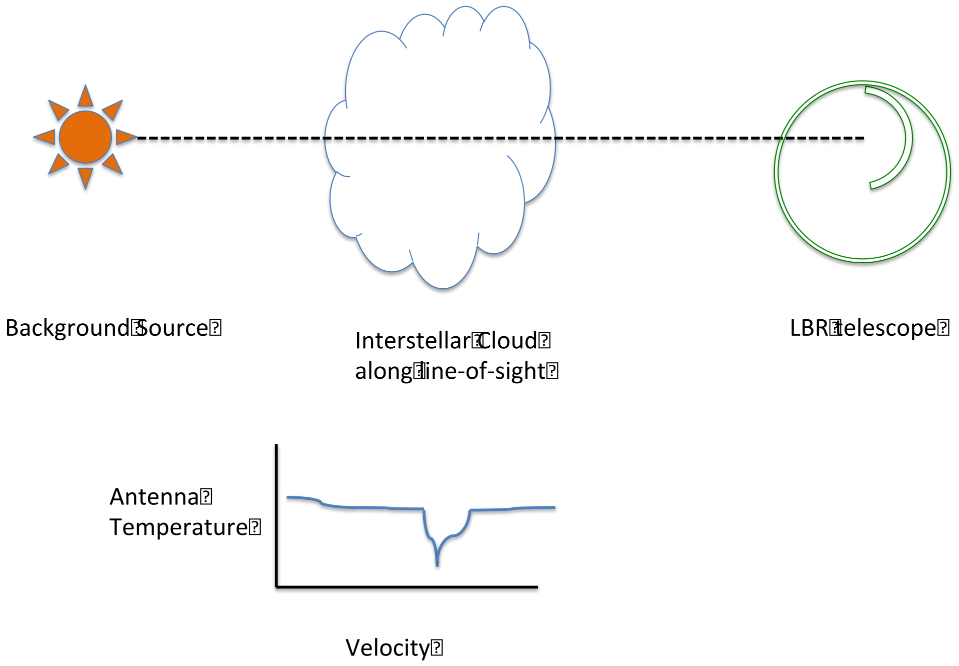

Figure VI.A.3: Schematic of spectral line seen in absorption from a diffuse interstellar cloud along the line of sight to a background source.

While hydrogen atoms and molecules are the most abundant species in the diffuse ISM, one of the most valuable tracers of this gas is water vapor. Its very strong ground-state transition at 556.9 GHz produces valuable diagnostic signals. Figure VI.A.4 shows a spectrum of this line taken towards the source G34.3+0.1. We see a multiplicity of clouds along the line of sight having different amounts of water and different line widths. This information allows determination of the density and temperature in these regions, as well as providing fundamental inputs for chemical modeling of these clouds. The background source providing the continuum (Antenna temperature ≅ 1.6 K) has a small angular size, and consequently this signal will be a factor ~8 stronger with LBR than with Herschel. This will allow sampling of many more lines of sight to gain a more complete picture of the ISM in the Milky Way. It will also allow use of extragalactic objects as background sources, opening up the possibility of studying the distribution of clouds outside the plane of the Milky Way.

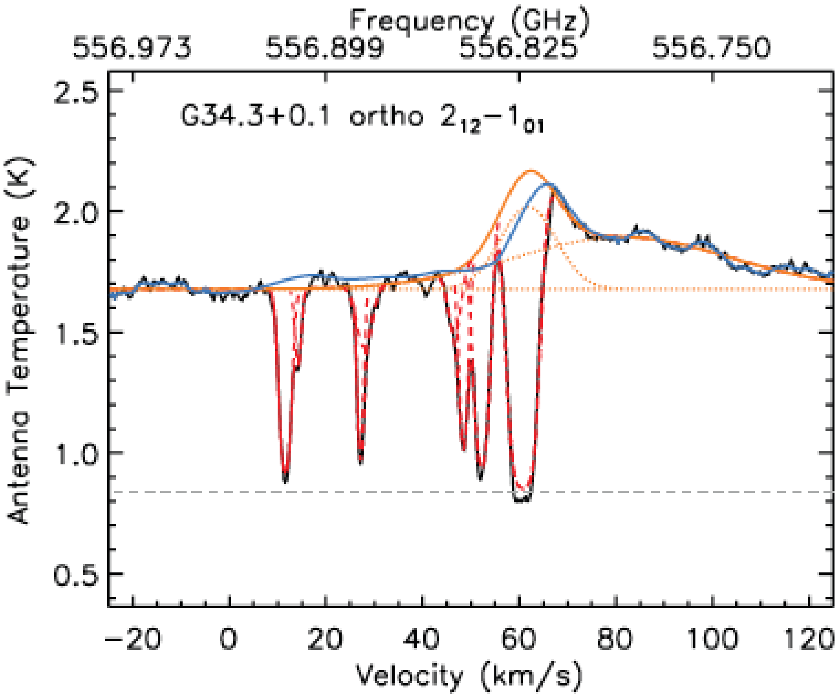

Figure VI.A.4: 556.9 GHz water vapor spectrum towards the Galactic source G34.2+0.1. Each of the components defined by the fitted spectrum (red) is a different interstellar cloud along the line of sight. The emission feature at 55 km/s to 100 km/s and also the absorption at 60 km/s are associated with the source itself. From Flagey et al. (2013).

VI.A.1.cStar Formation

Understanding the complex processes that determine how new stars are formed, the rate at which star formation occurs, and the distribution of masses of new stars is a key challenge of modern astrophysics. To unravel the physical conditions in regions of massive star formation requires a range of probes that can yield information about the wide range of densities, temperatures, and abundances that occur in these regions. Here, LBR has two major capabilities that complement what can be done using other platforms:

- High angular resolution compared to space-based (e.g. Herschel) and other suborbital facilities (e.g. SOFIA)
- Access to uniquely valuable probes such as water (compared to e.g. ALMA)

Thus, while ALMA offers superb angular resolution, it cannot observe water in the Milky Way, which is one of the key tracers of regions of star formation. The biogenic importance of water was the justification of a Herschel Guaranteed Time Project “WISH” (E. van Dishoeck, P.I) tracing the “water trail” from interstellar clouds to protoplanetary disks. However, with a factor of 8 times higher sensitivity and almost 3 times higher angular resolution at the 557 GHz frequency of the ground-state transition of ortho-H_2O, LBR will enable some very exciting new observations.

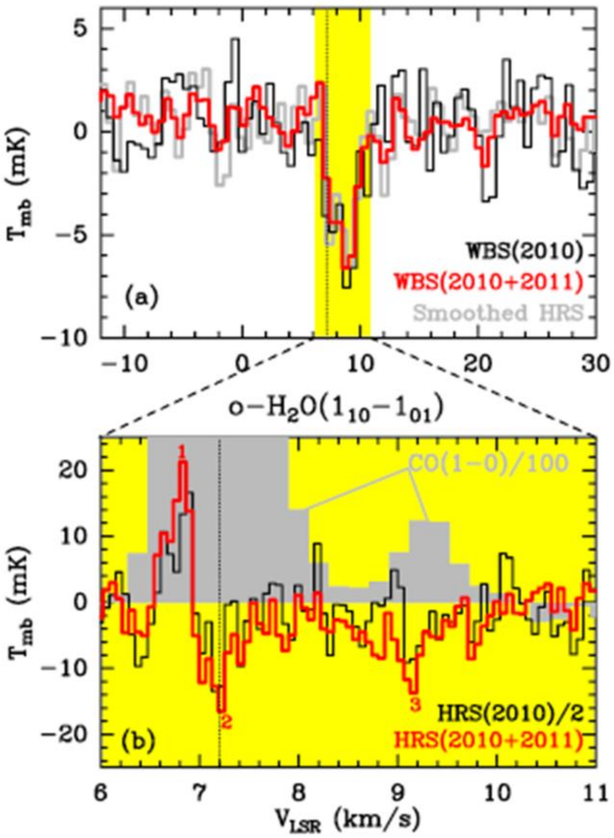

Figure VI.A.5: 557 GHz water vapor spectra of prestellar core L1544. The upper panel is relatively modest spectral resolution data, while the lower panel shows high resolution data from two different epochs as different-colored lines. From Caselli et al. (2012). A velocity resolution of better than 0.1 km/s ($R = 3\times10^6$, corresponding to $\delta f = 0.19$ MHz) is required to extract full information from the water vapor and

Prestellar cores are relatively small condensations in which a single star (or a small cluster of stars) is about to, or is in the process of forming. Figure VI.A.5 shows a spectrum of the first detection of water in the prestellar core, L1544. The upper panel shows “moderately high” velocity resolution (0.59 km/s) data, which suggest only an absorption line. But in the lower panel, “high resolution (0.067 km/s) spectra show that the actual line profile is a combination of narrow emission plus broad absorption components. This complexity reflects the varying abundance of water throughout this contracting dense core, in which the temperature and density also vary significantly with radius.

The 2011 observations of L1544 shown in Figure VI.A.5 took 10 hours of observing time with the Herschel HIFI instrument. L1544 is a very nearby star-forming region, about 140 pc from the Earth. More distant cores of this type will be highly beam diluted, and would thus have taken prohibitive amounts of observing time with Herschel. With LBR, we will have the capability to detect and study prestellar cores in different environments throughout much more of the Milky Way. This is critical for understanding how local conditions affect star formation. Equipped with a focal plane array of receivers, LBR could image water vapor in nearby cores in a reasonable amount of time, thus allowing construction of a full 3-D model of the collapse of a core to form a new star.

When a new star is formed from the contraction of a prestellar core, it is generally accompanied by a circumstellar disk. The disk contains the material out of which planets form, so that studying them is of critical importance in pinning down the process by which water might have gotten to the Earth. The biggest problems are (1) the angular diameters of even nearest circumstellar disks are very small – 3” to 12”, and (2) the abundance of gas-phase water seems to be quite small. LBR obviously has a huge advantage: with a beam size almost 3 times smaller than Herschel’s 40”, the largest disks will almost fill the main beam. Thus, water signals will be proportionately stronger and Herschel’s non-detections could be transformed into the capability to trace water in this next critical stage of planet formation. The reason that the water signals are weak is due to the structure of the disks – their midplanes are so cold that water is frozen as coating on dust grains that are present, while their outer layers are exposed to UV radiation from the young star, which destroys water molecules present in those regions. So it is only in an intermediate layer that we can expect to find water vapor, but with LBR we have for the first time a good chance of being able to finally pin down this important molecule in regions where material is being incorporated into planets.

It is evident that a high-altitude balloon such as LBR should be used only to observe spectral lines that are essentially unobservable from the Earth’s surface. Within the spectral regions that are rendered largely opaque by water absorption there are numerous transitions of other species. One type of observation that would have a major possible impact on astrochemistry would be to carry out small surveys of these obscured spectral regions. Certain molecules are expected to have enormously enhanced abundance only in warm regions of high density – regions which are typically very small and for which the high angular resolution of LBR would be a significant advantage compared to that of Herschel, for example. Some of this will be done as a “fringe benefit” of studies of H_2O itself, due to the broad bandwidth of the spectrometer to be used with LBR. But in other cases, targeted observations of massive star forming regions will be indicated, and these will complement similar observations that will be carried out by ALMA of spectral regions with good atmospheric transmission.

VI.A.1.d Cosmological Molecules

There are a number of important molecular species, sometimes called “cosmological molecules” because their constituent atoms were formed in the early universe, which can be observed at submillimeter wavelengths. Atoms of lithium and deuterium (heavy hydrogen) are believed to have formed exclusively in the “Big Bang” explosion that initiated the universal expansion of the universe. Deuterium can be observed in the HD molecule, and this is a high priority for astronomical study, but its transitions are at shorter wavelengths than can readily be observed with LBR (the longest wavelength transition is at 112 μm). However, LiH is a heavier molecule, and its ground-state transition is at 443.9 GHz for ^{6}LiH and 453.2 GHz for ^{5}LiH. These frequencies are marginally observable from the best ground-based sites, but the atmospheric transmission for typical sources will be ~0.1. Thus, LBR, with an antenna of comparable size to those available for these frequencies on the ground, will have an order of magnitude higher sensitivity. This could enable definitive detection of LiH, which so far has only been marginally detected in external galaxies for which the redshift moves the line into a region of the spectrum with better atmospheric transmission (Combes & Wiklind 1998; Friedel, Kemball, & Fields 2011). An LBR study could also result in a measurement of the ^{6}Li/^{5}Li isotopic ratio in LiH, which would give important limits on production of lithium in supernovae.

A recent Herschel detection that urgently needs follow-up is detection of the argonium ion, ArH^+, seen in absorption in diffuse clouds much like water vapor discussed above (Schilke et al. 2014). However, chemical models and observations are in agreement that ArH^+ is found EXCLUSIVELY in regions in which the hydrogen is almost entirely in atomic form. Thus, it is a quantitative probe of such regions, which in many other tracers such as C^+ are indistinguishable from regions in which H_2 is dominant. The atmospheric transmission at the 617.4 GHz frequency of the lowest transmission of this molecule is also extremely poor (typically ~0.05), and a large balloon-borne telescope such as LBR would have an order of magnitude sensitivity advantage over a ground-based study.

VI.B THz Earth Observing System

The terahertz portion of the electromagnetic spectrum offers major possibilities for Earth observing systems. Such systems are of several different types, but overall these have not yet been studied in detail because the required technology has not been available. With the rapid advance in terahertz receiver systems and the associated spectrometers that are required for radio astronomy and earth observations, the situation has dramatically improved. The availability of a platform such as LBR adds the final ingredient for a system with major capabilities.

One category is “limb sounding”, in which the antenna beam looks through the atmosphere with “cold space” as the background. The minimum height above the surface of the earth is called the tangent height. By looking at different tangent heights, the vertical distribution of a particular atmospheric constituent can be recovered. The narrower the beam, the greater the resolution in altitude that can be achieved, subject of course to instrumental considerations such as pointing accuracy and signal to noise ratio.

Limb sounding has been widely employed in satellites, and one of the prime examples of a spectrometric system is the Earth observing microwave limb sounder (EOS MLS) on the Aura Satellite (Waters et al. 2006). Figure V1.A.6 shows a selection of the chemical species observed by EOS MLS. Note that the 640 GHz band is particularly rich in important tracers of atmospheric chemistry.

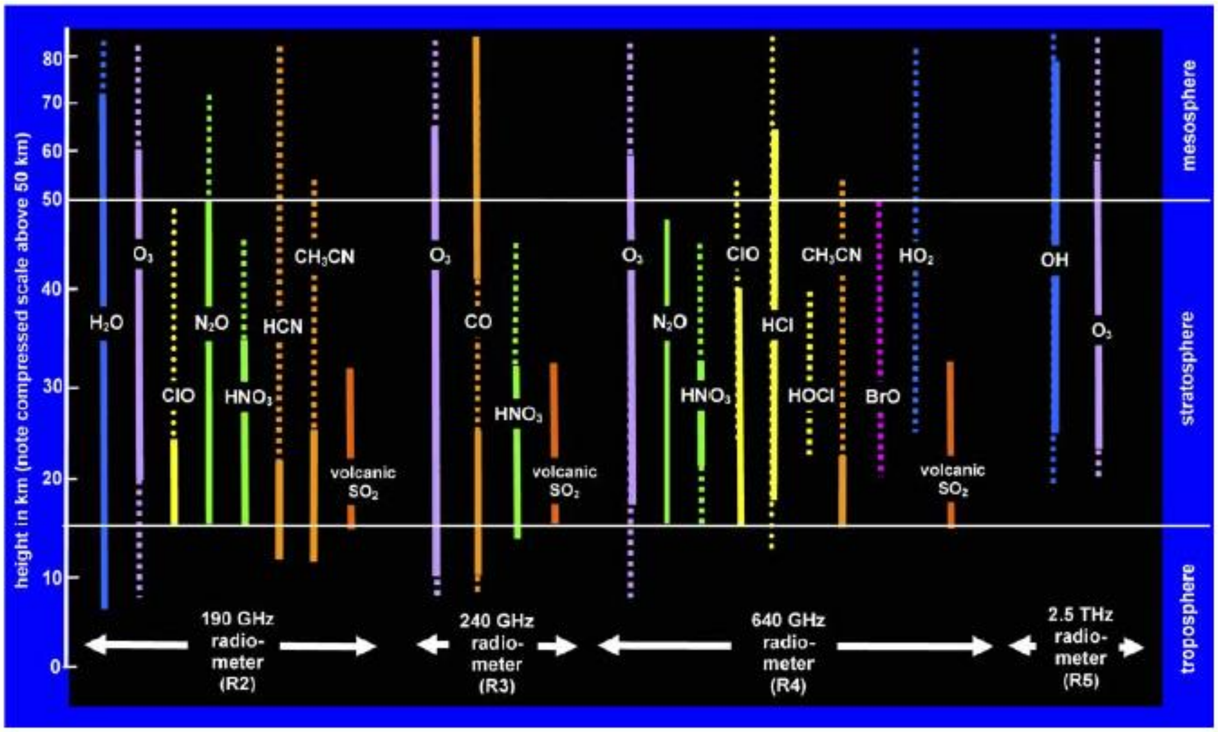

Figure VI.A.6. Atmospheric species observed by EOS MLS system on the Aura satellite. The ranges except the 2.5 THz should be accessible to LBR, with the 640 GHz region likely to be emphasized. From Waters et al. (2006).

LBR could supplement the observations that have been carried out remarkably successfully by EOS MLS. One area would be to carry out longer integrations in fixed directions to measure species below the sensitivity level that is currently achieved. Molecules such as BrO and HO_2 are important, but cannot be measured with current systems. It appears that the improved sensitivity of the radiometer that would be available on LBR plus the ability to obtain long integration times on a fixed path would result in significantly higher sensitivity that achieved by EOS MLS. Another advantage afforded by more modern technology is that the spectrometer used on LBR would have thousands of digitally defined channels, each on the order of 1 MHz width. EOS MLS, on the other hand, due to space and mass constraints on satellite, had to use analog filters with widths adjusted to their positions relative to the spectral line (narrower in the center to retrieve the Doppler-broadened core and wider at off-center frequencies to sample the pressure-broadened line wings). The LBR system will have higher resolution and wider coverage, and should be able to do a much better job recovering the vertical distribution of measured species. Another major advantage is that the LBR receiver will be a single sideband system, as compared to the double sideband mixer systems in EOS MLS. This means that the uncertainty due to the imprecisely known sideband gain ratio will be eliminated. This uncertainty is a major limitation for earth observing systems because one has a large continuum signal and contributions from different lines in both sidebands. All of this can be much more cleanly handled by the LBR system, which should result in higher accuracy as well as greater sensitivity.

Another interesting use of THz/submillimeter wavelength observations is to probe the composition of atmospheric clouds. Topics of interest include ice particles, whose size distribution is of great importance for understanding the properties of clouds and their role in the hydrological cycle of the upper troposphere. A relatively complex system to carry out these observations is described by Buehler et al. (2007), which employs bands between ~ 200 GHz and 650 GHz. A detailed system design for a system on board LBR has not yet been carried out, but there is no problem with having a multiband receiver that has any reasonable set of observing frequencies. Here, we are talking about moderate-bandwidth continuum observations (rather than spectral lines) but the frontends should be able to provide the required stability and will have exceedingly high sensitivity. The far-field distance of LBR is ~ 400 km at a frequency of 600 GHz. Thus the Earth's surface and most of the observable atmosphere are in the near field, and the beam size is essentially constant with a diameter of 10 m. At lower frequencies the beam will be larger, of course, but when looking not far from nadir, clouds down to the Earth's surface will be in the near field. The scanning capability together with the small beam width of LBR means that clouds can in fact be imaged with a resolution as small as 10 m, offering novel and powerful diagnostic capability.

VII APPROACH USED TO EVALUATE THE CONCEPT

VII.A Rooftop 3 meter LBR Prototype

Figure VII.1. 3 meter LBR rooftop prototype. The rooftop prototype is a fully functional 1/6th scale model of the flight version of LBR designed to operate at 115 GHz. An inflatable 3 meter diameter plastic sphere is used to simulate the 20 meter diameter flight version. A 1 meter diameter section of the sphere was made reflective by applying metallic spray paint. The black fork structure inside the sphere is a computer controlled az-el mount for steering the receiver system over the reflective surface. The 5 students who worked on LBR are in the foreground (3-Astronomy, 1-Electrical Engineering, and 1-Optical Sciences).

VII.A.1 Design

Figure VII.1 is a photograph of a 3 meter diameter, rooftop LBR prototype. The prototype was constructed to gain experience with the technological approaches needed to realize and operate a full 20 meter LBR. The prototype has all the key elements of the flight version. The sphere was purchased from a toy company and is formed from 0.8 mm thick, thermoplastic polyurethane (TPU) gores. The gores are thermally bonded together (as in the flight model) to create a spherical shape. The plastic sphere has a 1 meter long zipper through which hardware (and people!) enter and leave. As will be the case for the flight model, a blower is used to inflate the balloon with outside air. For the flight version the `outside' air is the helium gas that fills the carrier balloon. A liquid water monometer is used to regulate the pressure in the balloon to just above ambient. A reflective surface was first created by spaying a 1 meter diameter section of the sphere with metallized spray paint. Later we found that aluminized Mylar sheets stretched over the outer surface can achieve the same high reflectivity.

A computer controlled az-el telescope fork was designed and constructed to accurately position the instrument unit (IU) over the reflective surface (see Figure VII.2). The prototype IU has all the features of the flight unit shown in Figure V.C.1 (i.e. receiver, spectrometer, and instrument computer), except for the adaptive corrector, which was tested separately in the lab (see Sec. V.A.3d). For these tests an existing, uncooled, 115 GHz Schottky diode receiver was used for the receiver `frontend’ and an existing digital `iBOB’ Fourier Transform (FFT) spectrometer for the `backend’. The receiver has a double sideband noise temperature of ~1500K and an IF frequency of 1.5 GHz. The spectrometer digitizes the IF and produces a 1 GHz wide power spectrum of the downconverted sky signal.

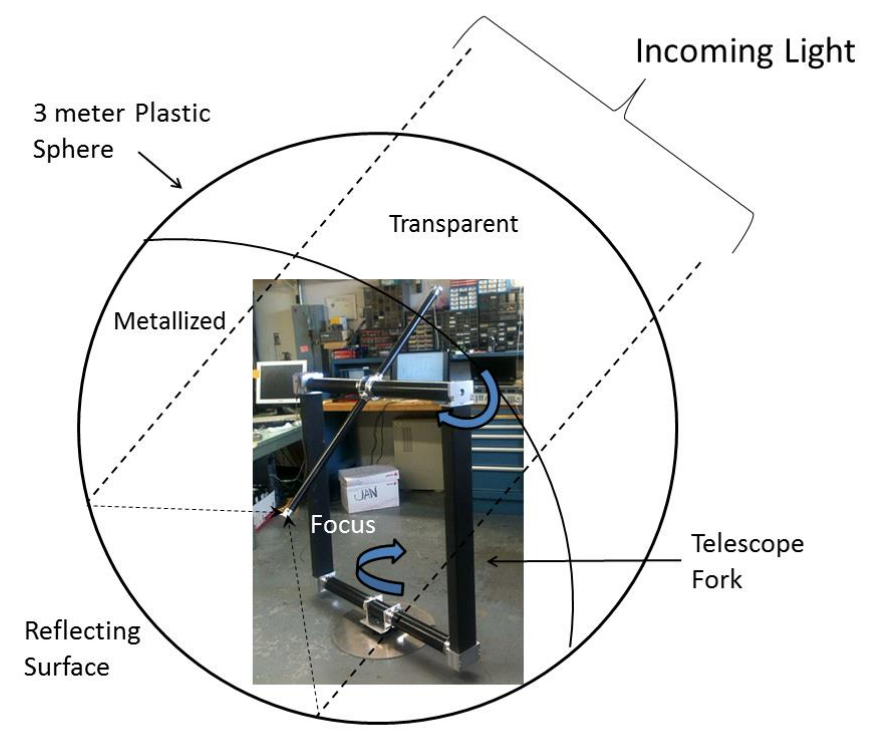

Figure VII.2. LBR prototype functional diagram.

To characterize the performance of the system a test transmitter was used to broadcast a 115 GHz tone across the roof to the 3 meter LBR which then produced a power spectrum of the received signal. As is a common practice in radio astronomy, the LO frequency of the receiver was switched by 3 MHz once a second, with the output of the receiver obtained with one LO frequency serving as the `Signal’ and the receiver output at the other LO frequency as the `Reference’. The two signals are differenced and normalized to suppress common mode noise from the receiver and atmosphere. A photograph showing the real time output of the LBR prototype with an incoming test tone is shown in Figure VII.3.

The optical performance of the rooftop LBR was characterized by performing a series of scans across the position of the test transmitter. In the first scan the IU was rotated so that the

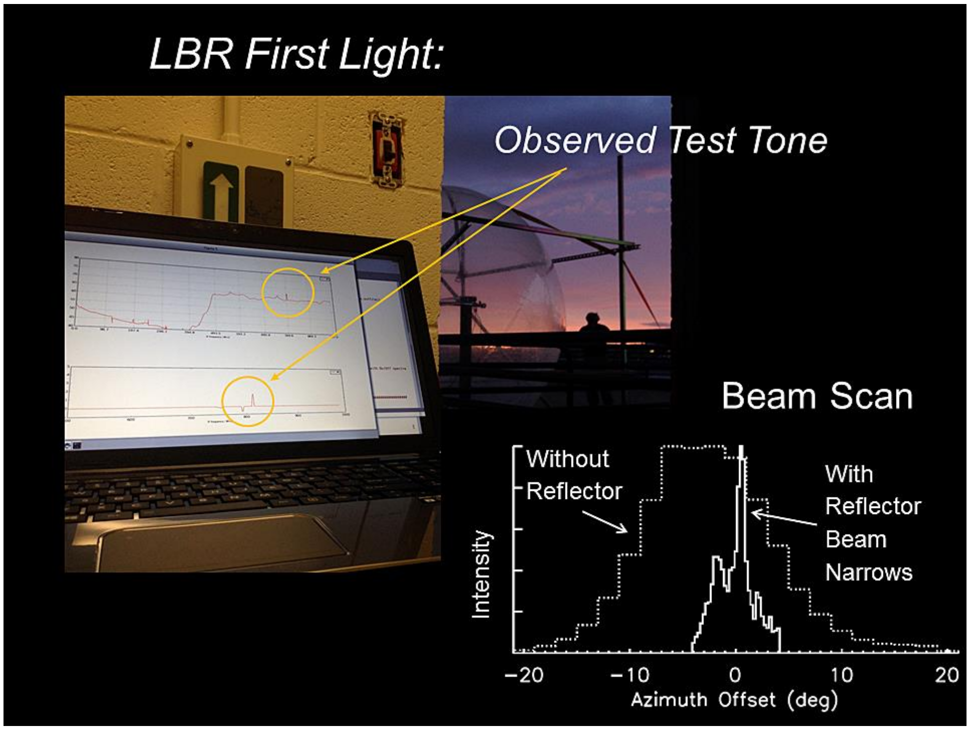

Figure VII.3. First light measurements with LBR. The laptop screen shows a real time display of a 115 GHz test tone being received by LBR. The inset shows two beam scans of the test transmitter, one made with the receiver alone and the other made with the receiver in combination with the spherical reflector. The peak of the scan made with the reflector is ~10x narrower, demonstrating the reflector is producing a diffraction limited main beam.

feedhorn of the transmitter was pointed 180° from the reflector surface. The resulting scan shows the broad, $\theta_h \sim 15^\circ$, full-width-half-maximum (FWHM) power pattern of the feedhorn. The IU was then rotated back 180°, so that the feedhorn was illuminating the reflector surface and another scan of the test transmitter performed. The resulting LBR scan shows a 10x improvement, producing a much narrower, $\theta_M \sim 1.5^\circ$, FWHM main beam. Here θ_M represents the convolution of LBR's diffraction limited beam ($\sim 0.5^\circ$) with that of the test transmitter. In the scan the main beam is seen to be on top of a broader beam component. This broad component is referred to as the error beam, θ_e, and is due to a combination of small scale random surface features (i.e. skin roughness, ε) and large scale correlated structural features (i.e. gore width, r_c) in the reflector surface. When pressurized the plastic surface of the sphere is exceptionally smooth compared to our wavelength of observation, $\lambda = 2.7$ mm. In such a case,

$$\theta_e \approx 0.53\frac{\lambda}{r_c} \ .$$

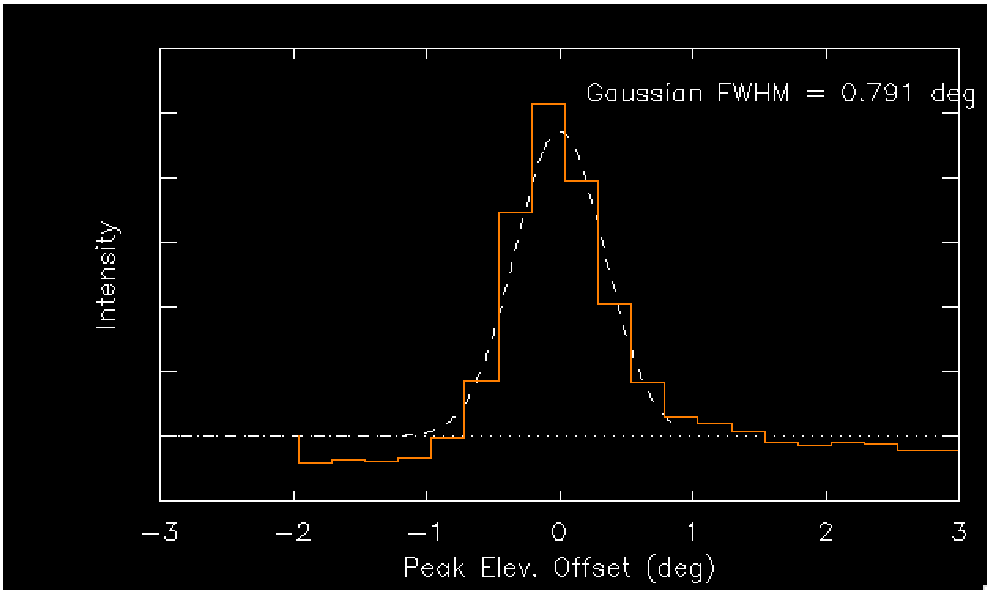

Figure VII.4. LBR Sun scan. The orange histogram is a scan of the Sun made with the LBR prototype at 115GHz. A Gaussian fit to the line yields a FWHM beam size of ~0.8°, indicating the reflector is providing diffraction limited performance.

From Figure VII.3, the size of the error beam is $\theta_e \approx 8^\circ$, yielding a value of $r_c \approx 26$ mm, suggesting there was a low-level ripple in the reflective surface at the time of measurement with a periodicity of ~ 2inches.

As a further test of optical performance, a Sun scan was also made with LBR. A 115 GHz total power scan of the Sun made with LBR is shown in Figure V.II.4. Since the projected size of the Sun on the sky is only ~0.5°, the scan yields a more faithful representation of the true LBR main beam. From the Sun scan we measure, $\theta_M \approx 0.8^\circ$, indicating the LBR prototype is providing diffraction limit performance. The fact that such a crude prototype works this well suggests the concept is robust and bodes well for the success of a full flight version. During flight the LBR beam quality will be routinely measured and optimized on a strong calibration source (e.g. Moon and planets).

VII.A.2 Lessons Learned

Several valuable lessons were learned in the construction and operation of the LBR rooftop prototype. We have incorporated these lessons into the proposed LBR design. These lesson include,

1) Pressure regulation of the balloon is essential. The internal pressure of the balloon and therefore its shape is very sensitive to diurnal temperature variations. Without a pressure regulator the diameter of the balloon would vary by as much as ~30% from dawn to midday. Similar day-night temperature excursions will be encountered by a stratospheric

flight launched at temperate latitudes (e.g. Ft Sumner, NM). The temperature excursions will be less during an Antarctic summer launch, since the Sun is up 24 hours a day.

2) The Instrument Unit (IU) should be secured in 3 dimensions within the LBR balloon otherwise it is easy for the receiver to go in and out of focus. As an added safeguard, the IU should include a focusing mechanism.
3) Small misalignments between the IU and reflector can lead to a significant pointing offsets. The offsets can be measured and removed. However, to eliminate the possibility of the receiver beam walking off the reflector surface, the entire back hemisphere of the LBR balloon should be metallized.
4) The IU should be fully tested before being mounted inside the balloon. During the IU development phase many trips in and out of the balloon were required before the system was fully operational, with each entrance leading to a partial deflation. The number of such trips could have been significantly reduced if the IU were more fully tested before installation. The flight version of LBR has been designed so that the IU is inserted into the carrier balloon just before the start of inflation. This approach allows the performance of the IU to be verified up to within few hours of launched.
5) Minimize the number of cables going into the balloon. Many of the problems we encountered were ultimately traced to faulty interconnects between instrument subsystems in and out of the balloon. At first our philosophy was to put as little hardware in the balloon as possible, but this led to an inordinate number of cables. System failures decreased dramatically when more of the IU subsystems were integrated *within* the balloon. We will adopt this approach in the flight version (see Sec. VI.).

VII.B Laboratory Measurements of Balloon Materials

As discussed in Sec. VI, LBR’s spherical reflector is inflated within the carrier balloon. The carrier balloon serves as the launch vehicle, radome, and stable mounting platform. On the way to the reflector the incoming light passes through the carrier balloon’s reinforced `EndCap’(see Figure VII.5. The EndCap is reinforced since it must support the majority of the LBR payload weight. It is typically constructed from 3 layers of 0.8 mil thick linear low-density polyethylene (LLDP) and 1 layer of 1.0 mil Mylar. As part of our Phase I study, the THz transmission of a sample of LLDPE balloon fabric was measured in a Fourier Transform Spectrometer (FTS). The resulting transmission curve is shown in Figure VII.6. One layer of LLDPE was found to pass $\geq$ 98%, of light at the LBR design frequency of 557 GHz. The properties of Mylar are well characterized at THz frequencies (Goldsmith 1996). From laboratory measurements, the total absorption of incoming light through the carrier balloon’s EndCap is estimated to be $\leq$ 8%.

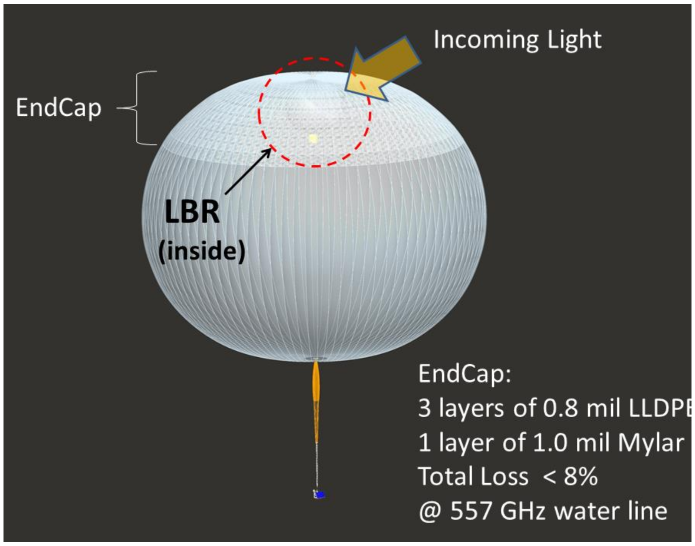

Figure VII.5. Observing through the EndCap. The top ~1/3rd of the carrier balloon forms the `EndCap'. The EndCap is reinforced to take the weight of the flight system. For astrophysical observation of the 557 GHz water line where LBR is looking up, the transmission of incoming light through the EndCap will be > 92%.

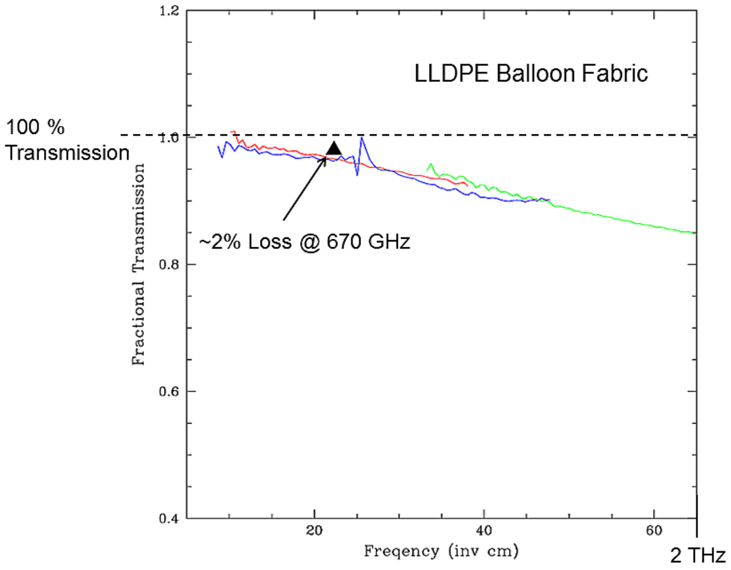

Figure VII.6. Measured transmission through one layer of LLDPE balloon fabric.

VIII LBR COST PROJECTION

A 10 meter class telescope capable of performing observations in the far-infrared/THz free of atmospheric absorption has long been a goal of NASA and the astrophysics community. However, the costs of such a mission have been daunting. LBR can make this dream a reality for spectroscopic studies at THz frequencies for a fraction of the cost of other mission approaches. NASA's only two missions operating in this spectral regime are SOFIA and JWST. SOFIA is an airborne observatory flying at ~45,000 ft that hosts a 2.5 meter, uncooled telescope in a modified Boeing 747SP. JWST is a 6.5 meter, radiatively cooled telescope that will perform observations from L2, ~ 1 million miles from Earth. The costs of both missions are staggering, over $1B for SOFIA and over $5B for JWST. Of the two missions, SOFIA is closest to LBR in capability and science goals. However, LBR has 16x the collecting area and flies ~3x higher than SOFIA, making it a superior platform from which to conduct high spectral resolution THz observations, at a cost < 1% of what has been spent on SOFIA to date. Table VIII.1 is the projected cost breakdown for building and flying a 10 meter sub-orbital LBR. The program includes both a test flight from Ft. Sumner, NM and an Antarctic science flight. The estimates are based on ROMs from balloon manufacturers and the actual cost of similar hardware built for the PI's ongoing Stratospheric TeraHertz Observatory (STO) program. During Phase II we will further refine these cost estimates.

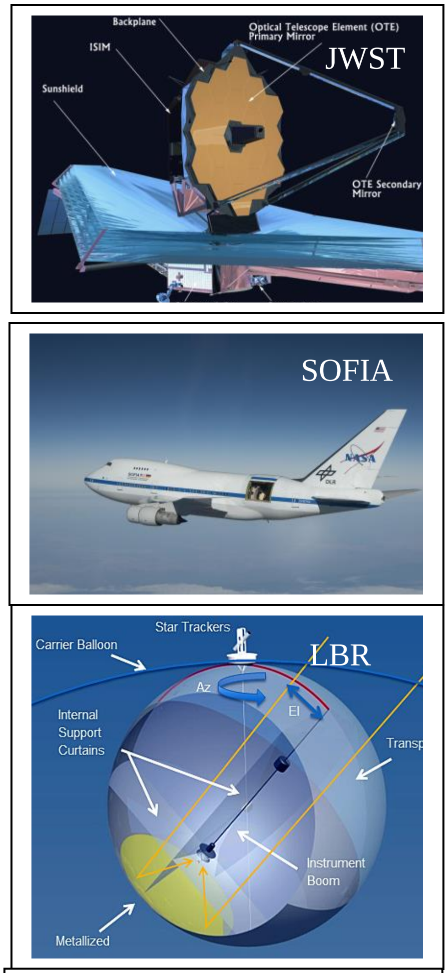

Figure VIII.1. *Top*: JWST is the NASA flagship IR/FIR mission with a 6.5 m telescope for >$5B. *Middle:* SOFIA is a 2.5 m airborne IR/FIR telescope for >$1B. *Bottom:* LBR is a 10 m FIR/THz sub-orbital telescope for <$0.01B.

Table VIII.1: Projected LBR Costs

Phase	Cost ($M)		Duration
Test Flight	LBR Balloon	1.0	2 years
	Service Gondola	1.5	
	Pointing System	1.0	
	Instrument	1.5	
Science Flight	LBR Balloon (+ spare)	1.5	2 years
	Service Gondola (refurb)	0.5	
	Pointing System	0.5	
	Instrument	1.5	
Total		9.0	4 years

IX REMAINING CHALLENGES

1. The Phase I study indicates an off-axis spherical corrector is likely to increase the effective collecting area of LBR. In Phase II a more detailed design of such a corrector system will be undertaken.
2. The small, table-top prototype of the adaptive corrector built in Phase I demonstrated the mechanics of the approach. However, a larger scale version of the corrector should be built and optically tested with a similarly scaled LBR to validate performance expectations.
3. A demonstration of the proposed optical parallax surface measuring system is needed to prove the validity of the approach. The system should be integrated with a scale model of LBR, together with the adaptive corrector. The performance of the closed-loop adaptive system should then be characterized under flight-like conditions.
4. Both the parallax and TOF laser ranging systems should be tested in day/night conditions.
5. A more detailed thermal and finite element analysis of the LBR balloon is needed in Phase II to quantify distortions due to thermal, differential pressure, stiffening, and gravitational factors that will influence the spherical LBR surface figure.
6. Several potential approaches to fabricating the LBR balloon have been identified in Phase I. In Phase II additional analyses and tests should be performed to identify the best approach to build LBR.
7. A more thorough analysis of the dynamic interaction between LBR, the carrier balloon, and the service gondola is needed to understand potential impacts on the reflector’s surface figure and pointing.
8. The best way to test the proposed deployment scheme and ultimate performance of LBR is to build a fully functional scale model. In Phase II we will build and test a 1/2 scale (10 meter diameter) version of LBR.
9. In Phase I resources were not available to conduct a more complete design study of the LBR pointing system and service gondola. In Phase II such a study should be undertaken.
10. The initial science driver for LBR is to observe the ground state water line at 557 GHz toward a variety of objects. Due to the presence of atmospheric water vapor, this line is unobservable toward astrophysical objects from anywhere but balloon or space-based telescopes. In Phase II a list of target objects, both galactic and extragalactic will be compiled and a detailed program for using LBR to probe greenhouse gases within planetary atmospheres will be formulated.

X REFERENCES

Buehler, S. A., Jiménez, C., Evans, K.F., et al. 2007, Quarterly Journal of the Royal Meteorological Society, 133, 109.

Caselli P., Keto, E., Bergin, E.A. et al. 2012, The Astrophysical Journal, 759, L37.

Chodimella, Surya, et al., 2006, Design Evaluation of a Large Aperture Deployable Antenna, American Institute of Aeronautics and Astronautics.

Combes, F. & Wiklind, T. 1998, Astron. Astrophys., 334, L81.

Farley, R., NASA 2010 Super-Pressure Balloon 14.915 MCG Test Flight Design Review.

Flagey, N., Goldsmith, P.F., Lis, D.C. et al. 2013, The Astrophysical Journal, 762, 11.

Friedel, D.N., Kemball, A., & Fields, B.D. 2011, The Astrophysical Journal, 738, 37.

Goldsmith, P.F. 1996, IEEE Potentials, 38, Aug.

Gordon, W.E. and Lalonde, L.M. 1961, IRE Trans. Antennas Propag., AP-9, 17.

Hartogh, P. 2014, private communication.

Herouni, P, Sixth International Conference on Antennas and Propagation, ICAP89, Conf. Pub. No. 301, 540.

Kildal, P.S., Baker, L.A., and Hagfors, T. 1974, Proc. IEEE, 82, 714.

Küppers, M., O'Rourke, L., Bockelée-Moran, D, et al. 2014, Nature, 505, 525.

Li, T. 1959, IRE Trans. Antennas. Propag. AP-7, 223.

North Sail, 2014, http://www.na.northsails.com/TECHNOLOGY/3DTechnology/Howis3DLMade/tabid/1934/Default.aspx

Schilke, P., Neufeld, D., Müller, H.S.P., et al. 2014, Astronomy & Astrophysics, in press.

Smalley NCAR-TN-25, "Balloon Shapes and Stresses Below the Design Altitude", Dec. 1966.

Smith, I.S., 2000, Ultra Long Duration Balloon Project, Briefing.

Smith, I.S. and Lee, Mike, 2007, "The HiSentinel Airship", American Institute of Aeronautics and Astronautics, Lighter Than Air Conference, Ireland.

Thomas, M and Veal, G., 1984, "Highly Accurate Inflatable Reflectors", AFRPL TR-84-021.

Waters, J.W., Froidevaux, L., Harwood, R.S., et al. 2006, IEEE Trans. Geoscience & Remote Sens., 44, 1075.

XI ACRONYMS AND ABBREVIATIONS

APL	Applied Physics Laboratory
BOPPS	Balloon Observation Platform for Planetary Science
BPO	Balloon Program OFFICE
BRRISON	Balloon Rapid Response for ISON
C&C	Command and Control
COTS	Commercial off the Shelf
CSBF	Columbia Scientific Balloon Facility
FOV	Field of View
GSE	Ground Support Equipment
IMU	Inertial Measurement Unit
IRIDIUM	
JPL	Jet Propulsion Laboratory
LBR	Large Balloon Reflector
LOS	Line-of-Sight
MLI	Multi-Layer-Insulation
MOC	Mission Operations Center
NASA	National Aeronautics and Space Administration
NFC	Narrow Field star Camera
OCC	Operations Control Center
PCS	Pointing Control System
PID	Proportional-Integra-Derivative
ROCC	Remote Operations Control Center
SIP	Support Instrumentation Package
STO	Stratospheric TeraHertz Observatory
TDRSS	
UofA	University of Arizona
VPN	Virtual Private Network
WFC	Wide Field star Camera